Department of Applied Physics

Cellulose Nanofibrils as a Functional Material

Marjo Kettunen née Pääkkö

Aalto University

DOCTORAL DISSERTATIONS

Aalto University publication series
DOCTORAL DISSERTATIONS 114/2013

Cellulose Nanofibrils as a Functional Material

Marjo Kettunen née Pääkkö

A doctoral dissertation completed for the degree of Doctor of Science (Technology) to be defended, with the permission of the Aalto University School of Scinece, at a public examination held at the lecture hall E of the school on 14 August 2013 at 12.

Aalto University
School of Science
Department of Applied Physics
Molecular Materials

Supervising professor
Acad. Prof. Olli Ikkala

Thesis advisor
Acad. Prof. Olli Ikkala

Preliminary examiners
Prof. Stephen Eichhorn, University of Exeter, UK
Prof.Sirkka-Liisa Maunu, University of Helsinki, Finland

Opponent
Prof. Akira Isogai, The University of Tokyo, Japan

Aalto University publication series
DOCTORAL DISSERTATIONS 114/2013

ISBN 978-952-60-5255-7 (printed)
ISBN 978-952-60-5256-4 (pdf)
ISSN-L 1799-4934
ISSN 1799-4934 (printed)
ISSN 1799-4942 (pdf)
http://urn.fi/URN:ISBN:978-952-60-5256-4

http://lib.tkk.fi/Diss/

Unigrafia Oy
Helsinki 2013

Finland

441 697
Printed matter

Author
Marjo Kettunen

Name of the doctoral dissertation
Cellulose Nanofibrils as a Functional Material

Publisher School of Science

Unit Department of Applied Physics

Series Aalto University publication series DOCTORAL DISSERTATIONS 114/2013

Field of research Engineering Physics, Physics

Manuscript submitted 11 June 2013 **Date of the defence** 14 August 2013

Permission to publish granted (date) 27 June 2013 **Language** English

☐ **Monograph** ☒ **Article dissertation (summary + original articles)**

Abstract

The recent developments to disintegrate nanocelluloses from plant and wood cell materials have attracted considerable interest in materials science. Nanocelluloses are considered as fascinating building blocks for functional materials, thanks to their high mechanical properties, rod-like or fibrous structure, biocompatibility and sustainability. In addition, they own high surface area with numerous free reactive groups offering great opportunities for chemical or physical functionalization.

Among nanocelluloses, native cellulose nanofibrils form an important class of materials, and this thesis explores them as building blocks for functional and responsive materials. The characteristics of enzymatically and mechanically prepared cellulose nanofibrils are studied in Publication I. The cellulose nanofibrils form strong inherent hydrogels at low concentration without chemical cross-linking, and show shear thinning which is useful both in processing and in applicability. Publication II demonstrates that the hydrogel enables vacuum freeze-drying to form light-weight aerogels which are ductile and deformable, even if the porosity totals 98%. The tunable morphology provides multiple length scale structures and porosity, as well as percolative template for conducting polymer, e.g. polyaniline to achieve highly porous conducting materials.

The aerogels, made from the long and entangled cellulose nanofibrils, are also versatile templates for titanium dioxide (TiO_2) and fluorosilane deposition to tune the wetting, and to enable responsive materials. In Publication III, the TiO_2-coated nanocellulose aerogel shows switchable water absorption between nonabsorbent and superabsorbent states upon exposure of UV light. In addition, TiO_2-coated aerogel shows improved photo-catalytic activity. The aerogel template not only serves as a support for TiO_2 but also enhances the effects due to its multiple scale structures. The superoleophobic and -hydrophobic bio-inspired nanocellulose cargo carrier, reported in Publication IV, is also shown to benefit from multiple length scaled structures and the pores. The TiO_2 approach is extended in Publication V, where the selective absorption of TiO_2-coated nanocellulose aerogels is applied, and floatable oil-absorbing nanocellulose aerogel is demonstrated for oil spill removal.

This thesis contributes to basic research on nanocelluloses, while yielding concrete benefits for the industrial context. It furthers the fundamental understanding of the behavior of cellulose nanofibrils, and suggests novel value-added applications beyond the classic cellulose applications. Nanocellulose can lead to strengthened competitiveness of the forest industry in its changing operational environment.

Keywords nanocellulose, microfibrillated cellulose, aerogel, foam, UV-switchable absorption, selective absoption

ISBN (printed) 978-952-60-5255-7 **ISBN (pdf)** 978-952-60-5256-4

ISSN-L 1799-4934 **ISSN (printed)** 1799-4934 **ISSN (pdf)** 1799-4942

Location of publisher Espoo **Location of printing** Helsinki **Year** 2013

Pages 144 **urn** http://urn.fi/URN:ISBN:978-952-60-5256-4

Tekijä
Marjo Kettunen

Väitöskirjan nimi
Selluloosan Nanokuidut Funktionaalisena Materiaalina

Julkaisija Perustieteiden korkeakoulu

Yksikkö Teknillisen fysiikan osasto

Sarja Aalto University publication series DOCTORAL DISSERTATIONS 114/2013

Tutkimusala Teknillinen fysiikka, fysiikka

Käsikirjoituksen pvm 11.06.2013 **Väitöspäivä** 14.08.2013

Julkaisuluvan myöntämispäivä 27.06.2013 **Kieli** Englanti

☐ **Monografia** ☒ **Yhdistelmäväitöskirja (yhteenveto-osa + erillisartikkelit)**

Tiivistelmä

Tässä työssä selluloosan nanokuidusta on valmistettu funktionaalisia ja ulkoisiin olosuhteisiin reagoivia materiaaleja. Nanoselluloosa on materiaalitieteen kannalta kiinnostava sen mekaanisen lujuuden, nanoskaalan kuiturakenteen, uusiutuvan alkuperän, sekä biologisen yhteensopivuuden vuoksi. Lisäksi nanoselluloosan suuri ominaispinta-ala, ja kuidun pinnalla olevat lukuisat kemiallisesti tai fysikaalisesti muokattavat ryhmät mahdollistavat mitä moninaisimpia funktionaalisia nanoselluloosamateriaaleja.

Natiivin selluloosan nanokuitujen kykyä muodostaa vahvoja hydrogeelejä hyvin alhaisilla konsentraatioilla on tutkittu julkaisussa I. Niiden osoitettiin olevan lujia ja voimakkaasti leikkausohenevia, mikä on tärkeää materiaalien valmistus- ja prosessointimenetelmissä sekä sovelluksissa. Julkaisussa II havainnolistettiin, miten vahva hydrogeeli voidaan kuivata kylmäkuivauksella, jolloin muodostuu aerogeelejä. Natiivin selluloosan nanokuiduista valmistetut aerogeelit ovat muokkautuvia ja taipuisia, huolimatta niiden 98 % huokoisuudesta. Niiden sisärakennetta ja huokoisuutta voidaan muunnella mm. kuivausolosuhteiden avulla, minkä vuoksi ne soveltuvat mitä erilaisimpiin käyttötarkoituksiin. Ne tarjoavat esimerkiksi perkoloivan substraatin johtavalle polymeerille, kuten polyaniliinille, jonka avulla saavutettiin erittäin huokoinen sähköisesti johtava nanoselluloosamateriaali. Lisäksi, päällystämällä aerogeeli titaanidioksilla (TiO_2), sen ominaisuuksia voidaan ohjata ulkoisesti. Julkaisussa III osoitettiin, että TiO_2-pinnoitetut nanoselluloosa-aerogeelit muuttuvat UV-valon vaikutuksesta vettä hylkivästä vettä superabsorboiviksi. Aerogeelin vaikutus on kaksijakoinen: se toimii sekä alustana että tehostaa omalla rakenteellaan pinnoitteen aiheuttamia ominaisuuksia. Myös TiO_2-nanoselluloosa-aerogeelin hyvä fotokatalyyttinen aktiivisuus perustuu suurehkoon ominaispinta-alaan ja hierarkkiseen huokoisuuteen.

Julkaisussa IV tarkasteltiin edelleen nanoselluloosa-aerogeelin rakenteen ja huokoisuuden merkitystä niin hydrofobisuuteen kuin myös oleofobisuuteen fluoraamalla aerogeeli. Julkaisussa V havainnollistetaan miten hydrofobiseksi TiO_2:lla pinnoitettu nanoselluloosa-aerogeeli absorboi selektiivisesti öljyä, mutta hylkii vettä. Tällaista veden pinnalla kelluvaa, öljyä imevää materiaalia voidaan käyttää esim. öljyn poistamiseen vedestä öljyvahingoissa.

Tässä työssä tutkitut funktionalisoidut nanoselluloosamateriaalit tarjoavat mahdollisuuksia uusiin erityissovellutuksiin materiaalitieteessä, ja yhtälailla nanoselluloosa luo mahdollisuuksia metsäteollisuuden kilpailukyvyn vahvistamiseen sen muuttuvassa ja haastavassa toimintaympäristössä.

Avainsanat nanoselluloosa, nanofibrillaarinen selluloosa, mikrobrillaarinen selluloosa, aerogeeli, valo-ohjautuva absorptio, selektiivinen absorptio

ISBN (painettu) 978-952-60-5255-7 **ISBN (pdf)** 978-952-60-5256-4

ISSN-L 1799-4934 **ISSN (painettu)** 1799-4934 **ISSN (pdf)** 1799-4942

Julkaisupaikka Espoo **Painopaikka** Helsinki **Vuosi** 2013

Sivumäärä 144 **urn** http://urn.fi/URN:ISBN:978-952-60-5256-4

Preface

The research that is presented in this thesis was carried out in the Molecular Materials group at the Department of Applied Physics at Aalto University (former Helsinki University of Technology). It has been a long and great journey to explore nanocellulose only to realize that this is only the beginning. I am grateful to my supervisor Academy Professor Olli Ikkala for providing the best possible scientific surroundings. I see myself privileged to be a member of his group, and enjoy Olli's never-ending ideas and enthusiasm for science. Without his ambition and contribution, this thesis would not have turned out as it is.

I would like to sincerely thank Professor Stephen Eichhorn and Professor Sirkka-Liisa Maunu for critical comments and valuable improvements as reviewers.

I am indebted to Professor Tom Lindström and Mikael Ankerfors for providing me the most fascinating material, cellulose nanofibrils to work with, and for the fruitful collaboration. I am ever grateful to Professor Lars Berglund for all discussions. In addition, I wish to thank Professor Janne Laine and Professor Monika Österberg for the collaborative journey we have gone. Moreover, Robin Ras and Professor Janne Ruokolainen, Sami Hietala and Mikko Karesoja are acknowledged for their valuable know-how and support.

I am most grateful to Harri Kosonen who was my instructor in the early years of my research. His guidance, ideas and practical advices had great impact to my work. I have greatly benefited from working with brilliant colleagues in our and in the collaborative labs. I would like to express my honest acknowledgement to all my numerous co-authors. I am very thankful to Hua Jin, Nikolay Houbenov, Marianna Kemell and Viljami Pore. Especially, I want to thank Jaana Vapaavuori for her enthusiasm and attitude towards the research we did. Your philosophy of life is astonishing!

I want to thank each and every member in the lab, past and present, for creating such a great working environment, we are like family. My very special thanks go to Antti N., Antti S., and Juuso: Antti N. is acknowledged for TEM imaging, Blender guidance, and all IT and technical help over the years. Antti S. is thanked for his patience for my never-ending IT problems and his valuable help in AFM image analysis. Antti, hölökyn kölökyn! Juuso is also thanked for, surprise surprise, IT support, but most of all for the spirit and the skill in our joint paper. Secretary Orvokki Nyberg and Timo Kajava are acknowledged for all help and the arrangements.

In 2005, I had pleasure to be a member of the research group of Professor Werner Blau at the Department of Physics at Trinity College Dublin. I am sincerely grateful for their hospitality and guidance. Especially I want to thank Adam, David, Estelle, Ronan, Shane and Yenny. Without your help and laughter I would not have survived. Shane is kindly thanked also for proof-reading of the manuscript. My warmest gratitude goes to Donna and John, you made the year in Ireland unforgettable.

It has also been pleasure to share the room with Panu Hiekkataipale. Thank you Panu for explaining me over and over again the same physical equations and curves, for listening my endless chatting, and for the friendship.

There is no other person who has shared the passion, ambition and joy for the cellulose research with me like Mari Granström. Our friendship, never-ending speculations about science and life are invaluable. Thank you, Mari.

I will always remember my great lecturers at University of Eastern Finland (former University of Joensuu) Leila Alvila and Tuure-Pekka Jauhiainen. Department of Chemistry is complimented for the years I studied there.

I would like to express my warmest gratitude to my friends: Andreina, Anne, Heta, Kirsi, Maria, Marjo, Sanna, Vuokko, ”biologit”, and family Ihanus for all the fun over the years, and for not losing my mind. I have been fortunate to get to known Riikka and Susanna during the maternity leave, and to share the everyday life ever since. Besides, I am thankful for my mother-in-law Liisa and great-grandpa Pauli for all the support.

This research was funded by the Academy of Finland, TEKES, EU FP7. Grants from Walter Ahlström foundation, Jenny and Antti Wihuri foundation, Emil Aaltonen foundation, and Tekniikan edistämissäätiö, are appreciatively acknowledged.

I am forever indebted to my parents, Terttu and Martti, who have supported me in so many ways. My sisters Salla and Menna, and my brother Lauri, and their families, have kept my feet on the ground.

Finally, I wish to express my deepest gratitude to my loving husband Mika for everything. Without him I would not have been able to finish this work. I dedicate this thesis to my dear children, Rasmus and Iisa, who have taught me more than no university ever can.

Havuja perkele!

Espoo, July 1st, 2013

Marjo Kettunen

Contents

List of Publications

This thesis consists of an overview and of the following publications which are referred to in the text by their Roman numerals.
Note, Marjo Kettunen published previously under her maiden name Marjo Pääkkö

I Pääkkö Marjo, Ankerfors Mikael, Kosonen Harri, Nykänen Antti, Ahola Susanna, Österberg Monika, Ruokolainen Janne, Laine Janne, Larsson Per Tomas, Ikkala Olli, Lindström Tom, *Enzymatic hydrolysis combined with mechanical shearing and high-pressure homogenization for nanoscale cellulose fibrils and strong gels*, Biomacromolecules, 8, 1934-1941, May **2007**

II Pääkkö Marjo, Vapaavuori Jaana, Silvennoinen Riitta, Kosonen Harri, Ankerfors Mikael, Lindström Tom, Berglund Lars A., Ikkala Olli, *Long and entangled native cellulose I nanofibers allow flexible aerogels and hierarchically porous templates for functionalities*, Soft Matter, 4, 2492-2499, September **2008**.

III Kettunen Marjo, Silvennoinen Riitta, Houbenov Nikolay, Nykänen Antti, Ruokolainen Janne, Sainio Jani, Pore Viljami, Kemell Marianna, Ankerfors Mikael, Lindström Tom, Ritala Mikko, Ras Robin. H. A., Ikkala Olli, *Photoswitchable Superabsorbency Based on Nanocellulose Aerogels*, Advanced Functional Materials, 21, 510-517, February **2011**.

IV Jin Hua, Kettunen Marjo, Laiho Ari, Pynnönen Hanna, Paltakari Jouni, Marmur Abraham, Ikkala Olli, Ras Robin H.A., *Superhydrophobic and Superoleophobic Nanocellulose Aerogel Membranes as Bioinspired Cargo Carriers on Water and Oil*, Langmuir, 27, 1930-1934, January **2011**.

V Korhonen Juuso T., Kettunen Marjo, Ras Robin H. A., Ikkala Olli, *Hydrophobic Nanocellulose Aerogels as Floating, Sustainable, Reusable, and Recyclable Oil Absorbents*, ACS Applied Materials & Interfaces, 3, 1813-1816, May **2011**.

Other publications

In addition to the articles included in this thesis, the author has contributed to the following publications and patent:

Granström Mari, **Kettunen née Pääkkö** Marjo, Jin Hua, Kolehmainen Erkki, Kilpeläinen Ilkka, Ikkala Olli. Highly water repellent aerogels based on cellulose stearoyl esters, *Polymer Chemistry,* 2**,** 1789-1796, **2011**.

Jin Hua, **Pääkkö** Marjo, Ikkala Olli, Ras Robin H. A. Liquid-repellent material. Patent Application FI 20095752, PCT/FI2010/050575, July 2, **2009**.

Ikkala Olli, Ras Robin H. A., Houbenov Nikolay, Ruokolainen Janne, **Pääkkö** Marjo, Laine Janne, Leskelä Markku, Berglund Lars A., Lindström Tom, ten Brinke Gerrit, Iatrou Hermis, Hadjichristidis Nikos and Faul Charl F. J., Solid state nanofibers based on self-assemblies: from cleaving from self-assemblies to multilevel hierarchical constructs, *Faraday Discussions*, 143, 95-107, **2009**.

Koponen Hanna-Kaisa, Saarikoski Inka, Korhonen Tuulia, **Pääkkö** Marjo, Kuisma Risto, Pakkanen Tuula T., Suvanto Mika, Pakkanen Tapani A., Modification of cycloolefin copolymer and poly(vinyl chloride) surfaces by superimposition of nano- and microstructures, *Applied Surface Science*, 253, 5208-5213, **2007**.

Author's Contribution

Publication I: "Enzymatic hydrolysis combined with mechanical shearing and high-pressure homogenization for nanoscale cellulose fibrils and strong gels"

The author designed, performed, and analyzed the rheological characterization, which formed the central part of the hydrogel properties. The nanofibrillated cellulose (NFC) was received from Prof. Tom Lindström (KTH/Innventia AB). The microscopy and other experiments were done by co-authors. The author wrote the first version of the manuscript and actively participated in finishing the article. The author list is extensive, as this was the first common article in an extensive Nordic collaborative nanocellulose project.

Publication II: "Long and entangled native cellulose I nanofibers allow flexible aerogels and hierarchically porous templates for functionalities"

The author designed, implemented, and evaluated the aerogels with the help of undergraduate student Jaana Vapaavuori. The NFC was received from KTH. The author designed and implemented the electrical functionalization of the aerogels. The author analyzed all the results and wrote the first draft of the manuscript and actively participated to complete the final form.

Publication III: "Photoswitchable Superabsorbency Based on Nanocellulose Aerogels, Advanced Functional Materials"

The author designed, executed and analyzed the UV-switchable superabsorbent aerogels. The CVD was carried out by Riitta Silvennoinen and Marianna Kemell. The photocatalysis was carried out by Viljami Pore and evaluated by the author. The other analytical experiments and microscopy were performed by co-authors. The NFC was received from KTH. The author wrote the first draft of the manuscript and actively participated to complete the final form.

Publication IV: "Superhydrophobic and Superoleophobic Nanocellulose Aerogel Membranes as Bioinspired Cargo Carriers on Water and Oil"

The author performed the first working demonstration of the desired wetting functionality, and collaborated with Hua Jin in the aerogel preparation. The author actively participated in the writing of the manuscript.

Publication V: "Nanocellulose Aerogels as Floating, Sustainable, Reusable, and Recyclable Oil Absorbents"

The author designed and implemented the sample preparation and experiments together with Juuso Korhonen. The author actively contributed in writing of the manuscript.

Abbreviations and Symbols

2D	Two-dimensional
3D	Three-dimensional
AFM	Atomic force microscopy
Ani	Aniline
APS	Ammonium peroxydisulfate
BC	Bacterial cellulose
BET	Brunauer, Emmett and Teller
BJH	Barret–Joyner–Halenda
CA	Contact angle
CMC	Carboxymethylated cellulose
CNC	Cellulose nanocrystal
CSA	Camphorsulfonic acid
CVD	Chemical vapour deposition
DBSA	Dodecylbenzenesulfonic acid
DP	Degree of polymerization
EGU	Endoglucanase unit
$FeCl_3$-$6H_2O$	Iron(III) chloride, hexahydrate
FE-SEM	Field emission scanning electron microscopy
FTCS	(Tridecafluoro-1,1,2,2-tetrahydrooctyl)trichlorosilane
HCl	Hydrochloric acid
IL	Ionic liquid
MFC	Microfibrillated cellulose
MCC	Microcrystalline cellulose
MWCNT	Multiwalled carbon nanotube
N_2	Nitrogen
NaBr	Sodium bromide
NaClO	Sodium hypochlorite
$NaClO_2$	Sodium chlorite
NCA	Nanocellulose aerogel
NFC	Nanofibrillated cellulose
MB	Methylene blue
NMMO	N-methylmorpholine-N-oxide
NaOH	Sodium hydroxide
PANI	Polyaniline
PANI-T	Polyaniline-toluene
Py	Pyrrole
PPy	Polypyrrole
RH	Relative humidity
SEM	Scanning electron microscopy

SO_4-TW	Sulfate-functionalized tunicate whiskers
TEM	Transmission electron microscopy
TEMPO	2,2,6,6-tetramethylpiperidine-1-oxyl
TiO_2	Titanium dioxide
TW	Tunicate nanowhisker
UV	Ultraviolet
XPS	X-ray photoelectron spectroscopy

ϕ	Weight fraction
γ	Shear rate
η	Shear viscosity
ρ	Density
ρ_s	Skeletal density
E'	Elastic modulus
G'	Storage modulus
G''	Loss modulus
m	Mass
σ_{yield}	Yield stress
$\%\ w/w$	Mass concentration
ω	Angular frequency

1. Introduction

Nanocelluloses are increasingly considered as suitable building blocks for designing of functional materials, thanks to their nanosize dimensions and unique rod-like or fibrous structure.[1-7] Native cellulose possess hierarchical structure covering the molecular scale (1–100 Å), the nanoscale (10–100 nm) and finally the mesoscale (1–100 μm). Their properties are closely related to the quality of arrangement of their multiple scale structures, and plant cell wall materials can be regarded one of the prototypic hierarchically structured materials in nature. More generally, over the last few decades, the design and use of hierarchical structures have become a major topic in nanotechnology areas as diverse as physics, chemistry, material science, biology, medicine, electronics and engineering.[8] On the other hand, among the nanomaterials, responsive materials with reversibly switchable properties are of great importance due to their foreseen technical applications. External stimuli, such as light illumination, temperature, electrical potential, pH, and others can change the properties of stimuli-responsive materials, which result for example in the change of surface properties such as wetting.[8, 9]

The recent environmental and political requirements encourage researchers to find sustainable alternatives to replace the existing non-renewable sources in material development. Also in this context, cellulose is excellent candidate being renewable and the most abundant polymer on the earth, not to mention its nanoscale fibrils. Importantly, these fibrils have outstanding mechanical properties and numerous free reactive groups on the surface offering great opportunities for functionalization.

The fact that future success in novel materials development is based on the transition from resource-intensive bulk products to knowledge-based value-added products goes for cellulose industry as well. The traditional forest products such as paper, packaging and viscose products have their place, but cannot meet the demands of the modern society for high performance materials. The increase in potential utilization of the cellulose as a

nanomaterial could improve the competitiveness of forestry materials. (Fig. 1.1)

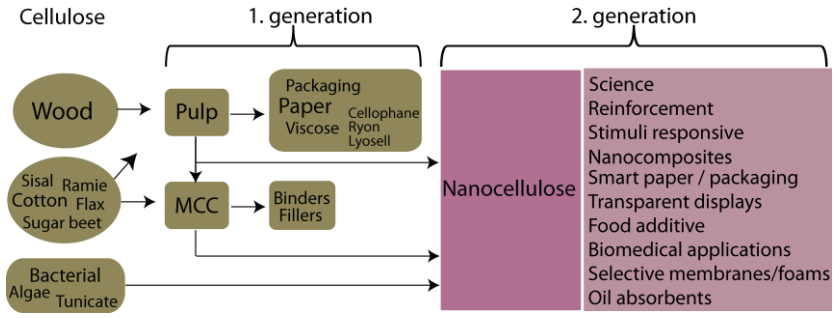

Figure 1.1. The traditional products (1. generation) of different cellulose sources and value-added and high performance nanocellulose based products (2. generation).

Native nanocellulose covers several types of materials involving the native crystalline structure, such as long and fibrous cellulose nanofibrils (also denoted as microfibrillated cellulose, MFC, or alternatively as nanofibrillated cellulose, NFC), rod-like cellulose nanocrystals (CNC), bacterial cellulose (BC) and tunicates, all having nanoscale lateral dimensions. The nomenclature will be discussed in more detail in next chapter. The state of the art in nanocellulose (fibrils and crystals) research has been summarized in several recent reviews, for example, Siró and Plackett 2010[6]; Eichhorn et al. 2011[1] and 2010[7]; Klemm et al. 2011[3]; Moon et al. 2011[2]; Lavoine et al. 2012[4] and Lin et al. 2012[10]. In the early 2000, the growing interest in nanotechnology resulted in a revival of MFC research pioneered by Turbak et al. and Herrick et al. in the 1980's, and many recent developments have prompted also industrial interest in cellulose nanofibrils. For instance DaiCel Chemical Industries (Japan), Innventia AB, UPM (Finland) and Stora Enso (Finland) built a pilot factory. In addition, Borregaard (Norway), J. Rettenmaier & Söhne (Germany), Oji Paper Company (Japan), Nippon Paper Group (Japan), and BASF (Germany) own patents and have started pilot projects and/or manufacture of cellulose nanofibrils. It is therefore reasonable to expect commercial nanocellulose products in near future. Within a few years the general interest in nanocellulose has increased tremendously, as has the number of research groups around the world that work with this material (illustrated by the growing number of relevant publications in Fig. 1.2.).

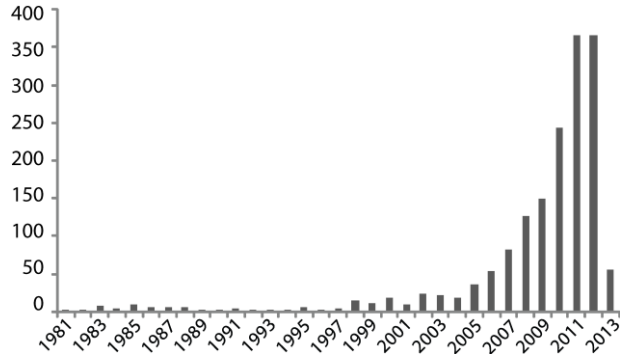

Figure 1.2. The number of publications released yearly in the field of nanocelluloses according to SciFinder(February 2013). Keywords used: microfibrillated cellulose, cellulose nanofibril, cellulose nanocrystal.

1.1 Outline of the Thesis

This thesis focuses in applying cellulose nanofibrils as building blocks for functional materials. The main advantages in applying cellulose nanofibrils are their mechanical strength and flexibility, ability to build hierarchically porosity, as well as the numerous free reactive hydroxyl groups on the surface that can be functionalized. The motivation for the present nanocellulose research was obvious both scientifically and industrially: when we started, only a few studies on the MFC/NFC existed and there was a need for new preparation methods and understanding how they behave. More importantly, novel value-added applications were considered to compensate the expected high production costs.

This thesis comprises six chapters as follows: Chapter 2 gives an introduction to the characteristics of the nanocelluloses, focusing on the NFC. Chapter 3 describes basics of aerogels and preparation methods used also in this work, including a brief review on state of art of cellulosic aerogels which are based on dissolved and regenerated cellulose. Chapter 4 contains simplified discussion on the photo-responsive wetting, influence of surface structure on the hydrophobicity, as well as examples of photocatalytic decomposition. The main results of this thesis are presented in Chapter 5, where the results are discussed in relation to the state of art. The strategy of the work is straightforward and presented schematically in Fig. 1.3. First, in Chapter 5.1, the characteristics of enzymatically and mechanically prepared cellulose nanofibrils are introduced. We demonstrate the creation of a strong inherent fibril network in the hydrogel by rheology (Publication **I**). Second, the behavior of these nanofibrils upon different drying conditions is investigated in Chapter 5.2. The first native nanocellulose aerogels with

tunable morphology, porosity and mechanical properties are shown, and they are applied as percolative template for a conducting material (Publication **II**). In Chapter 5.3, the versatility of the nanocellulose aerogel as a template is demonstrated by titanium dioxide coating: the UV-responsive superabsorbency and photocatalytic activity is shown (Publication III). Furthermore, the benefits of revealed multiple length scaled structures and porosity are discussed. In Chapter 5.4. the structure related superhydro- and oleophobicity of bio-inspired, fluorinated nanocellulose aerogel are discussed as a case study (Publication IV). Finally, the TiO_2 coating approach is extended in Chapter 5.5, where TiO_2 is employed to create selectively oil-absorbing nanocellulose aerogels for oil spill removal (Publication V).

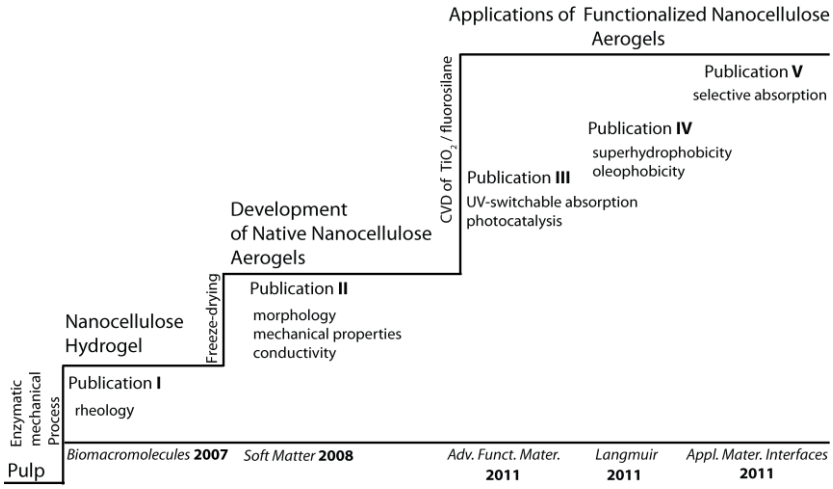

Figure 1.3. Schematic illustration of the structure of the research strategy and results presented in this thesis.

2. Cellulose: From Macroscopic Fibers to Nanocellulose

Cellulose is a homopolymer of β-1,4-linked anhydro-D-glucose rings in which every ring is rotated 180° with respect to each other.[11, 12] The repeat unit consists of two adjacent anhydroglucose rings and is known as cellobiose (Fig. 2.1.). In nature, cellulose chains have a degree of polymerization (DP) of approximately 10 000-15 000 glucopyranose units depending on the source.[12] However, the DP is greatly influenced by the source and the isolation treatment. For instance, the DP values of wood pulp vary typically from 300 to 1700. During the complex biosynthesis, cellulose chains arrange parallel-up and edge-to-edge, making flat sheets that are held together by van der Waals forces and an intra- and interchain hydrogen bond network.[13, 14] The intrachain hydrogen bonding between O3-H···O5 of the neighbouring molecules in the chain (Fig 2.1.) stabilizes the glucosidic linkages, resulting in a linear and rather stiff polymer structure. The interchain hydrogen bonds, i.e. hydrogen bonds between the adjacent chains within the sheets (Fig 2.1.), promote multiple chains to arrange into fibrils.[15, 16]

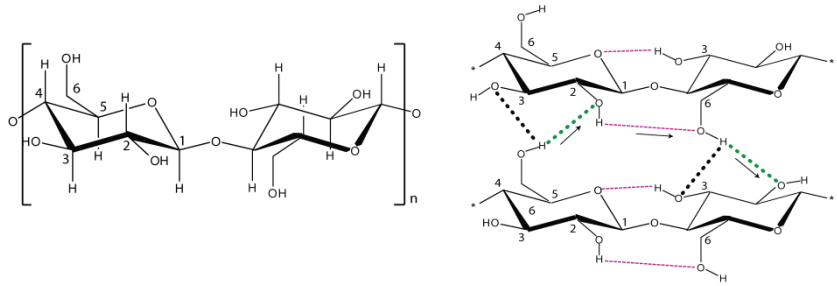

Figure 2.1. Molecular structure of cellobiose i.e. repeating unit of cellulose polymer and formation of the intrachain (red dashed line) and interchain (black and green dashed lines) hydrogen bonding. Note that, the O2 secondary alcohol and O6 hydroxymethyl groups are involved in both intrachain and interchain hydrogen bonds.[15]

Within these fibrils, cellulose chains are tightly packed together forming highly crystalline regions (crystallites), which are accompanied by disordered, amorphous-like regions, making cellulose semicrystalline. The cellulose

crystallites in the ordered regions exist in several polymorphs depending on the source, method of extraction, or treatment.[17] Cellulose I, so-called native cellulose, has two crystalline forms, Iα and Iβ that can coexist in various proportions.[18] Cellulose Iβ is dominant in plant cell wall cellulose and in tunicates. Cellulose II, i.e. regenerated cellulose crystal structure is formed by two processes, regeneration (solubilization and recrystallization) and mercerization, is the most stable structure with technical relevance (viscose products).[19, 20] The other polymorphs of cellulose, cellulose III and IV can be formed by ammonia and thermal treatments.[12]

Natural fibers are composite materials, resulting from the assembly of microfibrils and hemicellulose embedded in a matrix mainly composed of lignin.[21] For instance in wood cellulose, the polymer chains are packed into elementary fibrils with a lateral diameter of ~ 3-5 nm. They are further aggregated together with hemicellulose by hydrogen bonding to form what are classically known as microfibrils and their aggregates with a diameter of ~ 5 to 30 nm. The microfibrils are further packed into larger and larger aggregates finally forming macroscopic wood cellulose fibers (Fig.2.2.).

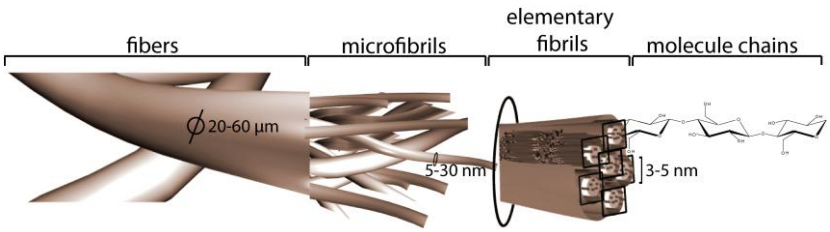

Figure 2.2. A simplified illustration of the morphological hierarchy in cellulose: the elementary fibrils contain both crystalline and amorphous regions.

What constitutes an elementary fibril and microfibril in terms of the number of chains and length and position of the disordered regions has been, and still is a subject of debate.[2, 5, 22, 23] In the end, it is the special hierarchical structure and the linear and symmetric packing of the chains that is stabilized by the strong intra- and interchain hydrogen bond network, which promotes the high axial stiffness and poor solubility of cellulose, as well as leads to the laborious delamination of the fibers to its nanoscale fibrils in MFC/NFC processes. However, upon cleaving and functionalization, the cellulose microfibrils have the ability to impart novel and significantly improved mechanical, optical, thermal, catalytic, filtration, biological, electrical, and magnetic properties. Therefore, the development and use of cellulose

nanofibrils with macroscopic fibers will increase the potential use of renewable materials. In the next sections, the basic principles to isolate the cellulose nanofibrils are discussed as well as their typical characteristics.

2.1 Preparation Methods Towards Cellulose Nanofibrils

First, a few words about the nomenclature of the different nanocellulose types for clarification: In this thesis, the terms nanofibrillated cellulose (NFC) and/or cellulose nanofibrils are used for describing the fibrous cellulose microfibrils. Currently, terms NFC and cellulose nanofibril are more and more commonly used instead of classical microfibril and MFC as they describe better the nanoscale nature of the individual fibrils. Indeed, here we distinguished NFC from traditional MFC not only to emphasize the size but also that a pre-treatment is applied in the fibrillation process, which enables the nanoscale and more individual fibrils as the aggregation is reduced. The term cellulose nanocrystal (CNC) is used for the rod-like cellulose crystals and tunicate nanowhiskers. Note that, the microcrystalline cellulose (MCC) is composed of aggregated bundles of multiple sized hydrolyzed cellulose microfibrils that are strongly hydrogen bonded to each other and have high crystallinity. The particles are typically 10-50 μm in diameter and they can be deagglomerated into smaller, 1-10 μm, sized particles prior to use.[2] MCC is commercial product and it is typically used in pharmaceutical applications and food industry, as well as source for CNC.

As cellulose microfibrils e.g. in wood fibers are composed of two regions, highly ordered chain packings i.e. *crystalline* regions and disordered *amorphous* regions, two main types of nanocellulose can be isolated: (i) cellulose nanocrystals and (ii) cellulose microfibrils (NFC/MFC) containing both regions.[24] The routes to different types are schematically presented in Fig. 2.3. in simplified terms. This thesis will cover only the type (ii), however, to put the topic and the results of this thesis in context, e.g. the rheological properties of CNC are discussed.

The typical procedures to prepare the rod-like CNC consist of subjecting e.g. pulp to strong acid hydrolysis under controlled temperature, agitation, and time, followed by sonication to separate crystals.[25] Sulfuric and hydrochloric acids have been extensively used, but phosphoric and hydrobromic acids have also been reported.[25] The origin of the cellulosic material demands which of the specific hydrolysis and separation protocols are used. In addition, the geometrical dimensions (length and width) as well as the morphology of the forming CNCs are found to vary widely depending on the source of the cellulosic material, and the conditions under which the hydrolysis is performed.[26] The self-assembly and chiral nematic nature of the

CNC,[27-29] as well as the their chemical modification, surface polymerization, and production of thin films, and finally applications in nanocomposites are have recently been reviewed.[1, 7, 10, 30]

Fibrous, long and entangled cellulose microfibrils, on the other hand, are isolated using different mechanical treatments, which most often involve a refining step followed by a high-pressure homogenization stage[31-34] although grinding[35-38] and cryocrushing[39] have also been reported.[4, 6] The resulting material is called microfibrillated cellulose and consisting of moderately degraded long fibrils that have greatly expanded surface area.[4, 40] Typically, traditional MFC consists of cellulose microfibril aggregates with a diameter ranging from 20 to even 100 nm with and length of several micrometers, rather than single nanoscale microfibrils. MFC can be manufactured from numerous different cellulosic sources. However, wood is obviously the most important industrial source, and thus it is also the main raw material to produce MFC.[4, 6] Bleached kraft pulp and sulphite pulp are frequently used as a starting material for MFC production. To prepare MFC, a pulp suspension is typically passed repeatedly through a mechanical homogenizer to increase the degree of fibrillation; inevitably, the energy consumption increases with the number of passes.[32, 41] Besides, these methods tend either to damage the microfibril structure by reducing the degree of crystallinity, and DP up to 27 %, or fail to sufficiently disintegrate the pulp fiber.[32, 41] Typical energy consumption reaches levels of approximately 27,000 kWh/tonne for homogenization and even higher values reaching up to 70,000 kWh/tonne have been reported.[42] In order to decrease the high energy consumption associated with these processes, and to isolate individual fibrils from the fibril aggregates, chemical[43-46] and enzymatic[40, 41, 47, 48] pre-treatments of the cellulose raw material have been developed. When the pre-treatments are applied, MFC is denoted more frequently NFC as it consists of nanoscale individual fibrils.

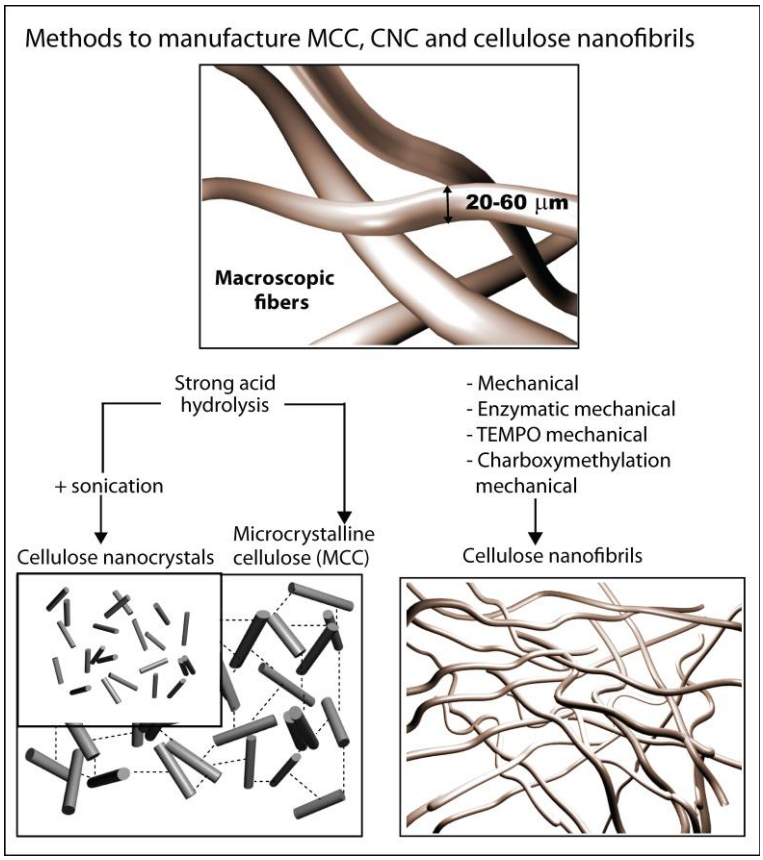

Figure 2.3. Preparation routes for MCC, CNC and cellulose nanofibrils (NFC/MFC).

Oxidation pre-treatment

Recently, Saito et al. introduced TEMPO-mediated oxidation as a pre-treatment for nanocellulose production.[49] In this procedure, cellulose fiber suspension is oxidized by 2,2,6,6-tetramethylpiperidine-1-oxyl radical (TEMPO) with NaClO as a primary oxidant and NaBr as an additional catalyst, at pH of 10-11.[44] Thereby, charged carboxylate groups are introduced on the surface of the fibers, as the C6 primary hydroxyl groups of cellulose (see Fig. 2.1.) are selectively converted to carboxylate groups via C6 aldehyde groups. As a result, the nanofibrils within the fibers separate from each other easier, as the electrostatic repulsion among the ionized carboxylates holds the hydrogen bonding between the fibrils. When the carboxylate contents reach approximately 1.5 mmol/g, the oxidized cellulose slurries are mostly converted to transparent, highly viscous dispersions with nanofibrils of 3-4 nm in width and a few microns in length.[44] Afterwards, they have developed the oxidation pre-treatment procedures that work at neutral or slightly acidic conditions, utilizing TEMPO/NaClO/$NaClO_2$ system.[50] Thus, the undesirable

side reactions such as depolymerization and discoloration, taking place under alkaline conditions, are avoided.[50] Consequently, aldehyde-free nanofibrils with uniform fibril distribution can be achieved, almost completely maintaining of the original DP.[50] The TEMPO oxidation pre-treatments are typically followed by mechanical treatment with a double-cylinder type homogenizer or sonication. The reported energy consumption for TEMPO mediated fibrillation process is ~ 7 MJ/kg i.e. ~ 2000 kWh/tonne.[45] This brings great potential in saving energy over the traditional processes.

Enzymatic pre-treatment

To weaken the fiber cell walls in the MFC fibrillation process, also enzymes can be utilized. Endocluganases, which are able to attack only in the amorphous, disordered regions, have been frequently applied.[40, 41, 48, 51] Typically, enzymatic pre-treatment combines a refining step prior the enzyme treatment as it swells the fiber walls, enabling the enzymes to penetrate into them, and potentially also to create damaged zones in the crystalline regions. This increases the number of possible attack points for the enzymes. It should be recalled that endoglucanases, used also in the present study, do not significantly degrade the DP of the cellulose, which in turn has an important impact on the mechanical properties of the end materials.[41] Henriksson et al. showed, that DP of dissolving sulfite pulp decrease from 1200 to only 910 due to the enzymatic treatment with enzyme concentration of 0.02 %.[41] Enzymatic pre-treatment is typically followed by homogenization, which liberates the cellulose nanofibrils from the fiber wall fragments. This is showed to lower DP and consequently has an effect on the mechanical properties.[41, 51] Henriksson et al. reported further the decrease in DP value from 910 to 740 as a consequence of the 12 passes through homogenizer.[41] The enzyme dosage should be low not only from the material property point of view, but also due to processing, as too high dosage cause severe clogging during homogenization.[42] According to calculations, the energy consumption for enzymatically hydrolyzed and homogenized cellulose nanofibrils is ~ 2300 kWh/tonne, including two refining steps and 8 passes (3 passes through the large chambers and 5 passes through the small chambers).[42] As the energy consumption was 27,000 kWh/tonne without pre-treatments, the reduction achieved is 91%.[42] However, it was later found that one cycle through the homogenizer was sufficient, and recent results have indicated that the energy consumption can be lowered further to be ~ 1800 kWh/tonne.[42]

Figure 2.4. Enzymatically and mechanically prepared 2% (w/w) aqueous gel of NFC (Innventia AB, Sweden)

Carboxymethylation

Another chemical pre-treatment for producing cellulose nanofibrils is carboxymethylation.[46] The goal is similar to TEMPO oxidation: introduce anionic charges on the fibril surface to increase the electrostatic repulsion between the fibrils, and thus facilitate the fibrillation. Wågberg et al. reported carboxylate content of ~ 0.5 mmol/g to isolate individual fibrils of 5 - 15 nm in width.[46] The procedure involves the solvent exchange from water to ethanol, impregnation of monochloroacetic acid by adding of NaOH in the mixture of methanol and isopropanol.[46] After carboxymethylation, the fibers are filtered and washed. Finally, the fibers are homogenized using a high-pressure fluidizer to liberate the fibrils.[46]

The main drawback of the above described method is the use of organic solvents, whereas for environmental reasons water-based processes are preferred.[42] Despite that the carboxymethylation is a commercial process, it can be considered fairly complex because several solvents must be handled.[42] However, Ankerfors made energy consumption calculations also for carboxymethylation process.[42] As only one pass through the homogenizer is needed, the mechanical energy consumption is thereby ~ 2200 kWh/tonne for 2 % w/w suspension.[42] Furthermore, the recent developments indicate that if carboxymethylation is used, NFC can be produced at higher concentration of ~ 8 % w/w, which gives a mechanical energy consumption only of 555 kWh/tonne (a 98% reduction).[42] This estimate is, though, preliminary and not yet takes all factors, such as the pump efficiency and pre-heating into account. According to developers, the energy consumption calculations could be further improved e.g. by considering the flow profiles, friction losses and viscosity changes in the suspension.[42]

The pre-treatment assisted MFC production is still under development. Despite the achievements to lower the energy consumption, the overall production costs are still rather high. The shipping and storage of a cellulose product with 2-8 % solid content is uneconomical. New approaches need to be considered, and novel value-added products to be developed to ensure the commercial success of nanofibrillated cellulose.

Bacterial cellulose

Bacterial cellulose networks differ significantly from NFC networks in that they consist of fully jointed fibril network of pure native cellulose, formed during cultivation. Under special culturing conditions the bacteria secrete a thick gel, called pellicle, that is composed of nanoscale cellulose microfibrils and 97% water.[52, 53] The most studied species of bacteria that produces cellulose is generally called Gluconacetobacter xylinus (reclassified from Acetobacter xylinum).

2.2 Structural, Rheological and Mechanical Properties of Cellulose Nanofibrils

The characteristics such as morphology, DP, dimensions (length and width), surface charge, rheological behavior and mechanical properties of nanocelluloses are greatly influenced not only by the processing method but also by the source of cellulose.[2, 4, 6] As there are a wide range of sources such as, wood pulp and plant fibers e.g. cotton, ramie, sisal, flax, sugar beet pulp, as well as tunicate, algae and bacteria, there are also numerous different nanocellulose materials with different properties.[2] Indeed, fibers show e.g. different initial fiber lengths and amounts of residual lignin and hemicellulose. The bacterial cellulose pellicle, on the other hand, consists of network of pure cellulose with extremely fine and interconnected, continuous and dimensionally uniform ribbon- like elements.[52] Therefore, a careful attention for the source and the processes is needed for comparison of the properties of the nanocelluloses.

The most typical sources for nanocellulose, MCC, wood pulp and BC as well as the different type of nanocelluloses, made via acid hydrolysis, TEMPO-oxidation, mechanical homogenization and carboxymethylation, are presented in Fig. 2.5. Even if CNCs are excluded in this thesis, it is important to show the morphological and dimensional differences between CNC and NFC/MFC as they further influence on e.g. rheological and mechanical properties. The dimensional and morphological characteristics of cellulose nanofibrils are generally investigated by electron microscopy, such scanning electron microscopy (SEM) and transmission electron microscopy (TEM).

While direct mechanical disintegration of wood pulp fibers typically produces aggregated fibrils with 20-100 nm in width, additional chemical and enzymatical pre-treatments result in fibrils with a width of ~ 5 nm and their aggregates of ~ 10 - 30 and nm as characterized by TEM and SEM.[37, 40, 44] The cross-section of bacterial cellulose ribbon fibril is ~ 6-20 nm in width.[52] The evaluation of the fibril length by microscopy is qualitative as the long fibrils are entangled and consist of junction points and kinks. On the other hand, the use of TEM or atomic force microscopy (AFM) for analyzing the dimensions of CNC is straightforward due to the rod-like character.[7, 26] However, fibrils can be several micrometer in length, and show generally higher aspect ratio than typical CNCs.[4, 45]

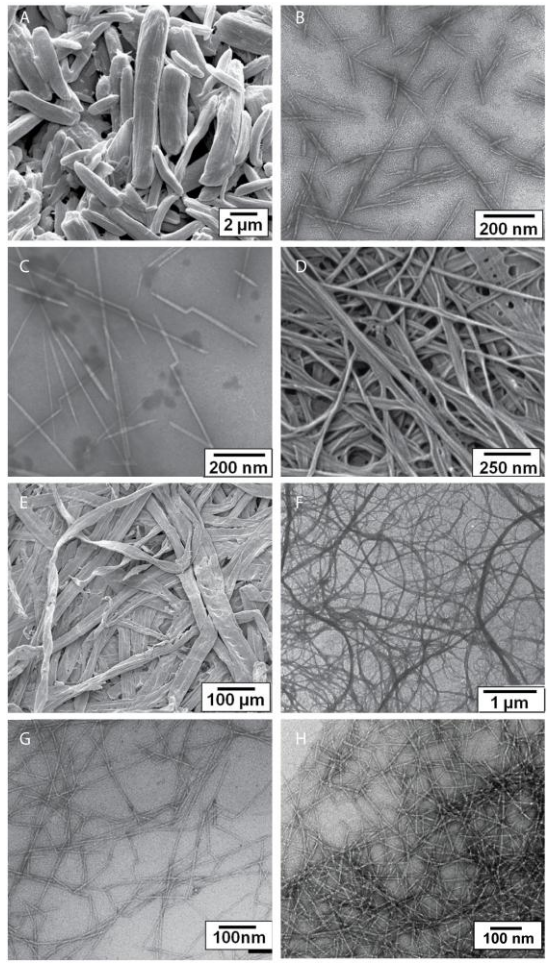

Figure 2.5. A) MCC from cotton[2] B) CNC via acid hydrolysis from wood[2], C) TWs[2] D) BC[54], E) wood pulp[2], F) mechanically homogenized MFC from sugar beet pulp[55] G) TEMPO-oxidized NFC from wood pulp[44], H) carboxymethylated NFC from wood pulp.[46] Image is adapted and reproduced from Moon et al. Chem Soc Rev. 2011 with the permission of RSC.

Nanocelluloses are typically produced to water dispersions in which they tend to aggregate and/or percolate to form networks depending on the surface charge[56] and concentration[56-59]. Rheology is a practical tool to investigate the aqueous suspension properties such as viscosity, elasticity, flow and alignment.[60] For instance, the storage modulus, *G'*, and loss modulus, *G"* express whether the system is an elastic gel or a viscous dispersion when measured as a function of the oscillation frequency ω. In addition, *G'* and *G"* also determine the rigidity of the gel. The early rheology studies of CNC and nanofibrils focused on shear viscosity. The flow and aligning behaviour of the crystals were investigated due to their liquid cristallinity,[61, 62] while shear thinning of MFC was important in both processability and applicability.[31, 32, 57] Shear viscosity experiments have confirmed the pseudoplastic behavior of nanocellulose suspensions. Indeed, CNC and fibrils showed a large decrease in viscosity with increasing shear rate, i.e. shear thinning.[56, 58, 61-66] In addition to shear thinning, Bercea et al. demonstrated further the flow orientation for tunicate nanowhiskers at large concentration range, as presented in Fig.2.6. [61]

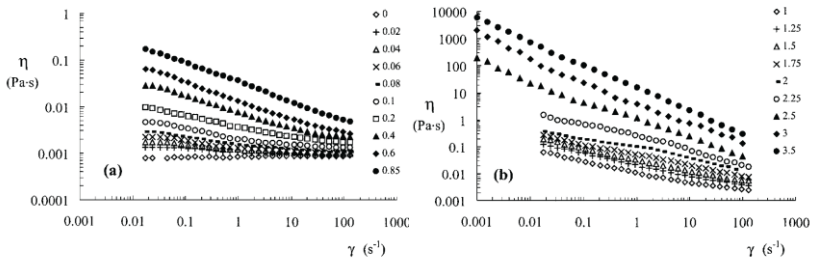

Figure 2.6. Shear thinning, i.e. decrease in viscosity with increasing shear rate, of CNC with different concentrations.[61] With permission from Langmuir © 2007 American Chemical Society**.**

Interestingly, Araki et al. showed that HCl treated CNCs form loose bulky aggregates, and show more complicated viscosity behaviour due to flocculation, induced by the lack of electrostatic repulsion.[56] On the other hand, H_2SO_4-treated suspension showed only a weak shear-rate dependence in viscosity, due to the possible flow induced orientation of the more charged rod-like particles.[56] H_2SO_4 treated CNCs with high surface charge showed also lower initial shear viscosity of 10^{-3} Pa, while that of HCl treated CNCs was 10^{-2} Pa. As both CNCs show similar length (<200 nm) and morphology, the differences in the initial viscosities at the same concentrations result from different distribution of the crystals in the suspension.[56] Accordingly, HCl treated CNCs form to loose flocs, which give rise to higher initial viscosity, while H_2SO_4 treated short crystals are dispersed and stabilized via

electrostatic repulsion suppressing the tendency for percolation, resulting in low initial viscosity.

The more recent rheology studies of cellulose nanofibrils concentrate more on moduli, i.e. elasticity/rigidity of the network. This is obvious as the high aspect ratio fibrils are entangled and form networks even with very low concentrations compared to CNCs. However, already the early rheology results suggested the applicability of fibrils and crystals as general thickeners in food, cosmetic, pharmaceutical and industrial products. [31,32,56]

The background for mechanical properties of the cellulose nanofibrils is briefly discussed next. A Young's modulus of a single native cellulose nanofibril has been estimated using two methods. An atomic force microscopy tip bending method yielded a value of 78 ± 17 GPa for BC,[67] while 114 GPa was suggested based on Raman spectroscopy.[68] The latter value is closer to a generally accepted value of 138 GPa for the crystal modulus of cellulose I, as suggested using an X-ray diffraction method.[69] Note that, highly crystalline plant derived CNCs and tunicate cellulose nanowhiskers, on the other hand, showed Young's modulus from 50 to 143 GPa when Raman spectroscopy was applied,[70, 71] and 145-150 GPa when AFM bending tests were utilized.[72]

Turning now to the Young's modulus of the fibrils in the networks. The effective moduli of single fibrils within NFC and BC networks are much lower than the generally accepted experimental value for the crystal modulus of cellulose I crystal structure, 138 GPa.[69] The moduli of cellulose nanofibril networks have been reported to be about 15 GPa, due to the lack of the alignment and reduced crystallinity.[6, 73] Aulin et al. used dynamic mechanical analysis (DMA) and model to predict the amorphous modulus of cellulose was utilized, values of 30 GPa for carboxymethylated NFC films have been reported.[74] Humidity scans in DMA showed how the modulus of a NFC film decreased from 30 to 19 GPa with increasing RH from 5 to 90%. Water in the amorphous regions is suggested to act as a plasticizer, reducing the intermolecular interactions between the NFC fibrils, and thus also the stiffness of the material.[74] Also the elastic component plays important role, as the mechanical behaviour of the films, is determined by the overall degree of crystallinity of the fibrils.[74]

Very recently, Tanpichai et al. applied Raman spectroscopy to study the Young's modulus of fibrous networks of BC and NFC.[73] They showed that Raman spectroscopy is a valuable tool as it records molecular deformation of both crystalline and amorphous regions that lie in the NFC material.[73] Thus, it enables some averaging of the stiffness recorded and results in a reduced value.[73] The Young's moduli of the BC networks ranged from 79 to 88 GPa, and that of enzymatically pre-treated and the carboxymethylated NFC fibril networks from 29 to 36 GPa.[73] The difference in the moduli between BC and

NFC is most likely due to the lower degree of crystallinity of NFC.[73] When the crystallinity is also taken into account, the moduli for enzymatically pre-treated and carboxymethylated randomly orientated NFC fibrils in the film are around 30 GPa.[73, 74] It is worth to mention, that although NFC fibrils themselves may have low modulus , the high bonding of the nanoscale entangled fibrils can contribute appreciably to the strength and modulus of the whole network. The effect of the fiber-fiber bonding on the overall strength of paper was early suggested by Page.[75] The contribution of bonding depends on the relative bonded area and efficiency of the interfacial fiber-fiber area to transfer load.[75] Thus, the overall load transfer efficiency of paper depends not only the inherent fiber strength, but also the number of fiber-fiber bonding and the nature of those interactions.[75] Accordingly, the very high fibril-fibril bonding in NFC network may contribute substantially to the overall modulus of the nanofibril networks in the film. Furthermore, the control of the fibril orientation in the network plays a role in mechanical properties. In the end, the potential applications for the mechanically high-performance nanofibrils are e.g. various nanocomposites[6, 7, 76] flexible electronics devices[77], wet-extruded multifunctional fibers[78, 79] and biomimetic materials[80, 81]

3. Aerogels

Aerogels have been pursued extensively towards highly porous and lightweight solid materials ever since introduced by Kistler in the 1930's.[82] An aerogel is a porous nanostructure containing ~ 90–99% air by its volume.[83] Aerogels are typically prepared from solvent swollen gels, i.e. percolative networks within a solvent medium. It is essential to avoid the collapse and shrinkage of the network upon solvent removal, as illustrated in Fig. 3.1. Drying process removes the liquid and leaves behind a network structure. This kind of delicate structure is responsible for the lowest known density, refraction index, thermal, electrical, and acoustical conductivities of any solid material.[83] As their porosities, densities and specific surface areas vary greatly depending on starting material, they have a variety of applications, such as thermal and acoustic insulation, catalysis, and templation. Most applications deal with inorganic silica aerogels,[83] but various types of organic aerogels[84-87] have also been reported, including carbon nanotube aerogels[88, 89] and cellulose derivative aerogels that can also be pyrolyzed into carbon aerogels[90-93]

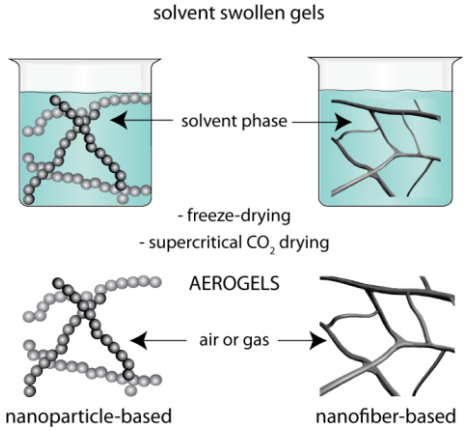

Figure 3.1. Schemes for aerogel process from wet gels to aerogels. For instance, silica aerogels and regenerated cellulose aerogels pearl-necklace morphology (left) while native nanocellulose aerogel show fibrous morphology (right).

Classically, the term “aerogels” was used to designate gels dried under supercritical conditions.[83] Supercritical drying prevents the formation a liquid-vapor meniscus during the drying. The meniscus is formed as a capillary pressure gradient is built in the pore walls due to the surface tension of the liquid. The formation of the menisci would lead to collapse most of the pore volume. However, from a practical point of view, supercritical drying is laborious and expensive.

As an alternative, freeze-drying[94-96] where the solvent in the wet gel is first frozen and then sublimated without entering the liquid state has been used. Therefore, the formation of a liquid-vapor meniscus is prevented or at least diminished. The surface area and mesopore volume of the freeze-dried aerogels tend to be slightly smaller than in supercritically dried aerogels. The gel network structure may eventually be affected by the nucleation and growth of solvent crystals, which tend to generate very large pores.[83] Indeed, ice crystals nucleate in the water or in other solvent, and grow in the same direction as the temperature gradient.[97] Consequently, solid material is entrapped between ice crystals. Homogeneous and unidirectional freeze casting, followed by the homogenous growth of ice crystals, results in ordered porous foam with unidirectional channel structures such as lamellar or cellular (honeycomb) structures.[97-99] Thus, by controlling and changing the location of the nucleation and the freezing temperature (rate), it is possible to control and tune the microstructure of the aerogels and foams.[97]

Despite all the advantages and delicate properties stated before, aerogels generally suffer from their brittleness. To overcome this problem and widen further their scope of applications, native cellulose has recently proven to be particularly useful source for aerogels and foams. Due to the biocompatibility and biodegradability, cellulose based aerogels open doors to application fields such as medical, cosmetic and pharmaceutical applications.

3.1 Cellulosic Aerogels

This chapter gives a brief review on the state of art of cellulosic aerogels, in which either cellulose derivatives[93, 100-103] or dissolved and regenerated celluloses[104-122] are applied. As the Publication **II**[123] was the first report on native nanocellulose aerogels, they will be introduced in chapter 5 (Results and Discussion). By contrast to native cellulose nanofibrils utilized in the present work, cellulosic aerogels exhibit cellulose II crystal structure, and preparation procedure involves several steps including dissolving, possible cross-linking, regeneration and typically supercritical drying. The cellulosic aerogels are greatly influenced by the source, solvent, regeneration bath, temperature, and drying method. Hence, the properties such as morphology,

porosity, surface area and mechanical properties may differ significantly even if the density of the aerogel would be the same. In most cellulosic aerogels, supercritical drying is required. Tan et al. demonstrated 2001 the first chemically cross-linked cellulose acetate butyrate derivatized aerogels showing very high surface areas up to 389 $m^2 g^{-1}$.[100] Fisher et al. investigated the influence of cross-linker content and cellulose DP and concentration, on formation of cellulose acetate aerogels reaching surface area of 250 $m^2 g^{-1}$.[101] Such high values can be explained by the morphologies and processing. The aerogels based on cellulose derivatives typically consist of cross-linked colloidal particles, which form pearl-necklace structures as seen in Fig. 3.1. However, the pearl-necklace structure of densely cross-linked colloidal particles causes also a large shrinkage, which in turn lowers the porosity to 41-82%.[101] Not surprisingly, such aerogels typically suffer from a fairly high density of 0.15–0.85 g cm^{-3}. Thereafter, cellulose derivative aerogels have been investigated to load silver nanoparticles in a controlled manner,[102] for energy applications[93], as well as for cell scaffolding and bone crafting[103] and an adsorbent for the selective capture of carbon dioxide from air[124].

A more fibrous aerogel structure can be obtained when MCC is dissolved followed by regeneration and drying.[104] Jin et al. reported highly porous cellulosic aerogels, which show order of magnitude lower density compared with cellulose derivative aerogels by dissolving cellulose in calcium thiocyanate solution followed by regeneration and freeze-drying.[104] The effects of the density and freeze-drying rate for 1 mm thick cellulose II aerogels were investigated, and the increase in the surface area from 70 to 120 $m^2 g^{-1}$ by increasing the density from 0.5 to 3 %w/w was shown. It was further demonstrated that, the lower the density, the bigger the pores were, and fibrils were pushed into film-like structures lowering the resulting surface area. If the density of the fibrils was increased, the growth of ice crystals was hindered and fibril aggregation was reduced, and thus resulting in finer fibrous structure and higher surface area.[104] To achieve higher surface areas, they use solvent exchange to tert-butanol prior the drying. Thereby, specific surface areas increased to 160–190 $m^2 g^{-1}$, depending on the density. Interestingly, Hoepfner et al. applied later the same dissolution route to show the effect of supercritical drying on the structure. By supercritical drying, the density of the aerogel was able to decrease down to 0.01 g cm^{-3}, and surface areas increased up to 250 $m^2 g^{-1}$.[105]

On the other hand, Innerlohinger et al.[106] and Liebner et al.[107, 110] performed comprehensive investigations regarding cellulosic aerogels utilizing NMMO as solvent and supercritical drying. As an alternative to NMMO, Gavillon and Budtova introduced cold aqueous NaOH for the dissolution, and produced similar types of aerogels by supercritical drying.[109] The combinations of NaOH and urea or LiOH and urea as solvent was tested by Cai et al., where

cellulose fibrils were regenerated from aqueous acid or methanol or ethanol.[111] Thereby, fibrous aerogels from cotton pulp with astonishingly high surface areas up to 485 m^2 g^{-1} were achieved by applying freeze or supercritical drying.[111] Note that the above-described cellulose II aerogel developments were under investigation at the same time as the first native nanocellulose aerogel development work presented in this thesis. Later, it was shown that the high surface area cellulosic aerogels can act as support medium for silver, gold, and platinum nanoparticles.[112] The nanoparticles dispersed and stabilized well due to the nanocellulosic network, and the yield and the size of the metal nanoparticles could be controlled through concentration, temperature, and the duration of reaction.[112] Very recently, also various aerogels utilizing LiCl/DMSO solvent path[113] and cellulosic-silica nanocomposite aerogels by in-situ formation of silica in the cellulosic gel were shown.[114] Similar NaOH/urea and LiOH/urea solution systems and freeze-drying were utilized for graphene-oxide modified cellulosic aerogels[115] and magnetic cellulosic composite aerogels[116].

Ionic liquids (ILs) have also attracted much interest recently as alternative benign solvents for cellulose,[125] also enabling aerogel production.[117-122] Cellulosic aerogels made from MCC dissolved in IL result in more globular morphology,[119] while wood based aerogels show more fibrous morphology. On the other hand, morphology also depends on the regeneration conditions, and direct conclusions are difficult to make. However, Li et al. showed that if wood flour is used as a source, aerogels cannot be prepared without a prior freeze-thaw process even when supercritical drying was utilized, but they collapsed.[120] Granström et al. showed IL route for porous cellulosic aerogels with dual length scale structures to achieve high water repellence based on stearoyl esters.[121]

While aerogels based on cellulose derivatives involve crosslinking, aerogels made from regenerated cellulose are typically based on the hydrogen bonds as physical crosslinks. Unfortunately, such aerogels generally suffer from brittleness. Depending on the source, solvent and concentration, elastic moduli are in a range of 0.6 - 85 MPa.[110, 115, 116, 119] For instance, supercritically dried sulphite pulp based aerogel with a density of 0.06 g cm^{-3} (3% in NMMO solution) showed a modulus of 9 MPa.[110] If cotton fibers where used, higher concentration of 5 and 10 % was required for gelation in LiOH/urea[116], and NaOH/urea[115] solutions. Accordingly, the resulted higher density of 0.2 g cm^{-3} leads higher moduli of 85 MPa and 35 MPa, respectively. There seems to be a contradiction, however, as the 5% solution results higher moduli than 10% solution and it is well know that the modulus correlate with density. On the other hand, the density and the morphology of the 10 % aerogel based on NaOH/urea solvent system were not reported.

The development of the cellulosic aerogels is still in progress. So far the focus has been in the process and source related issues and demonstrating the morphological variety arising from different solvents and regeneration, while practical applications have still played a minor role. The cellulosic aerogels show typically very high surface areas and uniform pore structure, and thus are interesting candidate for a sustainable substrate and template.

4. Responsive Materials

One of the main advantages in applying cellulose nanofibrils is the great number of reactive hydroxyl groups on the surface that can be functionalized. On the other hand, in many applications the functionalization is, in fact required, because the numerous hydroxyl groups give arise to also unwanted phenomena like aggregation of the fibrils and high excessive hygroscopicity. Generally, surface functionalization can be categorized into three groups: First, functionalization via synthesis i.e. modification of the fibril surface as a facilitating their extraction. Carboxymethylation, TEMPO-oxidation, and sulphuric acid degradation for CNC are included in this group. The main purpose is to introduce negative or positive charges on the surface of the fibrils to obtain better dispersion and/or to help in the delamination of the fibers. The second is adsorption of surfactants or polyelectrolytes for better dispersibility, dry and wet strength, as well as antistatic purposes. Third, chemical modification via covalent attachments of molecules or polymers utilizing e.g. esterification (acetylation), silylation, or "grafting-onto" and "grafting-from" methods. Thereby, properties such as mechanical, thermal, optical as well as humidity and gas barrier properties, of the fibrils can be enhanced and controlled.[2-4, 6] Functionalization also serves as a valuable tool to tailor the self-assembly of the nanocellulose.[1, 126, 127]

The functionalized NFC and CNC films with e.g. tuned thermal, optical and barrier properties as well as the nanocellulose based composite films have been reviewed e.g. by Lin et al.[10], Eichhorn et al.[1, 7], Lavoinne et al.[4], Moon et al.[2], and by Siró et al.[6] and will not be discussed further in this thesis. On the other hand, nanocellulose aerogels own various properties that can be benefited upon functionalization in versatile applications. Some practical functionalities such as conductivity, absorption, hydrophobicity, and photocatalytic activity combined with nanocellulose architecture will be discussed next in more detail.

4.1 Conductive Nanocellulose Materials

Conducting polymer composites with cellulose have received growing interest in recent years for applications such as batteries, sensors, antistatic coating, corrosion protection, and electrical devices to be employed in several fields including biology, medicine, agriculture, etc.[128] Cellulose nanofibrils can serve a dual purpose in the conducting polymer composites by mechanically reinforcing the brittle conductive polymers and providing a continuous 3D scaffold beneficial for conductivity.[129]

Among conducting polymers, polyaniline (PANI) is one of the most promising material because of its facile synthesis, good environmental stability, simple doping/dedoping chemistry, and controllable electrical conductivity. PANI is also one of the few conjugated polymers that is commercially available and therefore relevant for applications e.g. to enable electrical conducting coatings and composites.[130] The undoped emeraldine base form of PANI consists of benzene diamine and quinode diimine moieties. The latter ones can be doped with sufficiently strong acids to achieve a conducting emeraldine salt.[130, 131] Due to the rigidity, stacking, and mutual hydrogen bonds, emeraldine salts are generally not soluble in common solvents, unless the dopant acids are functionalized to incorporate spacers or surface active groups to limit mutual aggregation and to improve solubility.[131] The dopants, which can be also called counter-ions, may also modify the polymer or the polymer solution in other ways beyond the change in conductivity. These kinds of counter-ions are frequently called functional dopants. The effect of functionalised solubilising dopants is based on acid with *e.g.* a long alkyl tail that is compatible with nonpolar solvents, thus making the whole complex soluble in them. One of the first examples of functional dopants was dodecylbenzenesulfonic acid (DBSA) (see Fig. 4.1.).[131, 132]

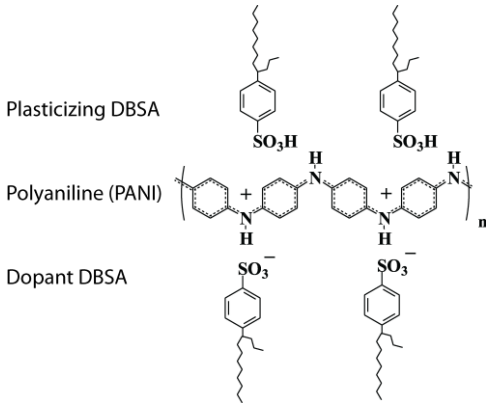

Figure 4.1. The structure of PANI(DBSA)1.0. Here branched, soft type DBSA is presented.

Even if the polyaniline chemistry is beyond the topic of this thesis, it is worth to mention, that the discovery of dopant-induced processability was an important step in conducting polymer, including polyaniline, research. Heeger, MacDiarmid, and Shirakawa were awarded a Nobel Prize in Chemistry in 2000 for the discovery and development of conductive polymers. Doping can increase the conductivity of conjugated polymers to high levels up to 1-10^4 S cm^{-1} range.

In a context of nanocelluloses, the state of art of the conducting nanocellulose composites based on BC, nanowhiskers and NFC, are briefly reviewed next. Yoon et al. demonstrated the first conducting nanocellulose films based on incorporation of multiwalled carbon nanotubes (MWCNT) into bacterial cellulose pellicles.[133] The electrical conductivity of the films ranged from 2.0x 10^{-2} to 1.4x10^{-1} S cm^{-1} with concentration of MWCNTs from 3.2 to 9.6 % w/w, which in turn depend on the immersion time and the initial concentration of MWCNTs in the dispersion.[133]

van den Berg et al. applied another type of nanocellulose, negatively charged tunicate whiskers, and adsorbed positively charged PANI doped with camphorsulphonic acid (CSA) in formic acid onto them.[134] They demonstrated PANI–CSA/SO_4-TW nanocomposites with good film-forming ability and high stiffness. Along with the Young's modulus, the electrical conductivity was increased with the nanowhisker content from 1.3 x 10^{-2} S cm^{-1} (at a whisker content of 66.7% w/w) to reach a maximum of 5 x 10^{-2} S cm^{-1} between 98 and 99.4% w/w of the nanowhiskers.[134] The percolation was observed at 0.6% w/w of PANI–CSA, suggesting that PANI–CSA was not homogeneously adsorbed by the individual nanowhiskers in a molecular scale.[134] They also showed a feasible combination of electrical conductivity and high mechanical properties.[134] These observations suggest that the PANI–CSA contributes the mechanical percolation within the nanowhisker network and, vice versa, nanowhiskers positively influence the electrical percolation of the PANI–CSA component.[134]

The contribution of percolative template comprising of nanocellulose fibrils was also utilized in Publication **II**, where we demonstrated the first highly porous conducting cellulose aerogels.[123] In contrast to previous studies, we generated the conductivity by post-functionalizing the aerogels by simply dipping the aerogels into PANI(DBSA)1.1-toluene solution. Despite the high porosity, similar conductivity levels were achieved. The results are introduced in detail in Chapter 5.2.

The subsequent investigations related to nanocellulose-based conducting materials contrast greatly the few previously reported. Instead of simple adsorption, they involve "in situ" polymerization process of pyrrole (Py) or aniline in the presence of cellulose nanofibrils. For instance, in situ

polymerization of Py on the surface of NFC results in individually PPy coated conducting cellulose nanofibrils.[129] Nyström et al. reported NFC/PPy composites process which is completely water-based and involves no time-consuming solvent-exchange and drying steps to maintain the large surface area of NFC upon water removal.[129] Such composites have surface areas of ~90 $m^2 g^{-1}$ and conductivities of 1.5 S cm^{-1}. Similar conductivity was achieved when bacterial cellulose was applied with PPy.[135] Thus, these composites can be applied in ion exchange membranes and novel energy storage devices.[129]

Bacterial cellulose polyaniline (BC/PANI) composites showed also similar electrical conductivity of 0.9 S cm^{-1}. Müller et al. prepared the composites through in situ oxidative chemical polymerization of aniline using HCl as dopant and $FeCl_3$-$6H_2O$ as an oxidant.[136] On the other hand, the PANI content was high, almost 40% w/w. At the same time, conducting composite membranes of BC/PANI doped with dodecylbenzenesulfonic acid, PANI(DBSA), shows low conductivities, even if the PANI content ranged from 30-50% w/w.[137] Very recently, Hu et al. showed very high electrical conductivity of 5.1 S cm^{-1} with well-controlled composite morphologies for BC/PANI nanocomposites.[128]

Interestingly and more related to the present work, Carlsson et al. demonstrated the polymerization route for conductive NFC aerogels.[138] The conductive composites were prepared by chemically polymerizing pyrrole onto TEMPO-oxidized cellulose nanofibrils dispersed in water, and the various nanostructures were obtained employing different drying methods.[138] Supercritical CO_2 drying was shown to generate highly porous aerogel composites with very high surface area of 246 $m^2 g^{-1}$. The all aerogel types showed similar specific charge capacities ranging between 212 and 226 C g^{-1} irrespective of porosity.[138] The average PPy content in the composite aerogels was as high as ~ 70%. The significantly higher conducting polymer mass fractions in these composites enable electric conductivity enhancement and thus improved electrochemical utilization.[138] The good mechanical properties of these composites are dominated by the NFC network, as chemically polymerized PPy usually forms a powder and cannot bear any load.[138] Recently, the nanoarchitecture-dependent electrical conductivity changes during redox state switching was shown in layer-by-layer deposited polyaniline–nanocellulose composite films.[139] Thereby, percolation speed can be tuned based on the cellulose nanofibril architecture. Also, cellulose nanowhiskers template reduces electrical percolation threshold 5-fold in conductive polymer nanocomposites.[140]

4.2 TiO_2 as Photo-Responsive Material

4.2.1 Photo-Response and Multiple Length Scales in Wettability

Titanium dioxide, TiO_2, is inexpensive, stable, nontoxic and biocompatible semiconductor. Ever since the discovery of photo-induced water splitting on TiO_2 electrodes by Fujishima and Honda,[141] there has been extensive research on potential applications of photocatalysis of the semiconductors in following fields: (i) photolysis of water to yield hydrogen fuel; (ii) photo-oxidative decomposition of organic pollutants; (iii) artificial photosynthesis; (iv) photo-induced superhydrophilicity; (v) photoelectrochemical conversion etc.[142, 143] Interestingly, TiO_2 shows both hydrophilic and lipo/oleophilic characters.[144, 145] As the hydrophilicity can be changed by UV-light, TiO_2 is a prototypic source for dynamically responsive materials. Such materials respond to external stimuli, such as light, temperature, solvents, electrical potential, pH, etc., and change their surface conformation and/or morphology, which results in the change of surface properties, such as wetting.[9] Light is one of the most important external stimuli used for switching the wettability, and TiO_2, in turn, the most studied material among the photosensitive semiconductors.[143] Fujishima's group discovered also the photo-induced superhydrophilicity. A flat TiO_2 surface can undergo an aqueous wetting transition from a contact angle (CA) of 72° to 0° upon UV illumination.[144] The original contact angle is recovered upon storage the sample in the dark.[144, 145] The mechanism for the photoinduced hydrophilicity was first proposed by Wang et al. the time of the discovery.[143] They suggest that UV-illumination generate the reduction of TiO_2 itself, resulting in Ti^{3+} ions, as oxygen atom ejects from the lattice. These defects, called thereby oxygen vacancies or Ti^{3+} sites, are created at the surface and are known to generate water dissociation, which would further produce hydroxyl groups on the surface, and thus increase the surface hydrophilicity.[144, 145, 146] However, subsequent studies brought new insight into the origin and the mechanism of photoinduced hydrophilicity of TiO_2.[142] In a secondly proposed model, UV-induced hydrophilicity is claimed to cause by major reconstruction of the surface –OH groups with presence of H_2O and UV-light, leading to an increased surface coverage of Ti-OH groups.[147] The third model simply suggests that superhydrophilicity is an inherent property of clean TiO_2 surface, which is revealed upon removal of hydrophobic hydrocarbon contaminants by photo-oxidation during the UV-illumination.[142]

Despite the ongoing debate on the actual mechanism and understanding of photoinduced hydrophilicity phenomenon, numerous commercial products are available based on this property, including windows and mirrors that are

self-cleaning and anti-fogging. Furthermore, with the development of techniques in fabricating hierarchically rough TiO_2 surfaces with combined microscale and nanoscale structures, UV switchable wetting even from CA > 150° to 0° have been reported (see example in Fig. 4.2.).[9, 148, 149]

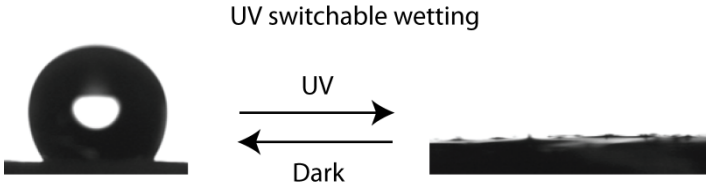

Figure 4.2. Water droplet on a rough TiO_2-coated surface exhibits contact angle of 140°. After UV illumination the CA is 0°. The surface shows reversible transition from hydrophilic state to hydrophobic upon storage in dark.

Generally, the increased surface roughness increases the surface area, and in combination with hierarchy and low energy coating, it can lead to even superhydrophobic surface with CA > 150°, as presented in Fig. 4.3. If a droplet is located on a rough superhydrophobic surface, where the solid/liquid interface follows the texture solid surface, droplet is at the Wenzel state.[150] On the other hand, if air can remain trapped underneath the droplet and droplet sits partially on air, droplet is at the Cassie state.[150] Lafuma and Quéré showed that even if the both states lead to very high CAs, they are very different from their adhesive properties: Wenzel droplets are pinned and shows adhesion, while Cassie droplets show reduced contact angle hysteresis and are able to roll off, typical to nonwetting Lotus leaves.[150, 151] Note, the definition of the superhydrophobicity is under constant debate: one claims, that surface is superhydrophobic only if it is non-wetting i.e. low contact angle hysteresis at Cassie state; the other defines also the Wenzel state superhyrdophobic only based on the high CA > 150°.[152]

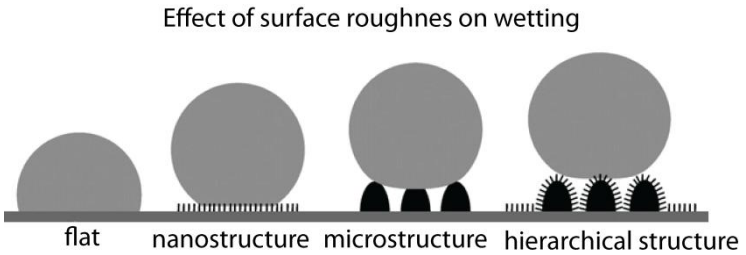

Figure 4.3. The largest wetted contact area between the droplet and the surface is given in flat and microstructured surfaces, but is reduced in nanostructured surfaces and is minimized in hierarchical structured surfaces. Adapted and reproduced from *Soft Matter* 2009, 5, p. 1387 with the permission of RSC .[151]

Recently, Bittoun and Marmur elaborated the role of multiple scale hierarchical roughness, and its strong dependency on the basic geometry in nonwettable surfaces.[153] The sinusoidal topography, similar to lotus leaf protrusions, generates the lowest wetted area among the several investigated geometries and lead to the highest CA.[153] The wetted area plays important role as it strongly effects on the adhesion of the drop to the solid surface and thus the further application.

In contrast to nonwetting surfaces, also superhydrophobic surfaces with high adhesion have been realized e.g. in aligned polystyrene nanotube films[154] and petal of the rose[155]. Such pinning of droplets has also been reported for paper surfaces.[156] The mechanism for high-adhesive pinning of the droplets is not clear. However, it is suggested that the capillary force between the micro-orifices/grooves and/or pores and water droplet, as well as the van der Waal's force between the surface and water, give rise to strong adhesion.[157] Another hypothesis is that adhesion is caused by the negative pressure induced by the volume change of the sealed air in the air pockets.[158] The common feature for high-adhesive superhydrophobic surfaces is the presence of such structures and pores that are able to trap air that is isolated from the atmosphere. It is important to note, that two kinds of trapped air is suggested to exist; air pockets in the open state (continuous with the atmosphere) leading to nonwettable surface, as well as sealed pockets of trapper air leading adhesion.[158] In addition to influence of multiple scales, geometry and air pockets, also height of the rough features as well as the droplet size play role in wetting phenomena of a rough surface.

Ever since Barthlott and Neinhuis suggested that "Lotus-effect"[159] can be transferred to artificial surfaces, researchers have been motivated mimicking also other biological structures in nature having specific wetting properties, such as water striders. The unique hierarchical micro- and nanostructures in the leg play important role in ability of water strider to walk on the water: they enhance the hydrophobicity of waxy surface, and enable air to trap in the hierarchical structures to form a cushion at the leg–water interface, thus preventing the legs from being wetted. Therefore, the hierarchical microsetae and nanogrooves in the leg are responsible for the water resistance and the strong supporting force.[160]

The need for hierarchical roughness was also realized in the previous (super)hydrophobization studies of cellulose, in which macroscopic cellulose fibers, such as in filter paper, provided the large microscale roughness, but it was necessary to generate a suitable hierarchy by additional means, e.g., by fluorinating nanostructures,[161, 162] nanoscale silicone,[163] metal oxide–silane nanocoatings,[164] gold nanoparticles,[165] or by etching the fibers.[156] On the other hand, in the native nanocellulose aerogels additional roughening is not

needed as they exhibit inherent hierarchical porosity and roughness due to the nanoscale fibrils and the aggregated sheets capable of some air trapping, as will be shown in chapter 5.3 and 5.4.

4.2.2 Photocatalytic Decomposition

In addition to photoinduced wetting, TiO_2 photocatalysis has received much attention also for degradation of environmentally harmful compounds.[143] Whereas the photo-induced hydrophilicity is caused by a topmost surface structural change, conventional photocatalytic oxidation activity depends on total amount of generated electron-hole pairs.[146] The higher the amount of photoinduced holes and electrons, the faster the decomposition, as more O^{2-} species and •OH radicals are induced to participate in degradation. Photocatalytic activity of TiO_2 coatings depend strongly on the phase, the crystallite size and the porosity of the coatings.[166] Furthermore, studies to control the morphology of TiO_2 are abundant, since both, the structural properties and the accessible surface area play a significant role in the efficiency of TiO_2 in many of its applications. For instance, macroscopic cellulose fibers within wood tissue and filter papers have been utilized as templates for organic–inorganic hybrids or for purely inorganic replicates of TiO_2, using sol–gel processes or atomic layer deposition.[167-172] The results show, that the sol-gel and deposition methods enable to template the morphological hierarchies of natural cellulosic substances from macroscopic to nanometer scales. Moreover, CNC has been reported to act as morphology-inducing and coordinate agent resulting crystal growth of TiO_2 particles and promoting the formation of nanocubes.[173]

On the other hand, cellulose fibers have been shown to serve as a good matrix for highly efficient TiO_2 photocatalysts.[166, 174-176] For instance, decomposition of gaseous acetaldehyde in TiO_2 containing pulp sheets with good deodorizing activity under room light illumination has been shown.[174] Further, TiO_2 containing pulp, filterpaper, and regenerated cellulose films showed good photocatalytic efficiency to decompose toxic organic pollutants and dyes.[166, 175, 176] Moreover, TiO_2-cellulose based photocatalysts exhibit also good photostability under weak illumination without any lost of photocatalytic activity after several cycles, or damage in the fiber matrix structure.[166, 176] However, if highly crystalline photoactive TiO_2 powder and intensive UV light is utilized, cellulose matrix can be damaged.[174, 175] Immobilization of the TiO_2 e.g. via bioconjugation, to form homogeneously distributed, non-aggregated TiO_2 particles on the cellulose, is suggested as a solution to protect the cellulose fibers during the very efficient photocatalysis.[175]

Reducing the particle size is generally beneficial for surface-dependent photocatalysis because it increases the specific surface area and hence the number of the reactive sites.[143] As mentioned earlier, one of the examples is applying the cellulose fibrils in the filter papers as templates for synthesis of TiO_2 using sol–gel processes or atomic layer deposition. Furthermore, particular effort is put on complex or hierarchical and/or porous hetero-nanostructures to facilitate the separation of photogenerated electron-hole pairs, which further improves the photocatalytic activity.[143, 177] Photocatalysis has been described dealing with a series of tasks involving optoelectronic conversion, surface/interface catalysis, and the post-treatment or recycling of the photocatalyst.[143] Therefore, it is important that all the above mentioned functions should be optimized and integrated into the photocatalytic system, in order to be practical in use.[143] This has generated the design and fabrication of advanced photocatalytic materials based on hierarchical composite nanostructures.[143] Thus, TiO_2-coated nanocellulose aerogels could be considered as an option. To date no single composition or structure is able to fulfil all the above mentioned tasks satisfactorily on its own.[143] As the stability and reasonable cost of the photocatalytic materials are called for, it is important to identify and design new photocatalytically active materials that are efficient, stable and abundant.[143]

5. Results and Discussion - Cellulose Nanofibrils as a Functional Material

This chapter presents the main results of this thesis. First, we introduce the characteristics of enzymatically and mechanically prepared NFC that enable strong networking and cause the superior mechanical properties (Publication **I**). Second, we demonstrate, for the first time, how these cellulose nanofibrils enables aerogels with tunable morphology, porosity and mechanical properties with suppressed brittleness, and that they provide a percolative template for conducting material (Publication **II**). Then we show versatility of these nanocellulose aerogels by coating them with titanium dioxide and fluorosilane. TiO_2-coated aerogels are applied as a photoswitchable superabsorbent and a photocatalytic material (Publication **III**), while fluorinated nanocellulose aerogels as a bio-inspired load carrier due its superhydro- and oleophobic properties (Publication **IV**). Last, we extend the TiO_2 approach to demonstrate floatable and selectively oil-absorbing nanocellulose aerogels for oil spill removal (Publication **V**).

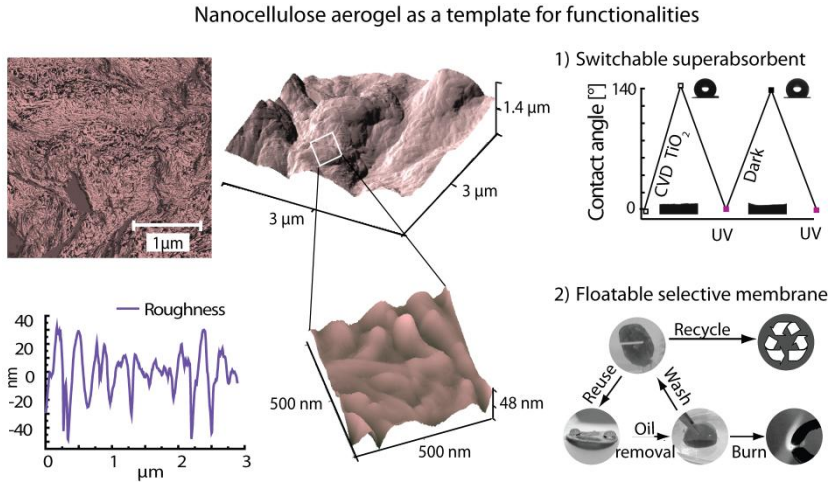

Figure 5.1. NFC aerogels provide multiple scale roughness and overhang structures beneficial for several functionalities, e.g. switchable superabsorbency and selective absorption.

5.1 Hydrogels Based on Native Cellulose Nanofibrils (Publication I)

Herric[31] and Turbak[32] succeeded to liberate nanoscale cellulose fibrils by only mechanical shearing but due to the major process-related problems MFC was never a commercial success, as discussed in Chapter 2.1. Subsequently, Taniguchi and Okamura[35] as well as Nakagaito and Yano[33] developed further the MFC processes that also were based only on the mechanical shearing but even if pulp slurry passed numerous times through the high-pressure homogenizer or grinder, the fibril sizes were still in the range of 20-100 nm, and the energy consumption was large. Importantly, harsh mechanical beating and shearing has the same disadvantages as acid hydrolysis, as at some point the fiber length and molecular weight and crystallinity are reduced.[32, 41] However, these are particularly important e.g. for mechanical properties and should, therefore, be preserved. These challenges motivated towards processes using less intensive shearing, thus lowering the process costs at the same time.

The source of the cellulose and the pre-treatments used in the fibrillation process effects greatly the characteristics of the NFC.[4, 6] In this study, sulfite pulp with a high hemicellulose content of ~ 15% was chosen as a raw material and selective, mild enzymatic hydrolysis as pre-treatment, as discussed in Publication I. Both the high hemicellulose content and enzyme hydrolysis facilitate the disintegration process.[37, 41] Therefore, the high energy input costs and clogging problems are largely overcome. The enzymatic pre-treatment does not only facilitate the process, but also enable selective hydrolysis of the amorphous parts of the cellulose, leaving hemicellulose intact. Hemicellulose plays an important role in the stability of the formed network by generating some electrostatic repulsion between the fibrils. The enzymatic assisted fibrillation process enabled a network of long and entangled nanoscale microfibrils that contain both amorphous and crystalline regions, as demonstrated in Publication **I**.

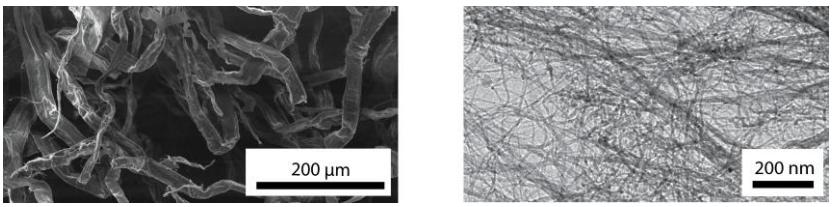

Figure 5.2. SEM image of macroscopic pulp fibers used as starting material (left). TEM image of cellulose nanofibrils resulted from enzymatically and mechanically assisted fibrillation process.

The cryo-TEM image in Fig. 5.2. shows cellulose nanofibrils disintegrated from pulp. The fibril size is reduced significantly from 20-100 nm to only 5-20 nm when compared to the previously reported solely mechanically fibrillated cellulose fibrils.[31-33, 35] Fibrils are several micro meter in length and entangled. There are also thicker, aggregated fibril bundles and junction points of the entangled fibrils.

At the same time, Saito et al. introduced chemical pre-treatment, TEMPO-mediated oxidation, which also resulted in individual cellulose nanofibrils with 3-5 nm in diameter.[44] Similarly, also carboxymethylation pre-treatment process yields very well fibrillated, individual cellulose nanofibrils.[46] Two main differences between the enzymatic-mechanically and chemically treated fibrils are, that the later are easier to fibrillate, and the lateral aggregation of the fibrils in the suspension is clearly suppressed leading to well-defined dispersions.[44, 46] This is due to the electrostatic repulsion between the fibrils, resulting from significant amount of carboxylate groups on the surface after oxidation/carboxylation process. The carboxylate content with negative surface charge, which causes the electrostatic repulsion, is typically 1.2-1.5 mmol/g and 0.5 mmol/g for the TEMPO-oxidized and carboxymethylated cellulose nanofibrils, respectively.[44, 46, 178] The surface charge density of the present enzymatically treated fibrils, that arouse from the hemicellulose, is only 0.05 mmol/g (44,2 μeq/g). The charge is substantially lower than the charge of chemically treated fibrils. The electrostatic repulsion is not strong enough to keep the fibrils ideally dispersed, and consequently, the fibrils aggregate to form interconnected flocs. The Figure 5.3. presents how the fibrils are distributed in the 2% w/w dispersion.

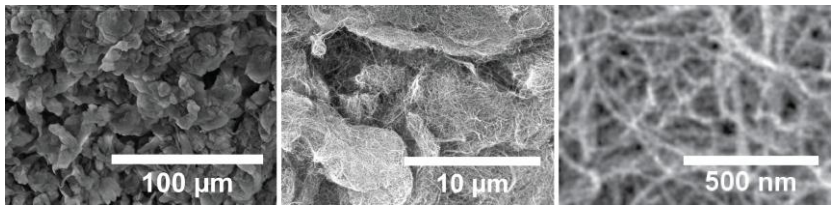

Figure 5.3. The 2% (w/w) enzymatically and mechanically homogenized cellulose nanofibril suspension is composed flocs that are closely interconnected by entangled fibrils. Inside the floc nanofibrils form dense network.

The low magnification SEM image from supercritically dried gel (Fig. 5.3. left) shows that the aqueous dispersion is composed of interconnected flocs with size of 5-20 μm and between the flocs there can be micron scale voids. The flocs are mutually connected with entangled nanofibrils, and inside the flocs the individual nanofibrils form dense network structures, demonstrated by the high magnification SEM images (Fig. 5.3. in the middle and in the

right). The effects of surface charge and possible flocculation of cellulose microfibrils and nanocrystals were discussed earlier by Dinand at al.[179] and Araki et al.[56] Note, that despite the micron scale flocs in the present structure which cause the turbidity, the suspension seems stable.

The entangled network structure itself illustrated by TEM and SEM should manifest in the mechanical and viscoelastic properties, as well as gelation. In Publication **I** we investigated the rheological properties of the aqueous suspension to find the strength of the network, and how the fibrils behave under the applied shear. In Fig. 5.4. the storage (elastic) modulus, *G'*, and the loss (viscous) modulus, G", of cellulose nanofibrils are shown. We found the storage modulus (*G'*) and loss modulus (*G"*) to be relatively independent of the angular frequency at all of investigated concentrations (%w/w). This means that the long and entangled fibrils are able to form a gel with all investigated fibril dispersions, even for the lowest mass fraction of 0.125 %w/w. Importantly, the values of the storage modulus are particularly high in comparison with the previously published results for cellulose short rod-like CNCs and MCC.[58, 180, 181] This is obvious as the storage modulus represent the elastic part of the network (elasticity).

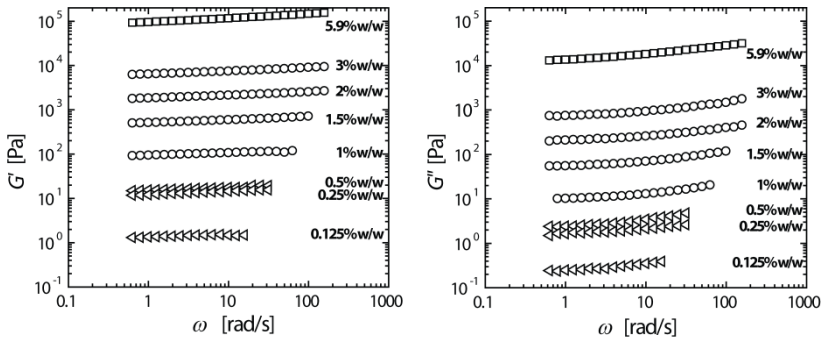

Figure 5.4. The storage modulus (*G'*) and the loss modulus (*G"*) of NFC as a function of angular frequency for all suspensions. Geometries used in the rheometer: steel plate for 5.9% w/w, aluminum cone-and-plate for 1-3% w/w, and acrylic plate for 0.125-0.5% w/w.

Another observation is that the elastic moduli are almost 10-fold higher than the loss moduli at the same concentration, also indicating a rather strong network, even for the lowest concentration. Furthermore, we noticed that the loss tangent (tan δ) values, which measure the ratio of the viscous modulus to the elastic modulus (G''/G'), were below 0.3 for all investigated dispersions: tan δ was 0.17 for 5.9-1% w/w dispersions, increasing to 0.24 for the range 0.5-0.125% w/w. This is a further indication that all dispersions are predominantly elastic. It is interesting that the *tan δ* values for all dispersions were fairly equal. However, the *tan δ* of NFC at the lowest concentration

exhibited the highest value, meaning that at low concentration there is a more viscous behaviour than at high concentrations. In addition, we found particularly strong concentration dependence in elastic moduli, as the storage modulus increases 5 orders of magnitude upon increasing the concentration from 0.125% w/w to 5.9% w/w, as seen in the Fig. 5.5.

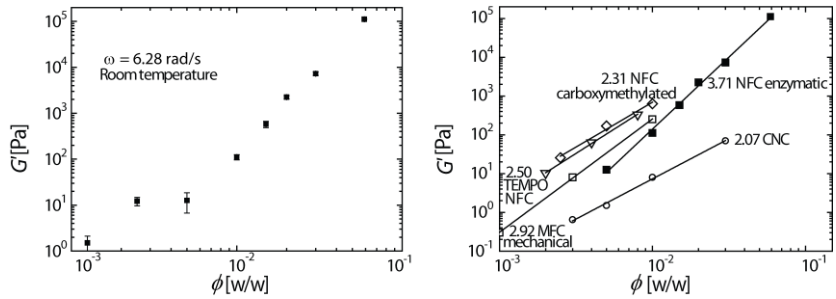

Figure 5.5. Storage moduli, *G'*, of present NFC as a function of weight fraction (left). *G'* of various nanocelluloses with different sources and preparation methods, as a function of weight fraction (right). CNC[58]; NFC enzymatic (the present study); MFC mechanical[57]; TEMPO NFC[178]; NFC carboxymethylated (Hiekkataipale et al. unpublished).

The influence of the nanocellulose source and processing method on the network moduli is obvious. In the Fig. 5.5. moduli of CNC and different NFC and MFC fibrils are plotted as a function of weight fraction. Acid hydrolysis, mechanical, enzymatical, TEMPO and carboxymethylation pre-treatments have been utilized for MCC, sugar beet pulp and wood pulp, respectively. 3% w/w of the present NFC leads to *G'* 10^4 Pa, whereas 3% w/w of rod-like CNC leads to *G'* 10^2 Pa[58] that is, a 2 orders of magnitude higher storage modulus. The present higher elastic modulus is due to high aspect ratio fibrils and fibril aggregates, which contain also *amorphous* parts. As the CNCs are typically short, they are not able to efficiently percolate, i.e. connect to each other to form a network gel at low concentrations. In contrast to rod-like CNC, the long and entangled fibrils in NFC are able to form an inherently interconnected network structure. Mechanically homogenized MFC from sugar beet pulp[57] and the present enzymatically and mechanically treated[40] NFC showed similar moduli. Both materials have low surface charges and tend to form flocs that effect on the overall moduli. Lowys et al. demonstrated that if subsequent ultrasonification was used, the moduli of sugar beet pulp fibrils were about twice as large as that of only mechanically stirred.[57] When more negative charges are introduced on the surface of the fibrils by TEMPO oxidation[178] or carboxymethylation, the moduli are increased one order of magnitude, at least at low concentrations. Saito et al. demonstrated also pH initiated gelation for TEMPO-oxidized NFC dispersion, where viscous 0.1 %

w/w aqueous dispersion became elastic by decreasing the pH from 8 to 2 with a droplet of HCl.[178] Moreover, the moduli increased two orders of magnitude for all investigated dispersions by decreasing the pH.[178] The higher moduli of TEMPO-oxidized NFCs are due to the more stabilized network structure of highly charged fibrils. The macroscopic mechanical behaviour of highly charged NFC is defined and dominated by the uniform network, while in low charged fibril suspensions (Publication **I**), the interfloc interactions are suggested to be dominant. Recently, also Fall et al. studied theoretically the influence of pH on colloidal interactions of cellulose nanofibrils[182] while Way et al. demonstrated pH-responsive gels, applying cellulose nanocrystals.[183]

Turning back to the Fig. 5.5, there is clear concentration dependence in the moduli ($G' \propto \phi^n$) for all the above-discussed materials, however, the slopes of the plots differ indicating different power-law exponents n. The materials can be divided roughly into two categories: those with $n \sim 2$ and those with a $n \sim 3$ or larger. The former group includes interestingly the both, rod-like CNC as well as the highly charged TEMPO and carboxymethylated NFC, whereas the latter group consist of less charged fibrils. Common to CNC and the charged NFCs is better stability and higher crystallinity, as they are not affected by several homogenization passes, unlike the mechanically and enzymatically treated low charge fibrils. The origin of the cellulose source influences also as kraft pulp, dissolving pulp, sulphite pulp and sugar beet pulp has different fiber length and hemicelluloses content. Moreover, the morphology of the highly charged fibrils resembles more rod-like CNCs than coiled and more amorphous low charged fibrils, which tend to flocculate. The scaling properties of elastic modulus depend not only on the size and degree of the interactions between the particles but also the shape. The shape of the group with power of ~ 2 can be considered as rod, and the shape of group with power of ~ 3 or larger more like spherical cluster. All the above-mentioned aspects suggest similar power law for CNC and TEMPO and carboxymethylated fibrils.

In Publication **I**, we also investigated the hydrogels under the continuous shear.[40] All (0.125-5.9 % w/w) suspensions show a large decrease of viscosity with increasing shear rate, that is, shear thinning as seen in Fig 5.6.

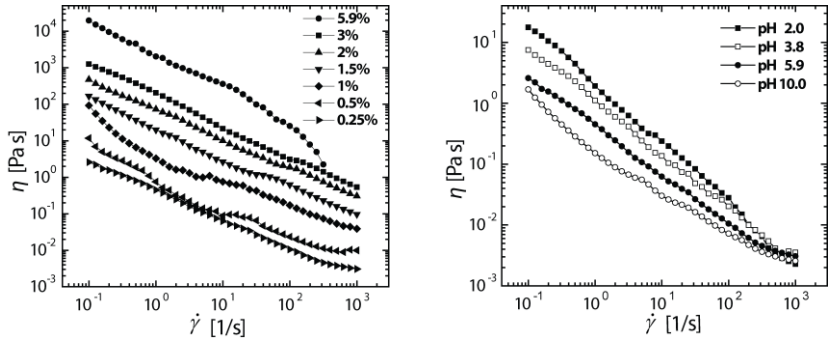

Figure 5.6. Influence of shear rate on the viscosity of NFC suspensions with different concentrations (left). Influence of pH on the shear viscosity of suspension with concentration of 0.25% w/w (right).

In addition, we demonstrated the influence of pH on the network structure by the shear viscosity experiments. The dependence of pH on shear viscosities is seen in Fig. 5.6. At lower pH, the hydrogen ions neutralize the charges of the hemicellulose associated with the fibrils, which reduces the homogeneous network. At higher pH, on the other hand, the number of charges increases leading to a higher electrostatic repulsion resulting in a lower interaction between the flocs and a lower viscosity.

The shear viscosities can be used as an indirect tool to compare structural and chemical differences between NFC and CNCs. The initial shear viscosity at very low shear rates shows the evident structural difference between long and entangled NFC[40] and low aspect ratio CNCs[56] and even with tunicates.[61] The enzymatically and mechanically homogenized NFC (1% w/w) exhibit initial shear viscosity of ~ 10^2 Pa s, that is, 3 orders of magnitude larger than that of TWs that showed initial shear viscosity of 10^{-1} Pa s at the same concentration.[61] On the other hand, the enzymatically and mechanically homogenized NFC shows similar shear viscosities as the mechanically homogenized MFCs manifesting the similarity of the fibrils.[31, 184]

The breakdown of the nanocellulose network (i.e. gel), causing the decrease in viscosity, is shown to take place via flocs.[56, 185] Viscous CNCs suspensions showed a clear plateau in the end of the shear viscosity curve.[61] It means that, CNC rods can be flow-oriented in the plateau region, and further increase in the shear rate does not change the rod orientation, or the viscosity.[56, 61] As there exists no plateau in the present NFC curves, it means that despite the high shear rates, the flocs are not broken into flow oriented individual fibrils. The fact that viscosities of the present cellulose nanofibrils remain higher compared to CNCs[56, 61] support the conclusion, that suspension is still composed of nanofibril aggregates or small flocs rather than individual fibrils. Recently, Saarikoski et al. demonstrated that shear viscosity of the NFC was strongly depended on the time, geometry and the gap size used in the

measurement.[185] Therefore, conclusions on the detailed shear thinning behaviour of NFC are still under debate. To investigate the initial viscosity under continuous shear, extremely low shear rates are required in order to avoid the breakage of the network. Furthermore, to overcome the geometry-related problems such as wall slip and uneven flow field, which would dominate the results, we suggest that measurement with small oscillatory amplitude should be applied instead of continuous shear. However, the shear-thinning behavior of the cellulose nanofibrils is beneficial e.g. in novel 3D cell culture and tissue engineering applications.[186, 187] Due to the shear thinning, cells can be mixed into the gel and thereafter the hydrogel cell cultures can be easily dispensed e.g. with a syringe and needle, a pipette tip, or a microfluidic device. Importantly, the high viscosity is established instantaneously after shearing (e.g. injection or mixing) has stopped.[186] In addition, shear-thinning is useful in material processing like extrusion and further processability, which is important for future success of NFC materials.[188-190]

Taking into consideration the characteristics of the NFC observed in Publication **I**, it become interesting to consider the long and inherently connected nanofibrils as construction units for nanoscale engineering of functional materials, which are discussed in the next section.

5.2 Robust Nanocellulose Aerogels with Tunable Morphology and Percolative Template (publication II)

The nanoscaled size, increased surface area and the superior mechanical properties of the nanofibrils, encouraged us to explore the applicability of the fibril network as a lightweight template. Previously, the potential of the fibril network as a reinforcement was shown[33, 36, 191-193] e.g. in optically transparent composites[36] and composite films.[24, 194, 195] In addition, promoted high toughness of nanopaper was shown based on purely cellulose nanofibrils.[51] However, no reports on applying the native cellulose nanofibril network to form aerogels were published by the time of this research. As discussed in chapter 3.1., previously reported derivatized cellulose aerogels require added cross-linkers to form a gel and stabilize the resulting aerogels due to a reduced number or total elimination of hydroxyl groups.[100, 101] Besides, gelation followed by solvent exchange prior to supercritical drying is usually a slow process, taking several days. Furthermore, such aerogels suffer from a large shrinkage, which lowers the porosity and increases the density, although the specific surface area can be very high. Dissolved and regenerated cellulose aerogels, on the other hand, suffered from quite laborious processing and brittleness.[104] In contrast to cellulosic regenerated aerogels,

we expected that native cellulose nanofibrils in the aerogels are held together not only by the physical hydrogen bonds, but also by mechanical entanglement of the fibrils. The rheological experiments showed strong networks, and that the high aspect ratio native nanofibrils would enable very low gel concentration for aerogels. Thus, the network was expected to be strong against the collapse upon drying, and possibly allowing new drying technique.

5.2.1 Drying Techniques and Morphological Characteristics of the Aerogels

Encouraged by these hypotheses, we tried particularly simple freeze-drying method i.e. drying in a vacuum oven without any preceding chemical cross-linking, or specific additional mechanism of physical cross-linking (Publication **II**). In our method, the gel is frozen relatively quickly due to the simple pumping action of the vacuum oven, resulting in ice sublimation from the frozen sample. For the first time, vacuum freeze-drying was demonstrated without significant collapse in the structure, and a robust and sponge-like native nanocellulose aerogel was achieved. In addition to vacuum freeze-drying, we applied the quick cryogenic freeze-drying method previously introduced for regenerated cellulose aerogels.[104] In our procedure the liquid propane was utilized instead of liquid N_2 in order to accelerate freezing. We placed the aqueous cellulose nanofibril gel on the mould and the mould was quickly plunged in liquid propane. Water is removed from the frozen state by sublimation in vacuum oven. The sublimation temperature was controlled only by cryogenic metal block underneath the metal mold. A lightweight nanocellulose aerogel was formed without significant collapse. Importantly, the aerogels seemed not to be brittle.

The both resulting nanocellulose aerogels reached a very high porosity of 98% and a density ranging from 0.02-0.03 g cm^{-3}.

$$Porosity = 1 - \frac{\rho}{\rho_s}$$

where ρ and ρ_s are the densities of the aerogel and cellulose fibrils (skeletal density). The value for ρ_s is 1.5 g cm^{-3}.[21]

Table 5.1. The properties of present aerogels

Drying method	Drying srinkage [%]	Density [g/cm^3]	Porosity [%]	BET surface area [m^2/g]
Cryogenic Freeze-dying	7	0.02	98	66
Vacuum Freeze-drying	max. 20	0.03	95-98	20

The different freezing rate in these two methods resulted in different morphologies and different pore size distribution into the aerogels (Fig. 5.7.). As we showed previously, the initial morphology of the present wet gel is composed of interconnected NFC flocs that, in turn, consist of dense network of long and entangled nanofibrils with diameters of 5–10 nm with occasional thicker fibril bundles. During the vacuum drying, however, the microstructure undergoes major changes as seen in Fig. 5.7. The SEM reveals that the nanofibrils inside the flocs collapse into 2-dimensional extended sheet-like morphology. This is due to the liquid–vapor menisci that can be formed prior the freezing in vacuum pumping, partially collapsing the flocs and pulling the nanofibrils together.

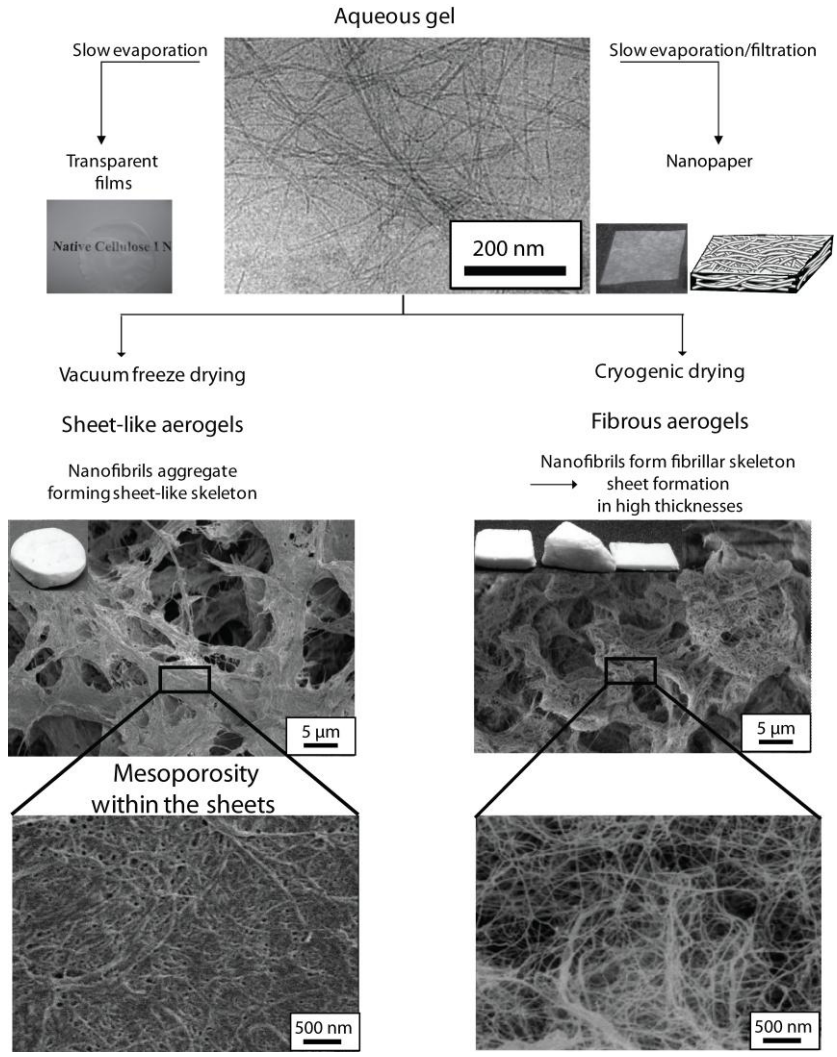

Figure 5.7. NFC allows transparent/translucent films and nanopapers as well as aerogels using different drying methods. Both aerogel types consist of nanoscale fibrils that are assembled into micronscale sheets or flocs, generating multiple length scales into the aerogel structure.

More importantly, large ice crystals are formed during the freezing that push the fibrils together leaving micrometer range voids. The 20% shrinkage caused by the aggregation is still relative small. SEM images show that the sheets are irregular and ~10-20 µm in width and oriented random-in-the-plan. The sheets form layered and interconnected skeleton structure to aerogel.

The cryogenically dried aerogels preserved better the interconnected and open fibrous morphology after the water extraction, as illustrated in Fig. 5.7.

According to SEM the skeleton is composed of nanofibril flocs and inside the flocs the 3D open network structure. This indicates that the freezing rate is relatively high to prevent the excessive ice crystals grow to separate the flocs and to destroy the network. The voids between the flocs originally in the wet gel are now slightly larger and form macrochannels in the aerogel. On the other hand, the voids between the sheets affected by the ice crystals are larger than the pores in the gryogenically dried aerogel.

N_2 adsorption–desorption measurements were carried out to determine the pore size distribution of the smallest pores. We found the existence of an additional mesoporosity, i.e. pores smaller than 50 nm (Table 5.2) evaluated from the desorption isotherm utilizing Barret–Joyner–Halenda (BJH) method. This suggests that the sheets, in fact, have also an internal porosity, which explains the high porosity even if 20% shrinkage took place. The internal porosity within the sheets can be also directly observed in the SEM micrographs (Fig. 5.7)

Table 5.2. The aerogel pore diameter distribution for < 100 nm pores based on N_2 desorption and BJH-method. The sample thickness is 3 mm.

Pore radius [nm]	Cryogenically freeze-dried [%]	Vacuum freeze-dried [%]	Classification
50-60		5	macroporous
40-50		10	mesoporous
30-3	98	84	mesoporous
1-2	2	< 1	microporous

As the final pore structure is formed during the sublimation, the final morphology of the aerogel is therefore directly related to the size and distribution of the ice crystals in the frozen system. Therefore, the morphology of the aerogel and the pore size distribution can be tuned: a higher freezing rate results in a smaller average pore size and a more homogenous pore structure, as well as preserves better the original gel body. In the both nanocellulose aerogels, nanoscale fibrils (5-10 nm) are assembled into micronscale sheets or flocs (5-20 μm), thus generating multiple length scales i.e. hierarchical structure into aerogel. Furthermore, aerogels contain also multiple scale pores: the voids between the sheets/flocs form macrochannels through the aerogel, while nanoscale pore network is formed within the fibrils.

Naturally, the BET surface areas of the aerogels differ from each other due to the differences in the freezing rate and consequently in morphology. The ca. 3 mm thick cryogenically dried aerogel shows a BET specific surface area

of ~ 70 $m^2 g^{-1}$, measured using an N_2 adsorption–desorption method and calculated from N_2 adsorption. Correspondingly, vacuum dried aerogel exhibits the BET surface area of only 20 $m^2 g^{-1}$. The large sheets with rather tightly aggregated fibrils result in lower BET surface area than more fibrous morphology. The more detailed effect of freezing rate on the morphology, porosity, and consequently on the surface area, as well as the mechanical properties, is still under investigation. However, the heterogeneity in the pore structure and in the different morphologies can be useful for controlling filtration properties for both gas and liquid phases. It is worth pointing out, that despite the collapse of the fibril flocs into the 2D sheets during the slow freezing, and the micron scale pores left by the ice crystals in the structure, the overall skeleton of the aerogel did not significantly collapse even upon the simplest vacuum drying.

Subsequent to this study,[123] freeze-drying has been the most frequently applied drying technique for native nanocellulose aerogels,[196-206] although supercritical drying is also utilized.[207-209] The density and morphology have been tuned by the freezing rate[204] or by selecting different concentration[198, 210] of the cellulose nanofibril gels before freeze-drying. Sehaqui et al. studied the effect of density on the structure, using the same enzymatically and mechanically homogenized NFC.[198] The freeze-dried nanocellulose aerogels showed cellular honey comb -like or polyhedral structures, with both open and closed cells, which are referred to as foams.[198] In addition to the structure and porosity, the density effects also on the surface area of the aerogel. The surface areas of the foams were similar to those of our aerogels. While the previous thin fibrous regenerated cellulosic aerogels showed increased surface area with increasing density,[104] the surface area of the foams decreased from 42 to 12 $m^2 g^{-1}$ upon increasing the density from 7 to 79 kg m^{-3} [198]. In the foams, thicker sheets are formed by increasing density or by decreasing the freezing rate, thus resulting in lower surface area.[123, 198]

A solvent, in which the fibrils are dispersed and dried, plays also an important role in controlling the structure, and consequently the surface area. To achieve very high surface area originating from cellulose nanofibril network, solvent exchange e.g. to tert-butanol has been applied prior the freeze-drying.[178, 204] For instance, totally fibrous native nanocellulose aerogels with very high surface area of 246 $m^2 g^{-1}$ were achieved by freeze-drying performing 6-step solvent exchange prior the drying.[204] If supercritical CO_2 drying is employed, the surface area can be further increased.[208] Moreover, the smaller and more stabilized TEMPO-oxidized cellulose nanofibrils results in even higher surface area than the enzymatically and mechanically homogenized nanofibrils that tend to aggregate more easily.[204] Therefore, also the fibril source should be taken into consideration, especially in

applications where high surface areas are required. The tunability of the morphology and pore structure makes the nanocellulose aerogels versatile materials e.g. as a template for catalysts.

5.2.2 Compression Studies of the Aerogels

The strong and inherently percolative skeleton structures of the native nanonanocellulose aerogels give arise to good macroscopic mechanical integrity. We noticed that the present vacuum and cryogenically freeze-dried aerogels were almost sponge-like and not as brittle as it would be expected regarding such low density and high porosity. The first indication of increased ductility and flexibility is that they can be reversibly folded into a loop (Publication **II**). Furthermore, the present aerogels can be compressed without disintegration into pieces. Next, we performed compression stress–strain tests to study the mechanical properties quantitatively, and apply the Gibson and Ashby deformation models[211, 212] for 2D and 3D cellular solids (open and closed) to discuss the mechanical behaviour of the aerogels. Three characteristics describes the stress-strain curves of cellular solid under compression: a *linear elastic* region, a *stress plateau,* and *densification*.[211, 212] The linear elastic region and accordingly the elastic modulus correspond to bending of the cell edges or face stretching.[212] The stress plateau, i.e. non-linear region, corresponds to cell collapse by elastic buckling, plastic yielding and brittle crushing.[212] The collapse mode depends on the properties of the solid from which the material is prepared.[212] In the densification, cells collapse throughout, pores become totally empty, and cell edges and faces press against to each other.[212] In the stress-strain curve, the densification can be seen as steep rise in the stress at high strains. The collapse mode of the non-linear region is important in the applicability point of view. If the cells collapse only by elastic bending and buckling, foam is flexible and recovers completely when unloaded. Rigid foams are also able to bend, however, cells collapse mainly by plastic yielding, initiated by formation of the plastic hinges, and break at higher loads.[212]

The compression stress-strain curves for present sheet-like and more fibrous aerogels are presented in Fig. 5.8. The behavior of the aerogels under the compression is similar. This could be explained by the asymmetry in the fibrous aerogel due to the possible aggregation of the fibrils, i.e. sheet formation in the interior of the aerogel. While brittle aerogels/foams show a flat collapse region in which the stress is constant with increasing the strain, the present native nanocellulose aerogels show gradual transition from linear to non-linear stress–strain region without clear yield point. Furthermore, collapse region shows strain hardening i.e. stress increases with strain in wide range, resulting in a rather linear curve until 40-50 % strain.

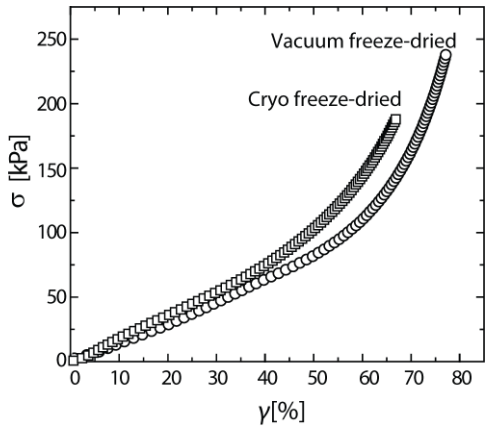

Figure 5.8. Compression stress-strain curves for fibrous (cryo freeze-dried) and sheet-like (vacuum freeze-dried) aerogels.

As the curves reveal, the sheet-like structure shows slightly more yielding behaviour than more fibrous-like, in which linear strain hardening dominates more. This was also observed later for the more closed foam structures and fibrous aerogel using the same NFC as in the present study.[204] As the stress–strain relationship is rather linear to large strains, the actual value of "modulus" is unclear, although the material is reported to be truly elastic (recovers after deformation) only at strains ranging from 3 to 12%.[204-206] The present aerogels show moduli of ~170 kPa, being comparable with moduli of 199 kPa and 249 kPa, reported for fibrous and irregular sheet structures, respectively.[204, 205] Therefore, the results support the observation of morphological irregularity of the sheet like aerogels, as well as the heterogeneity of the fibrous aerogels. The estimated yield stress for present aerogels is ~ 20-30 kPa. This is comparable with a recently reported yield stress of 35 (± 10) kPa for very similar type of aerogel with irregular sheet-like structures.[205] The deformation occurring in the non-linear, collapse region, is mainly associated with bending of the sheets and fibrils, as well as some cracking in at higher strains. After 50% strains, the sheets and fibrils press to each other and the materials show considerable stiffening due to densification of the porous structures. The present aerogels can be compressed to > 70 % strain.

As demonstrated subsequently, the mechanical properties of NFC aerogels scale strongly with density, besides, the morphology of the aerogels and the fibril source influence significantly. Sehaqui et al. reported a wide range of mechanical properties by controlling the density[198] and the fibril interaction by solvent exchange[204] resulting nanocellulose foams[198] or fibrous aerogels[204] as plotted in Fig. 5.9. For instance, it is possible to control the foam modulus

in a range as wide as 56–5310 kPa, and compressive yield strength in the range 7.8–516 kPa.[198] It is also shown that fibrous NFC aerogels depend more strongly on relative density than NFC foam (slope 2.2 for fibrous aerogel and 1.8 for NFC foams).[204]

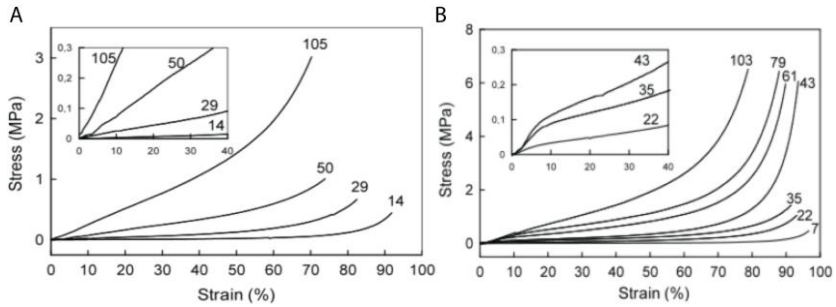

Figure 5.9. Compression stress–strain curves of (a) NFC fibrous aerogels and (b) NFC foams. Numbers next to each curve represent density values in kg m^{-3}. Magnified sections show (a) strain hardening behavior of the fibrous aerogels and (b) yield behavior of the NFC foams. Reprinted from Composites Science and Technology © 2011, with permission from Elsevier.[204]

To clarify the differences in the mechanical properties between the different structures, compression modulus (*E'*) and yield stress (σ_{yield}) of fibrous aerogel and foams, are presented in Table 5.3. All aerogels were prepared from the same enzymatically and mechanically homogenized cellulose nanofibrils, but they exhibit different morphology. Again, the one with totally fibrous structure refers to an aerogel and the others to foam. One of the foams show irregular sheet-like morphology with open cells,[205] and the other regular sheet-like polyhedral morphology with open and closed cells[198]. The fibrous aerogel has a lower modulus than that of NFC foams, particularly at low densities. Furthermore, the foam with a uniform cellular structure and regular sheets is significantly stiffer than the foam with irregular sheets and the fibrous aerogel.

Table 5.3. Mechanical properties of aerogels/foams with different morphology.

Structure	$NFC_{enzymatic}$ Fibrous	$NFC_{enzymatic}$ Foam (irregular)	$NFC_{enzymatic}$ Foam (regular)
Density (kg m^{-3})	29	27	28
E' (kPa)	199	249	718
σ_{yield} (kPa)	24.4	35	70.1

$NFC_{enzymatic}$ fibrous and foam (regular): Composites Science and Technology (2011), 71.; $NFC_{enzymatic}$ foam (irregular): Soft Matter (2013), 9.

Very recently, Ali and Gibson compared and modeled the difference in the deformation between these irregular and regular NFC foams.[205] The microstructure of the NFC foams they used differs significantly from that of regular NFC foams, as they are composed of irregular sheets that are occasionally connected to other sheets by smaller struts i.e. junctions of the sheets.[205] The irregular foams are less well connected and consist of smaller and thinner cell edges and larger sheets compared to regular foams reported by Sehaqui et al.[198, 205] The irregular foam deforms primarily by bending of the smaller struts (junctions of the sheets), with little deformation of the larger and more rigid sheets.[205] Therein the sheets contribute to the relative density of the NFC foam but do not resist the bending deformation.[205] Sheets were suggested to move slightly monolithically along with the bending of the struts.[205] Importantly, the Young's modulus of the irregular foam would be thus controlled by the bending of only the small and thin struts/junctions, which comprise only a fraction of the relative density of the foam.[205] Furthermore, they showed that also yield stress of the irregular foam arises from the plastic deformation of the smaller, thinner struts, along with some cracking at larger strains.[205] Consequently, the modulus and yield stress are smaller than those of foam made of regular sheets and more uniform pores.[205] Our aerogels exhibit more random organization of the sheets, multiple pore sizes, and uncontrolled pore connectivity, and thus resulting lower mechanical properties than those of reported by Sehaqui et al. and Ali and Gibson. Therefore, careful design and control of the overall aerogel and sheet structure would lead significant improvement in the mechanical properties.

Next, the mechanical properties of the aerogels are analysed according to the different sources. Table 5.4. shows the mechanical properties of the aerogels made form tunicate nanowhiskers, TEMPO-oxidized NFC, as well as enzymatically and mechanically homogenized NFC , with fibrous or sheet like morphology.

Table 5.4. Mechanical properties of aerogels/foams from different sources.

Source Morphology	Tunicate nanowhisker sheet		TEMPO-NFC fibrous	$NFC_{enzymatic}$ fibrous	$NFC_{enzymatic}$ sheet	
Density (kg m^{-3})	10	35	10	14	12	35
E' (MPa kg^{-1} m^3)	1.8	9.7	14	2.5	15	39
σ_{yield} (kPa)	-	-	20	3.2	29.6	92.7

Tunicate nanowhiskers: J. Mater. Chem. (2009)[206]; TEMPO-NFC: Soft Matter (2011)[178].; $NFC_{enzymatic}$ fibrous and foam: Composites Science and Technology (2011)[204].

Different sources lead to significant differences in the mechanical properties of the aerogel. For instance, the aerogel made from 0.8% w/w tunicate nanowhisker hydrogels showed specific moduli, *E'*, of 1.8 MPa kg^{-1} m^3, while the TEMPO-oxidized cellulose nanofibril hydrogel with the same fibril concentration resulted in the specific moduli of 14 MPa kg^{-1} m^3.[178, 206] Despite the rather high aspect ratio and very high crystallinity, the elastic modulus of the nanowhisker aerogel is almost one order of magnitude lower than that of the aerogel made of TEMPO-oxidized NFC. This is suggested to results from two structural aspects. First, there is a difference in the original network structure between the whiskers and the TEMPO-fibrils. While the TEMPO-oxidized nanofibrils form strong network due to the inherently connected nanofibrils already at very low concentrations, the individual tunicate nanowhiskers are just about to percolate i.e. to form a network (see also the morphologies in Fig. 2.5. c and h). Secondly, the nanowhiskers formed layered sheets, which are separated by large voids, and loosely connected through occasional thin fibrils, whereas the TEMPO oxidized nanofibrils show dense, uniform and rigid fibrous network throughout the sample. Furthermore, also the low-density sheet-like foam made from enzymatically and mechanically homogenized fibrils results in specific modulus of 15 MPa kg^{-1} m^3. The almost tenfold difference in modulus compared to that of the foam made from tunicate whiskers is generated by the structure. As discussed earlier, the sheets formed regular cellular structure, whereas the layered sheets in the whisker foam can span the entire cross-section of the sample being only loosely connected to each other. However, despite the structural change towards cellular structure upon increasing density, the nanowhisker aerogels showed still 4 times lower specific modulus compared to the long and entangled NFC foam, being 9.7 MPa kg^{-1} m^3 and 39 MPa kg^{-1} m^3, respectively. Finally, fibrous TEMPO NFC aerogel has a specific modulus of 14 MPa kg^{-1} m3, whereas the fibrous aerogel made from enzymatically and mechanically homogenized fibrils has that of 2.5 MPa kg^{-1} m^3. As the both aerogels were prepared by freeze-drying from tert-butyl alcohol, the difference in specific modulus is not affected by the structure but is generated only by the source. The TEMPO-oxidized fibrils show higher surface charge density, crystallinity, and form more uniform rigid network, and consequently a stiffer aerogel. Furthermore, it has been shown that the TEMPO oxidized fibrils may also orient locally within the hydrogel structures, which effect favourably on the mechanical performance of aerogels.[178]

To highlight the mechanical properties of native nanocellulose aerogels, regenerated cellulosic aerogels are not known to be able to form a stable aerogel at as low density as native fibrils are. Furthermore, there are two important and common features in the compression stress-strain curves of regenerated cellulose aerogels different from native ones. First, clearer yield

stress, where the material start to collapse can be observed. Although the yield stresses are rather high up to 160 kPa[110], the typical yield strains are only of 4 %.[110, 115] Second, beyond the yield point, aerogels show rather clear plateau, typical for plastic deformation, in which not only the skeleton bend but also the structures become irreversibly damaged.[110, 116, 119] The maximum compression strains are limited to 60%, while native nanocellulose aerogels can be compressed to very large strains of 70-99%.[123, 198, 205] This suggests that regenerated cellulose aerogels are rather rigid, and collapsed more by plastic yielding and brittle crushing, while native nanocellulose aerogels are more flexible and able to bend due to the alternating arrangement of crystalline and *amorphous* regions in the fibrils.

To put the effect of fibril size (aspect ratio) into perspective, the freeze-dried aerogels made from MCC show the compression modulus of only 17 kPa with a density of ~0.06 g cm^{-3} (note, concentration 5%).[213] That is one order of magnitude lower moduli despite of the higher density of MCC. Also tunicate nanowhisker aerogels[206] have shown lower moduli than NFC aerogels[178, 198] However, the high aspect ratio tunicate whiskers exhibit very interesting mechanical properties e.g. in stimuli-responsive bio-inspired nanocomposites.[214]

To conclude, the overall mechanical response of the aerogels is influenced by density, mechanical properties of the source itself, as well as the microstructural features of the aerogels and foams. Thus, one of the main advantages applying native cellulose nanofibrils in the aerogels and foams is the finer and more homogeneous and tunable cell structure compared to traditional fiber based porous structures.[205] Furthermore, native cellulose fibrils can be applied as reinforcement in other foams due to the low density and high mechanical properties and nanoscale size.[205]

5.2.3 Conductive Aerogels

Would the percolative skeleton of the nanocellulose aerogels enable and/or enhance electrical conduction at low weight fractions of conducting polymer? To answer this it is relevant to note that the present aerogels could be simply immersed in a wide variety of organic solvents, such as toluene and ethanol, and they could be re-dried in air or in a vacuum oven essentially maintaining the original aerogel properties without collapse. Encouraged by this observation, we demonstrated electrically functionalized aerogels using a conducting polymer (Publication **II**). In contrast to previous studies, we generated the conductivity by post-functionalizing the aerogels by simply dipping the aerogels into PANI(DBSA)1.1-toluene solution. In this system, the excess of the dopant (DBSA) enables solubility in toluene.[132]

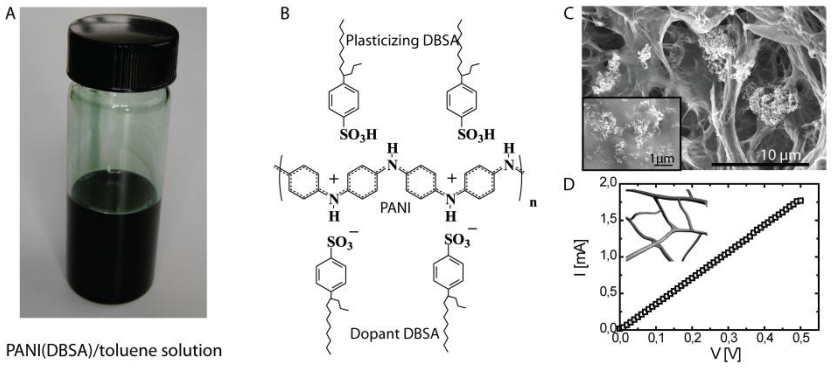

Figure 5.10. Nanocellulose aerogels were post-functionalized by dipping the aerogels into PANI(DBSA)1.1-toluene solution(A). Structure of polyaniline (PANI) doped and plasticized with branched, soft type DBSA (B). SEM image show the aggregated PANI on the skeleton of the aerogel (C). PANI-functionalized aerogels show ohmic conducting behaviour (D).

In our method, 2 mm thick vacuum dried aerogels were immersed in 6.2 %-wt PANI(DBSA)1.1 - toluene solution (commercial PANI-T, from Panipol Oy) for ca. one hour. We did not observe disintegration or significant swelling of the aerogel samples during such dipping, thus demonstrating the robustness of the network. As the aim was to explore whether a small amount of doped PANI on the aerogel skeleton could form conducting material, the excess, i.e. unbound, conducting polymer was rinsed off using a large excess amount of toluene until toluene was detected to be colourless. Finally, PANI(DBSA)1.1-nanocellulose aerogels were dried in the hood at mild heating to evaporate toluene, followed by vacuum drying. That PANI(DBSA)1.1 could be adsorbed on the nanocellulose aerogel skeleton, is qualitatively observed already by the green colour of the aerogels. The measured conductivities ranged from 7 x 10^{-3} to 4 x 10^{-2} S cm^{-1} being at same level than previously reported carbon nanotube and PANI(CSA) based nanocellulose composites.[133, 134] Note, taking into account the very high porosity of n. 98%, and the extremely small PANI(DBSA)1.1 volume fraction of below 0.5%, the aerogels showed astonishingly good conductivity compared with e.g. previously reported films. While we applied post-functionalization of the aerogels by simply dipping, the subsequently reported studies utilized in-situ polymerization of conducting polymer onto nanocellulose, as described in chapter 4.1. Thereby, the electrical conductivities are 1 to even 3 orders of magnitude higher than that of present aerogels. On the other hand, the mass fractions of the conducting polymer have been substantially higher. The recently reported PPy/NFC aerogels showed good electrical properties, however, the PPy content was 70% w/w.[138]

In summary, in the Publication **II** we showed many advantages of using long native cellulose nanofibrils to prepare aerogels. First, the high aspect ratio

and the inherent entanglements and junction points allow percolation and gelation in very low concentration. This means that very small amount of material is needed. Second, crosslinkers are not needed in the process, as entangled nanofibrils form rigid networks themselves. Besides, no solvent exchange or supercritical drying is required to inhibit or substantially suppress the collapse during the aerogel preparation, unlike in typical aerogel preparations. For the first time, we demonstrated that the present cellulose nanofibril network is strong and flexible thus allowing a highly porous and robust aerogel by in particular simple vacuum freeze-drying method. Besides, we showed that the fibril network enables nanocellulose aerogels with tunable hierarchical morphology and porosity and percolative template e.g. for conducting polymer.

5.3 Photoswitchable Superabsorbent and Photocatalytically Active Nanocellulose Aerogels (Publication III)

During the vacuum freeze-drying cellulose nanofibrils are assembled into micro- (sheets) and nanoscale (fibrils) structures within the aerogel. Furthermore, the aerogel contain voids and pores at different length scales: the voids between the sheets form macrochannels through the aerogel, while sheets show internal nanoscale porosity. As seen in Fig. 5.11., the multiple scale structures and pores in the aerogel generate hierarchical roughness, which is beneficial e.g. in catalysis, separation and wetting processes.

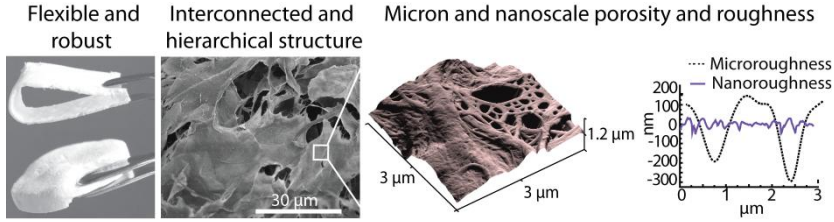

Figure 5.11. The native nanocellulose aerogels are robust, hierarchically rough and porous enabling template for functionalities.

In Publication **III** we applied the native nanocellulose aerogels as a template for TiO_2, which is a prototypic source for dynamically responsive material, e.g. TiO_2 changes its wetting properties by UV-light. Besides, it shows photocatalytic properties, stability, and biocompatibility. We wanted to explore whether the high porosity and multiple length scale in the aerogel promote wetting and photocatalytic properties resulting from TiO_2. Thus, the influence of a nanocellulose aerogel would be twofold: it would serve as a support for TiO_2 to act, and also enhance the effects due to its structure. On

the other hand, cellulose is very hydrophilic, and in many suitable applications water repellence is required. As inspired by the high porosity and very hydrophilic character of the nanocellulose aerogels, we showed that the originally very hydrophilic, superabsorbent nanocellulose aerogels are turned into water-repellent upon TiO_2 coating. Such TiO_2-coated aerogels further enable photoswitching of water absorption upon exposure to UV light, ranging from a very hydrophobic state to a superabsorbent. In addition, photocatalytic properties are explored in relation to the porous aerogel structure.

We chose chemical vapour deposition method (CVD) for aerogel functionalization, as it is feasible due to the high porosity of the aerogels. In the CVD process, the nanocellulose aerogels were exposed to titanium isopropoxide vapor at 190 °C at pressures of 1–5 kPa for 2 h (Publication **III**). TEM images showed quite uniform coating with a thickness of ~ 7 nm. We performed contact angle experiments to demonstrate the water repellence resulting from TiO_2 coating. The wetting and photoswitching between water-repellent and water-superabsorbent states in the aerogels are presented in Fig. 5.12.

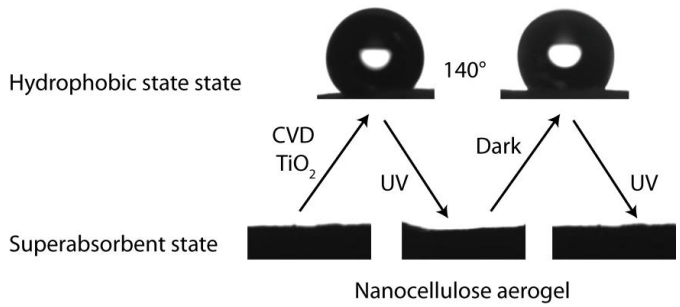

Figure 5.12. Switchable absorption and wetting upon TiO_2 coating of the nanocellulose aerogel and the effect of UV-illumination.

A water droplet on an uncoated nanocellulose aerogel surface is absorbed very quickly (within ca. 40 ms), and therefore the contact angle cannot be measured. The untreated nanocellulose aerogel is highly hydrophilic due to the numerous hydroxyl groups on the nanofibril surfaces, and the relatively high surface area in relation to nanofibril volume. We measured the amount of absorbed water by immersing an untreated aerogel in water for 30 min and weighing the aerogel after removal from the water. The untreated nanocellulose aerogel absorbs water ca. 35 times its own weight (absorbent capacity $m_{\text{absorbed water}}/m_{\text{aerogel}} = 35$). The measured volume increase was below 2%. Such a high absorption value is qualitatively expected, taking the aerogel porosity of 98%, and the densities of water and cellulose (1.00 and 1.55 g cm^{-}

^{3}, respectively) into account. Therefore, the material can be classified as superabsorbent. By contrast, upon TiO_2 deposition, the nanocellulose aerogel becomes highly hydrophobic, with contact angle of 140° (see Fig. 5.12.). The aerogel floats on the water and very little water is absorbed within the aerogel after TiO_2 coating: simple weighing suggested that after forced immersion in water, only 0.6 times the aerogel weight of water is absorbed (see Fig. 5.13.). However, it should be noted that a large fraction of this water might actually be adsorbed onto the surface due to the adhesive pinning of water despite of the high hydrophobicity.

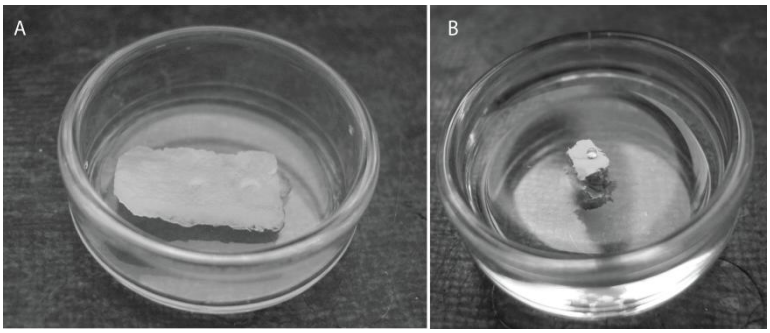

Figure 5.13. Untreated nanocellulose aerogel absorbs water 30 times its own weight (a), whereas the TiO_2-coated nanocellulose aerogel shows water repellency when floating on water (b). (Note that the aerogels in a) and b) were originally different in size.

Upon UV illumination, the TiO_2 -coated aerogels underwent a transition from the water-repellent state back to the water-absorbing state with a vanishing contact angle as seen in Fig. 5.12. UV illumination strongly increases the hydrophilicity of TiO_2. Therefore, absorption is drastically increased and 16 times of the aerogel weight of water is absorbed. The water repellence, with a high contact angle of 135°, recovers slowly upon storage in the dark (Fig. 5.12.).

The photocatalytic activity of these TiO_2-coated nanocellulose aerogels was demonstrated by methylene blue (MB) decomposition. The reaction was carried out in a quartz cell containing 3 mL of 0.03 mM aqueous MB solution. UV illumination was performed at wavelength of 365 nm, with intensity of ~2 mW cm^{-2}. The decomposition of MB can be observed from the variations in maximal absorption of the UV–visible spectra. Typically, MB solutions display maximal absorbance at 668 and 609 nm,[215] occurring at 665 nm in the present case. The UV-Vis spectra of the samples in the presence and absence of TiO_2 under UV illumination, as well as without UV illumination are presented in Fig. 15.14 a, c and d, respectively. The absorbance of MB decreased over time in all samples due to adsorption of MB on the fibril

surface. However, it can be clearly observed from the spectrum a, that when both TiO_2 and UV light is present, the main absorbance band of MB shifts strongly from 665 to 603 nm. This did not take place with the reference measurements. The shift results from N-demethylation of MB due to photocatalytic degradation.

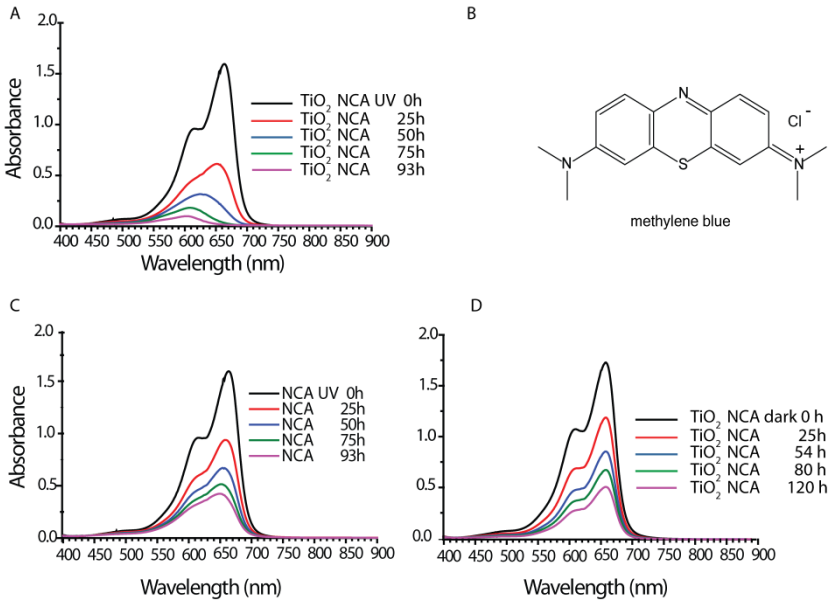

Figure 5.14. Spectral changes during the photodecomposition of methylene blue (MB) on TiO_2-coated nanocellulose aerogel (NCA) in the presence of TiO_2 and UV (a), absence of TiO_2(c) and absence of UV (d). The molecular structure of MB (b).

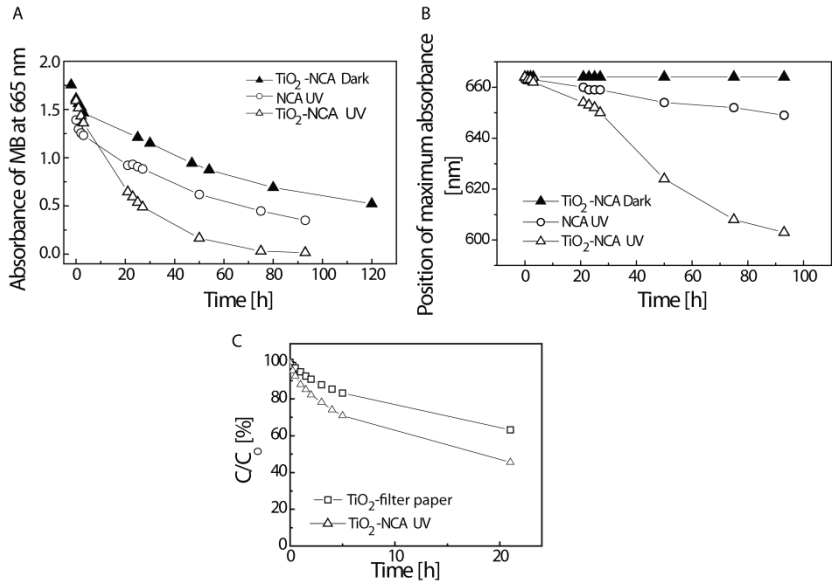

Figure 5.15. Absorbance of MB (a), and the position of maximum absorbance (b), as a function of time. As a reference for the TiO_2 -coated nanocellulose aerogel (NCA) sample illuminated with UV light (open triangles) the absorbance of MB with native NCA (i.e., no TiO_2 deposition) under UV radiation (open circles) as well as TiO_2 –coated NCA in the dark (filled triangles) are shown. (c) The photocatalytic activity of TiO_2-coated filter paper and NCA to decompose MB.

The photocatalytic decomposition is presented more clearly as a function of time in Fig. 5.15. When the absorbance of MB at 665 nm is plotted as a function of UV illumination time, the absorbance of MB decreased at a significantly higher rate than in the reference measurements, where either the TiO_2 or UV light was absent, as seen Fig. 5.15.a. The fact that absorbance of MB goes to zero, indicates that MB is photocatalytically decomposed. The shift results from *N*-demethylation of MB due to photocatalytic degradation.[215] Moreover, the main absorbance peak of MB shifted strongly from 665 to 603 nm when both TiO_2 and UV light were present, as presented in Fig. 5.15.b. This did not take place in the reference measurements. After 24 h of weak UV illumination 65% of the MB was decomposed. The activity is good taking into account the amorphous nature of the present CVD TiO_2 coating. Indeed, it has been reported that the amorphous TiO_2 nanoparticles show reduced photocatalytic activity.[170, 216] To put this result in perspective, the photocatalytic activity of the frequently used cellulose substrate, filter paper, was demonstrated under same conditions. As presented in Fig. 5.15.c, the decomposition is slower and the decomposed amount of MB is smaller in TiO_2-coated filter paper. After 24 h UV illumination ~ 45% of the MB was decomposed. Photocatalytic decomposition rates of MB in TiO_2 has been

shown to scale with light intensity.[215] Moreover, photocatalytic activity of TiO_2 coatings depend strongly on the phase, the crystallite size and the porosity of the coatings.[166] Previously, cellulose fibers coated with nanocrystalline TiO_2 particles by sol-gel process, showed only slightly higher photocatalytic decomposition activity in comparison with the present amorphous TiO_2 coating, even though the illumination intensity used was significantly higher than in the present system.[166] Interestingly, amorphous TiO_2 particles immobilized in regenerated cellulose film showed lower activity compared to present work.[176] Therefore, we believe that aerogel structure plays important role in photocatalytic activity. Next the influence of aerogel structure on wetting, absorption and photocatalytic activity is discussed more in detail by means of morphology and porosity based on SEM and AFM.

Structure-enhanced wetting

The large change of the aerogels from a strongly absorbing, very hydrophilic material to a near-superhydrophobic and water-repellent material after TiO_2 coating is remarkable, considering that initially both the substrate and the TiO_2 coatings are fairly hydrophilic. Indeed, the contact angle of water with a smooth and fresh TiO_2 surface is 15°.[145] As discussed in Chapter 4.2.1 surface roughness and porosity plays an important role in wetting as well as in catalytic activity. This was demonstrated by using TiO_2-coated filter paper as a reference. In the aerogels, nanofibrils are assembled into multiple length scales structures: micron scale sheets and nanoscale fibrils. Furthermore, the voids between the sheets form macrochannels through the aerogel while within the sheets there are nanoscale pore network, as seen in SEM images (Fig. 5.16.). Together these structures contribute multiple scale roughness.

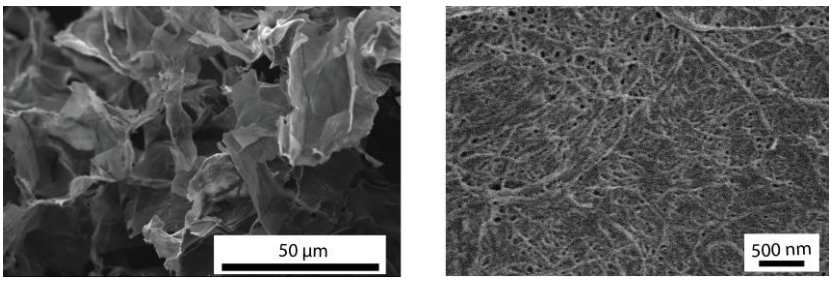

Figure 5.16. Low magnification SEM image of the TiO_2-coated aerogels shows the interconnected micronscale sheets and voids. The high magnification SEM image shows nanofibrils and nanoscale pore network within the sheet.

Accordingly, a 3D AFM topographical image of TiO2-coated aerogels (Figure 5.17.) reveals the internal porous network within the sheet forming the aerogel skeleton. The sheets, in turn, show microscale ridges and re-entrant

structures. The ridges result in the wavy structure to the sheets with typical height of over one micrometer (microroughness). Besides, at the smallest scale, the sheet shows hierarchical nanoscale roughness by AFM (Fig. 5.17.). Indeed, two roughness levels can be observed, one at 200 nm and the other at ~ 25 nm. Consequently, the aerogel consists of multiple length scale structures, which enable some air trapping and promotes high contact angle of 140°.

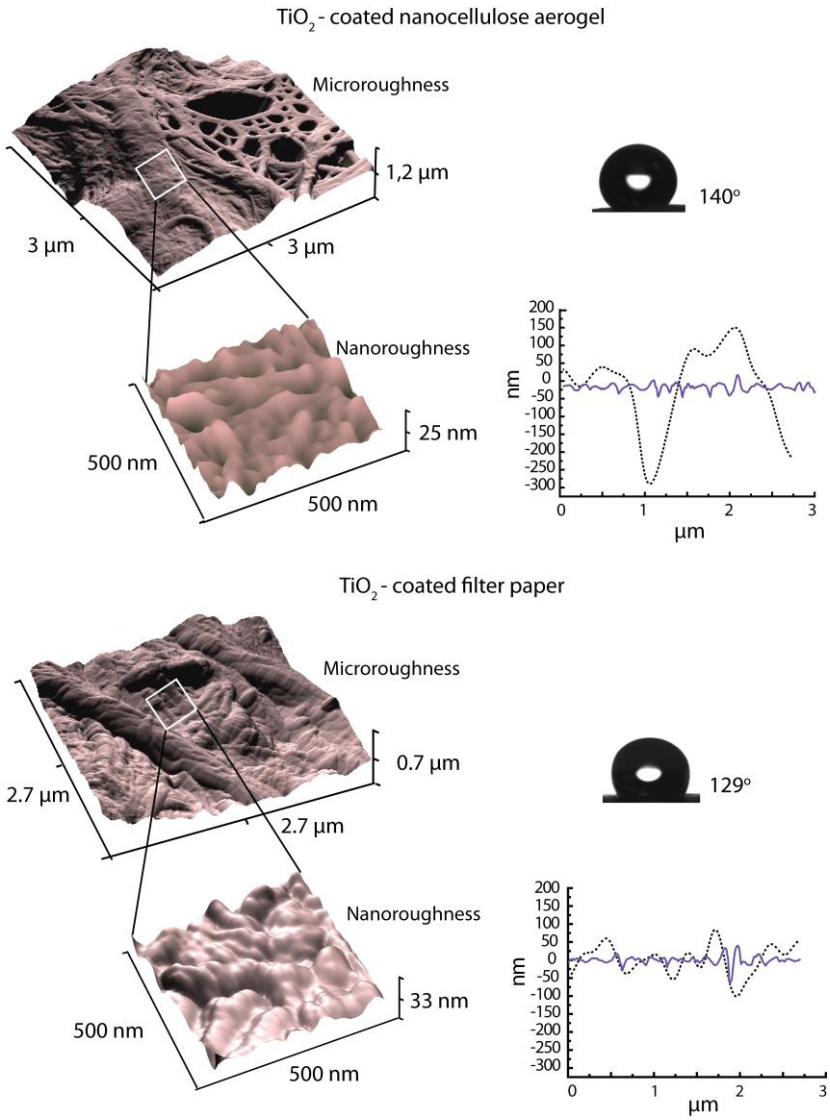

Figure 5.17. Topographical 3D AFM images of the TiO_2-coated aerogels and the TiO_2-coated filter papers, and resulted roughness.

By contrast, in the TiO_2-coated filter papers, the hierarchy and porosity is reduced. The TiO_2-coated filter paper is composed of macroscopic flattened

fibers that have topographical height of lower than 1 μm, as seen in the AFM image (Fig. 5.17.) The reduced hierarchical roughness and porosity leads to a smaller contact angle of 129°.

The need for structures at multiple length scales was also realized in the other cellulose (super)hydrophobization studies. While macroscopic cellulose fibers, such as in filter paper, provided the large microscale roughness, the hierarchy with nanoscale structures was necessary to generate by additional means, e.g. by fluorinating nanostructures,[161, 162] nanoscale silicone,[163] metal oxide–silane nanocoatings,[164] gold nanoparticles,[165] or by etching the fibers.[156] By contrast, in this work, cellulose nanofibrils provide both micro- and nanoscale structures and pores, due to their spontaneous aggregation, thus affording particularly simple preparations.

The impact of the hierarchically porous structure was observed also in absorption. An untreated hydrophilic filter paper with a rather high overall porosity of 73 %, can absorb only 1.4 times its own weight, while the nanocellulose aerogel absorbs 35 times its own weight. Even if the absorption and wetting are separate phenomena, being bulk and surface properties, they are still connected. The pores and structures at different length scales, formed during the vacuum freeze-drying, play an important role in both absorption and wetting of the TiO_2–coated aerogels. This material shows how the increased surface area with multiple length scale structures and pores increases the hydrophilicity of hydrophilic material, as well as the hydrophobicity of hydrophobic materials: at the superabsorbing state, the continuous pore network and structures at different length scales promote the facile water absorption, while at the water-repellent state, the structures promote formation of re-entrant structures, evidenced by a high contact angle.

Structure-enhanced photocatalysis

Photocatalytic activity of the TiO_2-coated nanocellulose aerogels is enhanced due to increased surface area and porosity. The BET surface area of filter paper is ~ 1 g m^{-2}, while the present aerogel exhibits a surface area of 20 g m^{-2}. Consequently, also the total amount of titanium deposited on the aerogel during CVD is higher, ~ 8.0 %, versus only 0.9 % of the filter paper (under the same conditions), explaining the difference in photocatalytic activity. Interestingly, according to roughness analysis based on the AFM, the nanoroughness of the aerogel actually decreased from 48 nm to 25 nm upon deposited 7 nm thick TiO_2 coating, still showing enhanced activity compared to filter paper. The roughness of the filter paper was not changed noteworthy upon the coating. The larger BET surface area results in the large contact areas between the active sites and the target substrate in photocatalysis. In

addition, the highly porous structure of the aerogel diffuses rapidly the reactants into the structure.

5.4 Structural Aspects in Bio-inspired Nanocellulose Aerogels (Publication IV)

As demonstrated in the previous publication and discussed earlier in chapter 4.2.1., multiple scale structures and air trapping play an important role in practical applications of the superhydrophobic surfaces. Inspired by the light weight and multiple length scales in the aerogel structure, common to water strider leg, we demonstrated a bio-inspired vacuum dried nanocellulose aerogel with load carrying capacity by CVD of fluorosilane[199] in Publication **IV**. In this thesis, the structural features of the fluorinated nanocellulose aerogel are discussed simplified with relation to hydrophobicity, strong adhesive force and supporting. In a rough analogy to water strider leg, our nanocellulose membranes show structures at several length scales, but in the present case fibrils form networks, from nanometer scale individual nanofibrils up to micrometer scale nanofibrous aggregates and sheets, as presented in Fig. 5.18. Rather than mimicking the setae that are connected only at one end to the water strider leg, we incorporate networks of fibrils, which are expected to be more robust.

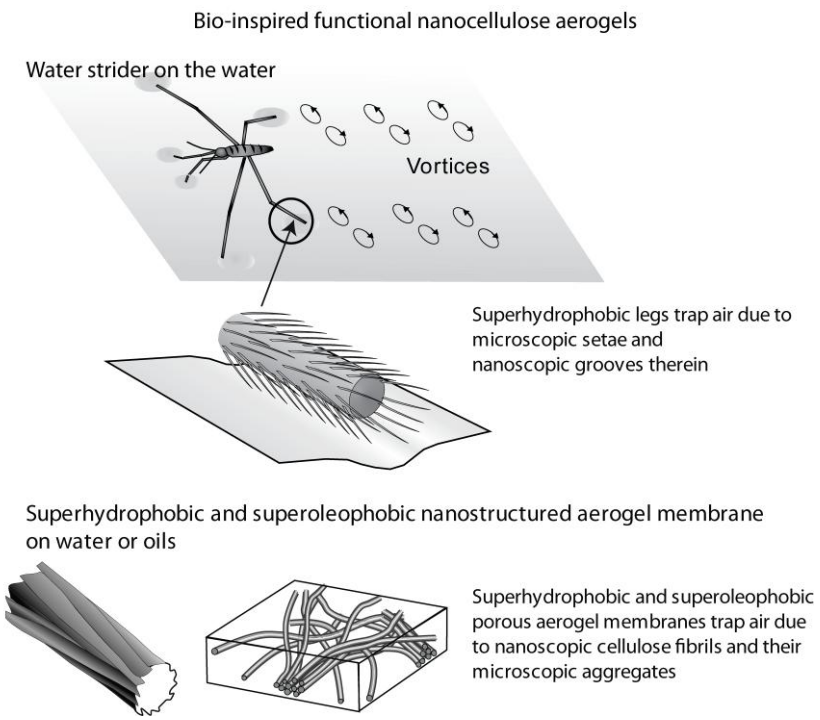

Figure 5.18. The nanocellulose aerogel shows structures at different length scales that promote air trapping and hydrophobicity of functionalized aerogel. The fluorinated aerogel is capable of floating and cargo carrying [199, 217]

The legs of water strider secrete a wax, which make the legs hydrophobic and cause surface tension effect. The contact angle of the flat surface of the secreted wax is only ~105°.[160] However, Gao et al. showed that it is not enough for that significant water repellence and strong supporting force but it is achieved by the hierarchical structures in the leg.[160] To generate hydrophobicity to nanocellulose aerogel, it was fluorinated by CVD with trichlorosilanes in "bottle-in-bottle" setup. It is known that maximum contact angle of flat fluorinated surface is roughly 120°.[218] Beyond that, contact angle value is influenced by the surface roughness. We observed water contact angles above 150° for the fluorinated nanocellulose aerogels, indicating superhydrophobicity, as seen in Fig 5.19. However, the droplet is highly pinned onto the surface even when tilted 180°. In addition to high water contact angles, we observed high contact angles of 153° and 158° also for paraffin oil and mineral oil, respectively, indicating additional superoleophobicity.

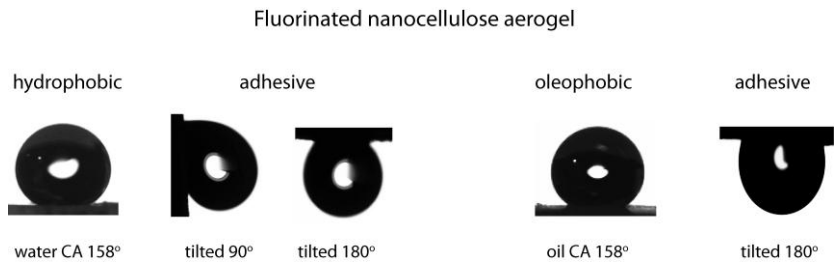

Figure 5.19. Fluorinated nanocellulose aerogels are high-adhesive superhydro- and superoleophobic materials.

The result is encouraging, as superoleophobic surfaces with CA > 150° for oils are rare and considerably more challenging to construct, as the surface tension of oils is only a fraction of that of water. In addition to chemical composition and roughened surface, a third parameter is required for superoleophobicity, that is, re-entrant surface curvatures in the form of overhang structures, introduced by Tuteja et al.[219] They showed that spacing ratios play important role in designing superoleophobic surfaces: not only the size of features but also the distance between features affects the wetting properties of surfaces. The overhangs can be realized as fibers[219], mushroom-like structures[219], and pores.[220] The oleophobicity confirms the existence of re-entrant structures in the present vacuum dried aerogels. Superoleophobic surfaces are appealing e.g. in antifouling, since purely superhydrophobic surfaces are easily contaminated by oily substances in practical applications, which in turn will impair the liquid repellence. However, the fluorinated nanocellulose aerogel shows also high adhesion, as the oil droplet remain pinned at tilted angles, as illustrated in Fig. 5.19.

Interestingly, also the previously introduced very hydrophobic TiO_2-coated nanocellulose aerogel shows adhesive pinning of the water droplet when tilted, as presented in Fig. 5.20. While the fluorinated nanocellulose aerogels are both hydrophobic and oleophobic, the TiO_2-coated aerogels are hydrophobic but oleophilic. The oleophilic character originates from TiO_2, as discussed in chapter 4.2. However, in the both aerogels, hydrophobicity is enhanced by the increased surface roughness, arising from multiple scale structures and pores on the surface.

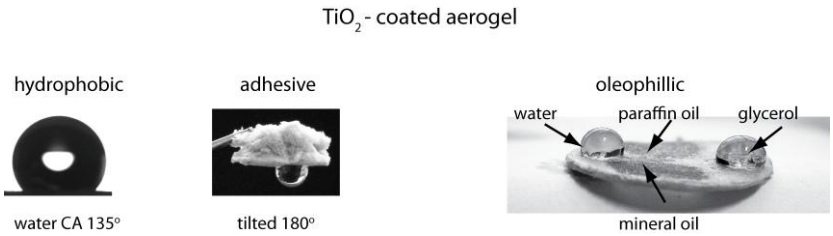

Figure 5.20. TiO_2-coated nanocellulose aerogels are highly adhesive hydrophobic but oleophilic materials.

In the adhesive superhydrophobic surfaces, generally, the hierarchical micro- and nanostructures are different in size from those of the lotus leaf which are nonwettable.[155] As discussed earlier, it is not only the multiple scale roughness which need to be taken into account when designing superhydrophobic surfaces, but also the right geometry, height and its ratio in the structures, play an important role. It is important to note, that the surface roughness of the present aerogels is comprised of heterogeneous structures, pores and voids that are irregularly distributed and uneven in height. However, the nanocellulose aerogels offer overhang structures and multiple length scales required for both superhydro- and oleophobicity. What comes to the high adhesion of the both surfaces, high porosity is suggested to play the key role: when wetted, the substantial number of nano- and micropores produce a miniscule capillary forces, and together with the roughness originating from the fibril aggregates create a large adhesion, as suggested by Guo et al. for sticky superhydrophobic surface[157]. Furthermore, the influence of high porosity on adhesion can be explained with the other suggested mechanism: pores and voids increase substantially the number of possible air pockets with sealed air, which induce negative pressure.

Despite the high adhesive pinning of the droplet, the superhydrophobic and superoleophobic character of fluorinated nanocellulose aerogel enable floating and load bearing capability on both, water and oily liquids. They are capable of supporting a weight nearly three orders of magnitude larger than the weight of the aerogel itself.[199] This could be conceptually interesting for, for example, autonomous devices sensing pollution on water or oil.

5.5 Bio-Based Selective Membrane for Oil Spill Removal (Publication V)

As we previously demonstrated the floating and superabsorbing characters, as well as the hydrophobicity and the oleophilicity of functionalized nanocellulose aerogels, we wanted to further benefit from these properties. Therein, it became particularly attractive to extend the TiO_2-coating approach and investigate the functionalized aerogels as a selectively absorbing membrane for oil spill removal. Cleaning oil spills under a marine environment is a challenging task. The collection of oil is often preferred instead of in-situ burning or using dispersing agents that facilitate natural degradation, as it enables proper disposal of the oil. In oil collection, traditional choice for absorbent material is sawdust, which however, suffers from large coincident water absorption along with the oil that needs to be separated. Thus, there is a need for selective materials that do not absorb water but are able to rapidly absorb a large amount of oil. The materials should be robust, floating, reusable, recyclable and environmentally friendly, and able to incinerate along with the oil they absorb. Despite that the previously reported materials, such as polypropylene fiber mats[221, 222], silica aerogels,[223-225] carbon nanotube aerogels[226] and manganese oxide nanofiber membranes[227] showed various oil intake from 15[222] to even 180[226] times their original dry weight, they suffered from poor retention, brittleness, sustainability and safety issues. Porous nanocellulose materials fulfil all the above-mentioned requirements, being also widely abundant, renewable, sustainable and safe material for environmental applications.

We utilized similarly TiO_2-coated nanocellulose aerogels described in chapter 5.3. which show small density of 20-30 mg cm^{-3} and a porosity of >98%, and that are hydrophobic and oleophilic (Publication **V**). This functionalized aerogel absorbs a variety of organic solvents and oils, and on the other hand, repels water as shown previously in Fig 5.20. The droplets of water and also glycerol (as another example of a polar, viscous liquid) on the surface demonstrate the hydrophobicity (contact angle >90°) of the material, while paraffin oil and mineral oil demonstrate the oleophilicity, as the oils readily absorb into the aerogel. When a hydrophobic aerogel is immersed in water, the water absorption is unsubstantial, as discussed previously. On the contrary, the aerogel absorbs a large amount of oil within the interior pores from the surface of water as demonstrated in Fig. 5.21. An oil spill with a volume almost equal to the overall volume of the aerogel is absorbed when the aerogel is placed onto the paraffin oil spill (colored with Nile Red dye for clarity).

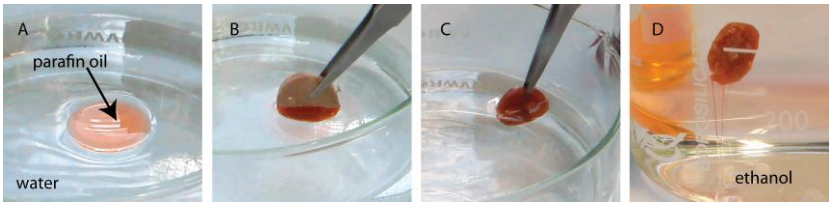

Figue 5.21. Oil spill removal from water (a) paraffin oil (colored for clarity) floating on water;(b) the oil being absorbed into the aerogel; and (c) all of the floating oil has been absorbed;(d) the oil-filled aerogel can be washed simply by immersing it in a solvent, such as ethanol. The oil gets removed as shown by the red streaks.

The weight of the absorbed oil is ca. 30 times the dry weight of the aerogel. By immersing the aerogel directly into paraffin oil, up to 40 times of the original weight could be absorbed. However, the excess seemed to be oil adhering outside the aerogel. The oil-filled aerogel can be left floating on water without water penetration into the structure, or oil release, as the weight of the soaked aerogel decreases only by 5% after 24 h. Besides, floating of oil-filled aerogel on water dyed with Reactive Blue, showed no color after removal, which also confirms that oil is not replaced by water. When weighing the oil filled aerogel 24 h after removing it from water, 95% of the oil was still retained in the aerogel. Importantly, we showed that the absorbed paraffin oil could be completely removed by immersing the oil-soaked aerogel into an organic solvent, such as ethanol or octane. Fig. 5.21.d shows a paraffin oil-filled aerogel dropped into a glass jar containing ethanol. The oil is immediately released as shown by the red stained streaks. The weight difference of the dry aerogel after and before the oil immersion was very low (ca. 0.6% of the absorbed amount) manifesting that practically no oil was left in the aerogel.

To test the reusability of the aerogel we immersed an aerogel in an organic solvent (toluene) for 10 times and measured the weights before and after drying. The results shown in Fig. 5.22.a indicate that the absorption capacity does not deteriorate and the dry weight of the aerogel does not change when the aerogel is reused multiple times. After this reusability experiment, the aerogel was immersed in water and it still did not absorb water, which indicates that the hydrophobicity was not lost. After the cycles, a number of different organic solvents along with some oils were absorbed and the aerogel was dried a total of 20 times without any measurable change in the dry weight or the absorption capacity indicating durability and reusability. The ratios of the final and initial weights upon full absorption m/m_0 (w/w) are shown in Fig. 5.22.b along with theoretical maximum lines corresponding to given constant volume (100% and 80% vol/vol plotted) intake within the aerogel.

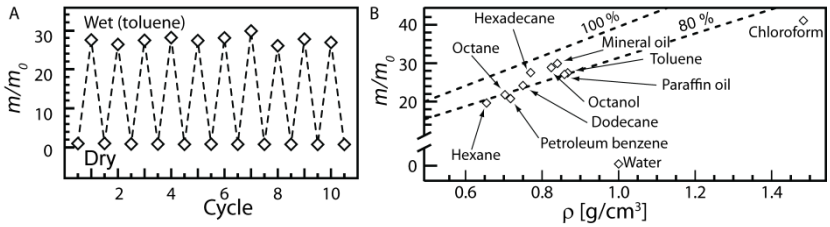

Figure 5.22. The reusability of aerogel absorbent (a) and the mass-based absorption capacity for different organic solvents and oils as a function of the density of the liquid (b).

The aerogels are made from nanocellulose, which is sustainable and can be simply incinerated along with the absorbed oil. Here the low-surface energy coating was TiO_2, but other inorganic coatings, such as octyltrichlorosilane,[228] or surfactants could lead to similar results. In the end, as the TiO_2-coated nanocellulose aerogels can be reused, recycled, or incinerated with the absorbed oil, and cellulose as well as titanium dioxide are environmentally friendly, this work paves way for nanocellulose-based oil absorbents for sustainable applications.

In various other functionalization of the n[22]ative nanocellulose aerogels, demonstrated after the present work, the morphology and mechanical properties have been utilized in various ways. The network of bacterial cellulose aerogel can serve as a substrate for non-agglomerating growth of ferromagnetic cobalt ferrite nanoparticles, to form magnetic aerogels.[203] They showed superior mechanical properties, higher porosity, lower density, as well as smaller and more controlled nanoparticles than accordingly prepared magnetic regenerated cellulose II aerogels.[116] The native nanocellulose aerogels have been also applied as a template for inorganic hollow nanotube aerogels, that are suitable for fast response resistive humidity sensor.[207] Furthermore, they can be considered as an effective supporting material for metal ion catalysts.[202] The mechanical behaviour of the native nanocellulose aerogels has been further improved by cross-linking, which turn the aerogel into shape recoverable in water.[201] In addition to floating and cargo carrying, the fluorinated native nanocellulose aerogels have been showed to allow Marangoni-driven self- propulsion as they are gas permeable from their open-porous structure.[217] Moreover, spray dried porous fluorosilane modified microparticles show self-cleaning and water droplet manipulation.[229] Importantly, these recently developed native cellulose aerogels have shown their superiority in functionality, mechanical properties, and in sustainability, as well as in biocompatibility compared to previous aerogels, thus expanding the applicability of aerogels even more.

6. Conclusions and Outlook

The results presented in this thesis demonstrate the applicability of the native cellulose nanofibrils as building blocks for functional and responsive materials. First, we have shown in Publication I that NFC, as isolated by mechanical and enzymatic treatments forms inherent hydrogel networks in water without chemical cross-linking, leading to high storage modulus even at very low concentrations. Furthermore, the NFC hydrogel shows strong shear thinning, which is beneficial in processability and in applications, considering the easy mixing and dispensing. Next, in Publication II it was demonstrated that the strong nanofibril network enables porous aerogels. In contrast to most previous aerogels, which are brittle, the shown native nanocellulose aerogels are ductile and deformable, despite the high porosity of 98% and randomly organized structure. Controlling of the overall aerogel structure by freeze-drying allow tuning of to the mechanical properties and the morphology. The present nanocellulose aerogels are composed of micronscale sheets or flocs that, in turn, consist of nanoscale fibrils, generating dual scale structure into the aerogel. Furthermore, the aerogels contain hierarchical porosity: the pores between the sheets and flocs form macrochannels through the aerogel, while a nanoscale pore network is formed between the fibrils. These aerogel skeletons provide a percolative template for conducting material, e.g. polyaniline to achieve highly porous conducting materials.

The nanocellulose aerogels are also versatile templates for functional coatings to tune the surface activity, and to allow responsive materials as demonstrated in Publications III, IV and V. The TiO_2-coated nanocellulose aerogels are functional, i.e. show photo-triggered wetting and absorption transformations. We have shown that the original nanocellulose aerogel is very hydrophilic and act as a superabsorbent, absorbing water 35 times its own weight. Upon CVD of TiO_2 on the nanocellulose aerogel, it became hydrophobic with negligible absorption. The UV illumination, on the other hand, changes the surface structure of the TiO_2-coated nanocellulose aerogel and switches the material to be superabsorbent again. Besides the photoresponsive wetting and adsorption, we demonstrated the improved photocatalytic decomposition of organic matter based on the enhanced

surfaced area and hierarchical porosity of the TiO_2-coated nanocellulose aerogel. In addition, TiO_2 coating on the nanocellulose aerogel provides means to tailor the selectivity of the absorption due to its hydrophobic but oleophilic character. By exploiting the selectivity of the TiO_2-coated aerogel for water and oil and the superabsorbency of porous nanocellulose template, we demonstrated sustainable and water floating selectively absorbing membrane for oil spill removal.

Moreover, we showed combined superhydro- and oleophobicity based on fluorinated nanocellulose aerogels. The result is encouraging, as superoleophobic surfaces are rare and considerably more challenging to construct. Superoleophobic surfaces are appealing e.g. in antifouling, since purely superhydrophobic surfaces are easily contaminated by oily substances in practical applications, which in turn will impair the liquid repellence.

The results presented in this thesis demonstrate that nanocelluloses allow novel properties within the class of cellulose-based materials. One of the most obvious advantages of exploiting cellulose nanofibrils e.g. for preparation of porous templates is that the high aspect ratio cellulose nanofibrils enable very low gel concentrations, and very low density and highly porous light weight aerogels. Importantly, the cellulose nanofibril network is robust against the collapse upon drying, thus allowing a facile drying process. Moreover, the results presented in this thesis show that the nanocellulose aerogels enable feasible templates, not only by serving as a support for functional materials, but also enhancing the effects of functional coating. The native nanocellulose aerogels offer re-entrant curvatures, and multiple length scaled structures and pores required for both superhydro- and oleophobicity, as well as improve the absorption and photocatalysis.

We believe that these results will not only contribute to the basic understanding of the behavior of cellulose nanofibrils but they also suggest novel types of sustainable applications in materials science beyond the classic cellulose applications. During and after the publications shown in this work, significant development has taken place regarding the production, modification, and use of nanocellulose aiming for sustainable materials, driven by various research groups around the world. Importantly, nanocellulose materials can lead to strengthening of the competitiveness of the forest industry in its changing operational environment.

Altogether, this work has aroused a number of questions, many of which remain unanswered. Therefore, the work as such should be considered as a beginning, not the end. What are the key advantages and ultimate limitations of the use of cellulose nanofibrils in future material development? Despite the fact that the nanocellulose materials have been proven to be able to compete successfully in various properties with extensively used synthetic polymers, the production methods and the costs still limit the final commercial success.

How to find the feasible preparation method, which is able to maintain as many valuable properties as possible needed in the applications? Or which preparation method generates fibrils that can best be utilized in the various applications? How to fully exploit the superior mechanical properties of the cellulose nanofibrils in various applications? What are the key value-added products, which ensure the commercial success of cellulose nanofibrils in the future? Those are some of the questions that will be answered in the near future.

7. Bibliography

[1] S. J. EICHHORN, *Soft Matter* **7**, 303 (2011).

[2] R. J. MOON, A. MARTINI, J. NAIRN, J. SIMONSEN, J. YOUNGBLOOD, *Chem. Soc. Rev.* **40**, 3941 (2011).

[3] D. KLEMM, F. KRAMER, S. MORITZ, T. LINDSTRÖM, M. ANKERFORS, D. GRAY, A. DORRIS, *Angew. Chem. Int. Ed.* **50**, 5438 (2011).

[4] N. LAVOINE, I. DESLOGES, A. DUFRESNE, J. BRAS, *Carbohydr. Polym.* **90**, 735 (2012).

[5] Y. HABIBI, L. A. LUCIA, O. J. ROJAS, *Chem. Rev.* **110**, 3479 (2010).

[6] I. SIRÓ, D. PLACKETT, *Cellulose* **17**, 459 (2010).

[7] S. J. EICHHORN, A. DUFRESNE, M. ARANGUREN, N. E. MARCOVICH, J. R. CAPADONA, S. J. ROWAN, C. WEDER, W. THIELEMANS, M. ROMAN, S. RENNECKAR, W. GINDL, S. VEIGEL, J. KECKES, H. YANO, K. ABE, M. NOGI, A. N. NAKAGAITO, A. MANGALAM, J. SIMONSEN, A. S. BENIGHT, A. BISMARCK, L. A. BERGLUND, T. PEIJS, *J. Mater. Sci.* **45**, 1 (2010).

[8] G. A. OZIN, A. C. ARSENAULT, *Nanochemistry; A Chemical Approach for Nanomaterials*. RSC Publishing: Cambridge, 2005.

[9] B. XIN, J. HAO, *Chem. Soc. Rev.* **39**, 769 (2010).

[10] N. LIN, J. HUANG, A. DUFRESNE, *Nanoscale* **4**, 3274 (2012).

[11] D. KLEMM, T. HEINZE, U. HEINZE, K. J. EDGAR, B. PHILIPP, P. ZUGENMAIER, *Comprehensive cellulose chemistry* 2. ed., Wiley-VCH: 2009.

[12] A. O'SULLIVAN, *Cellulose* **4**, 173 (1997).

[13] Y. NISHIYAMA, P. LANGAN, H. CHANZY, *J. Am. Chem. Soc.* **124**, 9074 (2002).

[14] Y. NISHIYAMA, J. SUGIYAMA, H. CHANZY, P. LANGAN, *J. Am. Chem. Soc.* **125**, 14300 (2003).

[15] Y. NISHIYAMA, G. P. JOHNSON, A. D. FRENCH, V. T. FORSYTH, P. LANGAN, *Biomacromolecules* **9**, 3133 (2008).

[16] M. JARVIS, *Nature* **426**, 611 (2003).

[17] P. ZUGENMAIER, *Prog. Polym. Sci.* **26**, 1341 (2001).

[18] R. H. ATALLA, D. L. VANDERHART, *Science* **223**, 283 (1984).

[19] P. LANGAN, Y. NISHIYAMA, H. CHANZY, *J. Am. Chem. Soc.* **121**, 9940 (1999).

[20] P. LANGAN, Y. NISHIYAMA, H. CHANZY, *Biomacromolecules* **2**, 410 (2001).

[21] S. J. EICHHORN, C. A. BAILLIE, N. ZAFEIROPOULOS, L. Y. MWAIKAMBO, M. P. ANSELL, A. DUFRESNE, K. M. ENTWISTLE, P. J. HERRERA-FRANCO, G. C. ESCAMILLA, L. GROOM, M. HUGHES, C. HILL, T. G. RIALS, P. M. WILD, *J. Mater. Sci.* **36**, 2107 (2001).

[22] Y. NISHIYAMA, *J. Wood Sci.* **55**, 241 (2009).

[23] A. N. FERNANDES, L. H. THOMAS, C. M. ALTANER, P. CALLOW, V. T. FORSYTH, D. C. APPERLEY, C. J. KENNEDY, M. C. JARVIS, *PNAS* **108**, E1195 (2011).

[24] T. ZIMMERMANN, E. PÖHLER, T. GEIGER, J. SCHLEUNIGER, P. SCHWALLER, K. RICHTER, Cellulose Fibrils: Isolation, Characterization, and Capability for Technical Applications. In *Cellulose Nanocomposites*, ACS: 2006; Vol. 938, pp 33.
[25] S. BECK-CANDANEDO, M. ROMAN, D. G. GRAY, *Biomacromolecules* **6**, 1048 (2005).
[26] S. ELAZZOUZI-HAFRAOUI, Y. NISHIYAMA, J. L. PUTAUX, L. HEUX, F. DUBREUIL, C. ROCHAS, *Biomacromolecules* **9**, 57 (2008).
[27] G. GRAY DEREK, M. ROMAN, Self-Assembly of Cellulose Nanocrystals: Parabolic Focal Conic Films. In *Cellulose Nanocomposites*, American Chemical Society: 2006; Vol. 938, pp 26.
[28] J. F. REVOL, H. BRADFORD, J. GIASSON, R. H. MARCHESSAULT, D. G. GRAY, *Int. J. Biol. Macromol.* **14**, 170 (1992).
[29] K. FLEMING, D. G. GRAY, S. MATTHEWS, *Chem. Eur. J.* **7**, 1831 (2001).
[30] M. A. S. A. SAMIR, F. ALLOIN, A. DUFRESNE, *Biomacromolecules* **6**, 612 (2005).
[31] F. W. HERRICK, R. L. CASEBIER, J. K. HAMILTON, K. R. SANDBERG, *J. Appl. Polym. Science: Appl. Polym. Symp.* **37**, 797 (1983).
[32] A. F. TURBAK, F. W. SNYDER, K. R. SANDBERG, *J. Appl. Polym. Sci.: Appl. Polym. Symp.* **37**, 815 (1983).
[33] A. N. NAKAGAITO, H. YANO, *Appl. Phys. A* **78**, 547 (2004).
[34] T. ZIMMERMAN, E. PÖHLER, T. GEIGER, *Adv. Eng. Mater.* **6**, 754 (2004).
[35] T. TANIGUCHI, K. OKAMURA, *Polym. Int.* **47**, 291 (1998).
[36] S. IWAMOTO, A. N. NAKAGAITO, H. YANO, M. NOGI, *Appl. Phys. A* **81**, 1109 (2005).
[37] K. ABE, S. IWAMOTO, H. YANO, *Biomacromolecules* **8**, 3276 (2007).
[38] M. HASSAN, A. MATHEW, E. HASSAN, N. EL-WAKIL, K. OKSMAN, *Wood Sci. Technol.* **46**, 193 (2012).
[39] B. WANG, M. SAIN, *Polym. Int.* **56**, 538 (2007).
[40] M. PÄÄKKÖ, M. ANKERFORS, H. KOSONEN, A. NYKÄNEN, S. AHOLA, M. ÖSTERBERG, J. RUOKOLAINEN, J. LAINE, P. T. LARSSON, O. IKKALA, T. LINDSTRÖM, *Biomacromolecules* **8**, 1934 (2007).
[41] M. HENRIKSSON, G. HENRIKSSON, L. A. BERGLUND, T. LINDSTRÖM, *Eur. Polym. J.* **43**, 3434 (2007).
[42] M. ANKERFORS, Microfibrillated cellulose:Energy-efficient preparation techniques and key properties, Licentiate Thesis, KTH, Stockholm, (2012).
[43] T. SAITO, Y. NISHIYAMA, J. L. PUTAUX, M. VIGNON, A. ISOGAI, *Biomacromolecules* **7**, 1687 (2006).
[44] T. SAITO, S. KIMURA, Y. NISHIYAMA, A. ISOGAI, *Biomacromolecules* **8**, 2485 (2007).
[45] A. ISOGAI, T. SAITO, H. FUKUZUMI, *Nanoscale* **3**, 71 (2011).
[46] L. WÅGBERG, G. DECHER, M. NORGREN, T. LINDSTRÖM, M. ANKERFORS, K. AXNÄS, *Langmuir* **24**, 784 (2008).
[47] S. JANARDHNAN, M. SAIN, *BioResources* **1**, 176 (2006).
[48] M. HENRIKSSON, Cellulose Nanofibril Networks and Composites. Preparation, Structure and Properties Doctoral Thesis, KTH, Stockholm, (2008).
[49] T. SAITO, A. ISOGAI, *Tappi Journal* **4**, 3 (2005).
[50] T. SAITO, M. HIROTA, N. TAMURA, S. KIMURA, H. FUKUZUMI, L. HEUX, A. ISOGAI, *Biomacromolecules* **10**, 1992 (2009).
[51] M. HENRIKSSON, L. A. BERGLUND, P. ISAKSSON, T. LINDSTRÖM, T. NISHINO, *Biomacromolecules* **9**, 1579 (2008).
[52] D. KLEMM, D. SCHUMANN, U. UDHARDT, S. MARSCH, *Prog. Polym. Sci.* **26**, 1561 (2001).
[53] D. KLEMM, B. HEUBLEIN, H.-P. FINK, A. BOHN, *Angew. Chem. Int. Ed.* **44**, 3358 (2005).

[54] S. IFUKU, M. NOGI, K. ABE, K. HANDA, F. NAKATSUBO, H. YANO, *Biomacromolecules* **8**, 1973 (2007).
[55] A. DUFRESNE, J. Y. CAVAILLE, M. R. VIGNON, *J. Appl. Pol. Sci.* **64**, 1185 (1997).
[56] J. ARAKI, M. WADA, S. KUGA, T. OKANO, *Colloids Surf., A* **142**, 75 (1998).
[57] M.-P. LOWYS, J. DESBRIERES, M. RINAUDO, *Food Hydrocolloids* **15**, 25 (2001).
[58] D. TATSUMI, S. ISHIOKA, T. MATSUMOTO, *J. Soc. Rheol., Japan* **30**, 27 (2002).
[59] E. LASSEUGUETTE, D. ROUX, Y. NISHIYAMA, *Cellulose* **15**, 425 (2008).
[60] J. D. FERRY, *Viscoelastic properties of polymers*. 3 ed., John Wiley & Sons, Inc.: New York, 1980.
[61] M. BERCEA, P. NAVARD, *Macromolecules* **33**, 6011 (2000).
[62] M. M. DE SOUZA LIMA, R. BORSALI, *Macromol. Rapid Commun.* **25**, 771 (2004).
[63] C. GOUSSE, H. CHANZY, M. L. CERRADA, E. FLEURY, *Polymer* **45**, 1569 (2004).
[64] H. ONO, Y. SHIMAYA, K. SATO, T. HONGO, *Polym. J.* **36**, 684 (2004).
[65] H. ONO, H. YAMADA, S. MATSUDA, K. OKAJIMA, T. KAWAMOTO, H. IIJIMA, *Cellulose* **5**, 231 (1998).
[66] H. ONO, Y. SHIMAYA, T. HONGO, C. YAMANE, *Trans. Mater. Res. Soc Japan* **26**, 569 (2001).
[67] G. GUHADOS, W. WAN, J. HUTTER, *Langmuir* **21**, 6642 (2005).
[68] Y. C. HSIEH, H. YANO, M. NOGI, S. J. EICHHORN, *Cellulose* **15**, 507 (2008).
[69] T. NISHINO, K. TAKANO, K. NAKAMAE, K. SAITAKA, S. ITAKURA, J. AZUMA, K. OKAMURA, *J. Polym. Sci. Part B* **33**, 611 (1995).
[70] A. STURCOVA, G. R. DAVIES, S. J. EICHHORN, *Biomacromolecules* **6**, 1055 (2005).
[71] R. RUSLI, S. J. EICHHORN, *Appl. Phys. Lett.* **93**, 033111 (2008).
[72] S. IWAMOTO, W. KAI, A. ISOGAI, T. IWATA, *Biomacromolecules* **10**, 2571 (2009).
[73] S. TANPICHAI, F. QUERO, M. NOGI, H. YANO, R. J. YOUNG, T. LINDSTÖM, W. W. SAMPSON, S. J. EICHHORN, *Biomacromolecules* **13**, 1340 (2012).
[74] C. AULIN, M. GÄLLSTEDT, T. LINDSTRÖM, *Cellulose* **17**, 559 (2010).
[75] D. H. PAGE, *TAPPI* **52**, 674 (1969).
[76] K. OKSMAN, M. SAIN, ACS Symposium Series *Cellulose Nanocomposites Processing, Characterization, and Properties*, ACS: 2006; Vol. 938.
[77] M. NOGI, H. YANO, *Adv. Mater.* **20**, 1849 (2008).
[78] S. IWAMOTO, A. ISOGAI, T. IWATA, *Biomacromolecules* **12**, 831 (2011).
[79] A. WALTHER, J. V. I. TIMONEN, I. DÍEZ, A. LAUKKANEN, O. IKKALA, *Adv. Mater.* **23**, 2924 (2011).
[80] A. WALTHER, I. BJURHAGER, J.-M. MALHO, J. PERE, J. RUOKOLAINEN, L. A. BERGLUND, O. IKKALA, *Nano Lett.* **10**, 2742 (2010).
[81] H. JIN, A. CAO, E. SHI, J. SEITSONEN, L. ZHANG, R. H. A. RAS, L. A. BERGLUND, M. ANKERFORS, A. WALTHER, O. IKKALA, *J. Mater. Chem. B* **1**, 835 (2013).
[82] S. S. KISTLER, *Nature* **127**, 741 (1931).
[83] A. C. PIERRE, G. M. PAJONK, *Chem. Rev.* **102**, 4243 (2002).
[84] R. W. PEKALA, *J. Mater. Sci.* **24**, 3221 (1989).
[85] H. TAMON, H. ISHIZAKA, T. ARAKI, M. OKAZAKI, *Carbon* **36**, 1257 (1998).
[86] R. W. PEKALA, C. T. ALVISO, J. D. LEMAY, *J. Non-Cryst. Solids* **125**, 67 (1990).
[87] R. W. PEKALA, D. W. SCHAEFER, *Macromolecules* **26**, 5487 (1993).

[88] X. Cui, J. Wei, K. Wang, A. Cao, H. Zhu, Y. Jia, Q. Shu, D. Wu, *Adv. Mater.* **21**, 1 (2009).
[89] J. Zhou, J. Liu, A. S. Karakoti, A. Kumar, D. Joung, Q. Li, S. I. Khondaker, S. Seal, L. Zhai, *ACS Nano* **4**, 7293 (2010).
[90] B. Grzyb, C. Hildenbrand, S. Berthon-Fabry, D. Begin, N. Job, A. Rigacci, P. Achard, *Carbon* **48**, 2297 (2010).
[91] M. Nogi, F. Kurosaki, H. Yano, M. Takano, *Carbohydr. Polym.* **81**, 919 (2010).
[92] J. Rooke, C. Matos, M. Chatenet, R. Sescousse, T. Budtova, S. Berthon-Fabry, R. Mosdale, F. d. r. Maillard, *ECS Transactions* **33**, 447 (2010).
[93] C. Hildenbrand, F. Fischer, A. B.-F. Rigacci, S.;, B. Simon, P. Achard, *Polymer Preprints (ACS, Division of Polymer Chemistry)* **52**, (2011).
[94] H. Tamon, H. Ishizaka, T. Yamamoto, T. Suzuki, *Carbon* **37**, 2049 (1999).
[95] H. Tamon, H. Ishizaka, T. Yamamoto, T. Suzuki, *Carbon* **38**, 1099 (2000).
[96] S. Kuga, D.-Y. Kim, Y. Nishiyama, R. M. Brown, *Mol. Cryst. Liq. Cryst.* **387**, 13 (2002).
[97] S. Deville, E. Saiz, R. K. Nalla, A. P. Tomsia, *Science* **311**, 515 (2006).
[98] J. Lee, Y. Deng, *Soft Matter* **7**, 6034 (2011).
[99] A. J. Svagan, M. A. S. A. Samir, L. A. Berglund, *Adv. Mater.* **20**, 1263 (2008).
[100] C. Tan, B. M. Fung, J. K. Newman, C. Vu, *Adv. Mater.* **13**, 644 (2001).
[101] F. Fischer, A. Rigacci, R. Pirard, S. Berthon-Fabry, P. Achard, *Polymer* **47**, 7636 (2006).
[102] N. D. Luong, Y. Lee, J.-D. Nam, *Eur. Polym. J.* **44**, 3116 (2008).
[103] F. Liebner, R. Dunareanu, M. Opietnik, E. Haimer, M. Wendland, C. Werner, M. Maitz, P. Seib, M.-A. Neouze, A. Potthast, T. Rosenau, *Holzforschung* **66**, 317 (2012).
[104] H. Jin, Y. Nishiyama, M. Wada, S. Kuga, *Colloid Surf. A* **240**, 63 (2004).
[105] S. Hoepfner, L. Ratke, B. Milow, *Cellulose* **15**, 121 (2008).
[106] J. Innerlohinger, H. K. Weber, G. Kraft, *Macromol. Symp.* **244**, 126 (2006).
[107] F. Liebner, A. Potthast, T. Rosenau, E. Haimer, M. Wendland, *Holzforschung* **62**, 129 (2008).
[108] M. Litschauer, M.-A. Neouze, E. Haimer, U. Henniges, A. Potthast, T. Rosenau, F. Liebner, *Cellulose* **18**, 143 (2011).
[109] R. Gavillon, T. Budtova, *Biomacromolecules* **9**, 269 (2008).
[110] F. Liebner, E. Haimer, A. Potthast, D. Loidl, S. Tschegg, M.-A. Neouze, M. Wendland, T. Rosenau, *Holzforschung* **63**, 3 (2009).
[111] J. Cai, S. Kimura, M. Wada, S. Kuga, L. Zhang, *ChemSusChem* **1**, 149 (2008).
[112] J. Cai, S. Kimura, M. Wada, S. Kuga, *Biomacromolecules* **10**, 87 (2009).
[113] Z. Wang, S. Liu, Y. Matsumoto, S. Kuga, *Cellulose* **19**, 393 (2012).
[114] J. Cai, S. Liu, J. Feng, S. Kimura, M. Wada, S. Kuga, L. Zhang, *Angew. Chem. Int. Ed.* **51**, 2076 (2012).
[115] J. Zhang, Y. Cao, J. Feng, P. Wu, *J. Phys. Chem. C* **116**, 8063 (2012).
[116] S. Liu, Q. Yan, D. Tao, T. Yu, X. Liu, *Carbohydr. Polym.* **89**, 551 (2012).
[117] C. Tsioptsias, A. Stefopoulos, I. Kokkinomalis, L. Papadopoulou, C. Panayiotou, *Green Chem.* **10**, 965 (2008).
[118] O. Aaltonen, O. Jauhiainen, *Carbohydr. Polym.* **75**, 125 (2009).
[119] R. Sescousse, A. Smacchia, T. Budtova, *Cellulose* **17**, 1137 (2010).

[120] J. LI, Y. LU, D. YANG, Q. SUN, Y. LIU, H. ZHAO, *Biomacromolecules* **12**, 1860 (2011).
[121] M. GRANSTRÖM, M. KETTUNEN NEE PÄÄKKÖ, H. JIN, E. KOLEHMAINEN, I. KILPELÄINEN, O. IKKALA, *Polym. Chem.* **2**, 1789 (2011).
[122] H. CHEN, J. LI, *Adv. Mater. Res.* **280**, 1912 (2011).
[123] M. PÄÄKKÖ, J. VAPAAVUORI, R. SILVENNOINEN, H. KOSONEN, M. ANKERFORS, T. LINDSTRÖM, L. A. BERGLUND, O. IKKALA, *Soft Matter* **4**, 2492 (2008).
[124] C. GEBALD, J. A. WURZBACHER, P. TINGAUT, T. ZIMMERMANN, A. STEINFIELD, *Environ. Sci. Technol.* **45**, 9101 (2011).
[125] R. P. SWATLOWSKI, S. K. SPEAR, J. D. HOLBREY, R. D. ROGERS, *J. Am. Chem. Soc.* **124**, 4974 (2002).
[126] J. MAJOINEN, A. WALTHER, J. R. MCKEE, E. KONTTURI, V. ASEYEV, J. M. MALHO, J. RUOKOLAINEN, O. IKKALA, *Biomacromolecules* **12**, 2997 (2011).
[127] M. WANG, A. OLSZEWSKA, A. WALTHER, J.-M. MALHO, F. H. SCHACHER, J. RUOKOLAINEN, M. ANKERFORS, J. LAINE, L. A. BERGLUND, M. ÖSTERBERG, O. IKKALA, *Biomacromolecules* **12**, 2074 (2011).
[128] W. HU, S. CHEN, Z. YANG, L. LIU, H. WANG, *J. Phys. Chem. B* **115**, 8453 (2011).
[129] G. NYSTRÖM, A. MIHRANYAN, A. RAZAQ, T. LINDSTRÖM, L. NYHOLM, M. STRÖMME, *J. Phys. Chem. B* **114**, 4178 (2010).
[130] A. PRON, P. RANNOU, *Prog. Polym. Sci.* **27**, 135 (2002).
[131] Y. CAO, P. SMITH, A. J. HEEGER, *Synth. Met.* **48**, 91 (1992).
[132] W.-Y. ZHENG, R.-H. WANG, K. LEVON, Z. Y. RONG, T. TAKA, W. PAN, *Macromol. Chem. Phys.* **196**, 2443 (1995).
[133] S. H. YOON, H.-J. JIN, M.-C. KOOK, Y. R. PYUN, *Biomacromolecules* **7**, 1280 (2006).
[134] O. VAN DEN BERG, M. SCHROETER, J. R. CAPADONA, C. WEDER, *J. Mater. Chem.* **17**, 2746 (2007).
[135] D. MULLER, C. R. RAMBO, D.O.S.RECOUVREUX, L. M. PORTO, G. M. O. BARRA, *Synth. Metals* **161**, 106 (2011).
[136] D. MULLER, J. S. MANDELLI, J. A. MARINS, B. G. SOARES, L. M. PORTO, C. R. RAMBO, G. M. O. BARRA, *Cellulose* **19**, 1645 (2012).
[137] J. MARINS, B. SOARES, K. DAHMOUCHE, S. L. RIBEIRO, H. BARUD, D. BONEMER, *Cellulose* **18**, 1285 (2011).
[138] D. O. CARLSSON, G. NYSTROM, Q. ZHOU, L. A. BERGLUND, L. NYHOLM, M. STROMME, *J. Mater. Chem.* **22**, 19014 (2012).
[139] S. SHARIKI, S. LIEW, W. THIELEMANS, D. WALSH, C. CUMMINGS, L. RASSAEI, M. WASBROUGH, K. EDLER, M. BONNE, F. MARKEN, *J. Solid State Electrochem.* **15**, 2675 (2011).
[140] E. TKALYA, M. GHISLANDI, W. THIELEMANS, P. VAN DER SCHOOT, G. DE WITH, C. KONING, *ACS Macro Lett.* 157 (2013).
[141] A. FUJISHIMA, K. HONDA, *Nature* **238**, 37 (1972).
[142] T. L. THOMPSON, J. T. YATES, *Chem. Rev.* **106**, 4428 (2006).
[143] H. TONG, S. OUYANG, Y. BI, N. UMEZAWA, M. OSHIKIRI, J. YE, *Adv. Mater.* **24**, 229 (2012).
[144] R. WANG, K. HASHIMOTO, A. FUJISHIMA, M. CHIKUNI, E. KOJIMA, A. KITAMURA, M. SHIMOHIGOSHI, T. WATANABE, *Nature* **338**, 431 (1997).
[145] R. WANG, K. HASHIMOTO, A. FUJISHIMA, M. CHIKUNI, E. KOJIMA, A. KITAMURA, M. SHIMOHIGOSHI, T. WATANABE, *Adv. Mater* **10**, 135 (1998).
[146] T. WATANABE, S. FUKAYAMA, M. MIYAUCHI, A. FUJISHIMA, K. HASHIMOTO, *J. Sol-Gel Sci. Technol.* **19**, 71 (2000).
[147] N. SAKAI, A. FUJISHIMA, T. WATANABE, K. HASHIMOTO, *J. Phys. Chem. B* **107**, 1028 (2003).
[148] X. FENG, J. ZHAI, L. JIANG, *Angew. Chem. Int. Ed.* **44**, 5115 (2005).
[149] J. MALM, E. SAHRAMO, M. KARPPINEN, R. H. A. RAS, *Chem. Mater.* **22**, 3349 (2010).

[150] A. LAFUMA, D. QUERE, *Nature Mater.* **2**, 457 (2003).
[151] K. KOCH, B. BHUSHAN, Y. C. JUNG, W. BARTHLOTT, *Soft Matter* **5**, 1386 (2009).
[152] A. MARMUR, *Soft Matter* **8**, 6867 (2012).
[153] E. BITTOUN, A. MARMUR, *Langmuir* **28**, 13933 (2012).
[154] M. JIN, X. FENG, L. FENG, T. SUN, J. ZHAI, T. LI, L. JIANG, *Adv. Mater.* **17**, 1977 (2005).
[155] L. FENG, Y. ZHANG, J. XI, Y. ZHU, N. WANG, F. XIA, L. JIANG, *Langmuir* **24**, 4114 (2008).
[156] B. BALU, V. BREEDVELD, D. W. HESS, *Langmuir* **24**, 4785 (2008).
[157] Z.-G. GUO, W.-M. LIU, *Appl. Phys. Lett.* **90**, 223111 (2007).
[158] S. WANG, L. JIANG, *Adv. Mater.* **19**, 3423 (2007).
[159] W. BARTHLOTT, C. NEINHUIS, *Planta* **202**, 1 (1997).
[160] X. GAO, L. JIANG, *Nature* **432**, 36 (2004).
[161] D. NYSTRÖM, J. LINDQVIST, E. ÖSTMARK, A. HULT, E. MALMSTRÖM, *Chem. Commun.* 3594 (2006).
[162] G. GONCALVES, P. A. A. P. MARQUES, T. TRINDADE, C. P. NETO, A. GANDINI, *J. Colloid Interface Sci.* **324**, 42 (2008).
[163] S. LI, H. XIE, S. ZHANG, X. WANG, *Chem. Commun.* 4857 (2007).
[164] S. LI, Y. WEI, J. HUANG, *Chem. Lett.* **39**, 20 (2010).
[165] T. WANG, X. HU, S. DONG, *Chem. Commun.* 1849 (2007).
[166] M. J. UDDIN, F. CESANO, F. BONINO, S. BORDIGA, G. SPOTO, D. SCARANO, A. ZECCHINA, *J. Photochem. Photobiol. A* **189**, 286 (2007).
[167] Y. SHIN, J. LIU, J. H. CHANG, Z. NIE, G. J. EXARHOS, *Adv. Mater.* **13**, 728 (2001).
[168] J. HUANG, T. KUNITAKE, *J. Am. Chem. Soc.* **125**, 11834 (2003).
[169] A. DONG, Y. WANG, Y. TANG, N. REN, Y. ZHANG, Y. YUE, Z. GAO, *Adv. Mater.* **14**, 926 (2002).
[170] M. KEMELL, V. PORE, M. RITALA, M. LESKELÄ, M. LINDÉN, *J. Am. Chem. Soc.* **127**, 14179 (2005).
[171] T. H. HAN, J. K. OH, J. S. PARK, S.-H. KWON, S.-W. KIM, S. O. KIM, *J. Mater. Chem.* **19**, 3512 (2009).
[172] D.-H. YU, X. YU, C. WANG, X.-C. LIU, Y. XING, *ACS Appl. Mater. Interfaces* **4**, 2781 (2012).
[173] Y. ZHOU, E.-Y. DING, W.-D. LI, *Mater. Lett.* **61**, 5050 (2007).
[174] H. MATSUBARA, M. TAKADA, S. KOYAMA, K. HASHIMOTO, A. FUJISHIMA, *Chem. Lett.* **767**, (1995).
[175] L. YE, C. D. M. FILIPE, M. KAVOOSI, C. A. HAYNES, R. PELTON, M. A. BROOK, *J. Mater. Chem.* **19**, 2189 (2009).
[176] J. ZENG, S. LIU, J. CAI, L. ZHANG, *J. Phys. Chem. C* **114**, 7806 (2010).
[177] X. WANG, R. A. CARUSO, *J. Mater. Chem.* **21**, 20 (2011).
[178] T. SAITO, T. UEMATSU, S. KIMURA, T. ENOMAE, A. ISOGAI, *Soft Matter* **7**, 8804 (2011).
[179] E. DINAND, H. CHANZY, R. M. VIGNON, *Food Hydrocolloids* **13**, 275 (1999).
[180] V. S. RUDRARAJU, C. M. WYANDT, *Int. J. Pharm.* **292**, 53 (2005).
[181] V. S. RUDRARAJU, C. M. WYANDT, *Int. J. Pharm.* **292**, 63 (2005).
[182] A. FALL, S. LINDSTRÖM, O. SUNDMAN, L. ÖDBERG, L. WÅGBERG, *Langmuir* **27**, 11332 (2011).
[183] A. E. WAY, L. HSU, K. SHANMUGANATHAN, C. WEDER, S. J. ROWAN, *ACS Macro Letters* **1**, 1001 (2012).
[184] G. AGODA-TANDJAWA, S. DURAND, S. BEROT, C. BLASSEL, C. GAILLARD, C. GARNIER, J. L. DOUBLIER, *Carbohydr. Polym.* **80**, 677 (2010).
[185] E. SAARIKOSKI, T. SAARINEN, J. SALMELA, J. SEPPÄLÄ, *Cellulose* **19**, 647 (2012).
[186] M. BHATTACHARYA, M. M. MALINEN, P. LAUREN, Y.-R. LOU, S. W. KUISMA, L. KANNINEN, M. LILLE, A. CORLU, C. GUGUEN-GUILLOUZO, O. IKKALA, A. LAUKKANEN, A. URTTI, M. YLIPERTTULA, *J. Controlled Release* **164**, 291 (2012).

[187] C. EYHOLZER, A. B. DE COURACA, F. DUC, P. E. BOURBAN, P. TINGAUT, T. ZIMMERMANN, J. A. E. MANSON, K. OKSMAN, *Biomacromolecules* **12**, 1419 (2011).
[188] P. MATHEW AJI, A. CHAKRABORTY, K. OKSMAN, M. SAIN, The Structure and Mechanical Properties of Cellulose Nanocomposites Prepared by Twin Screw Extrusion. In *Cellulose Nanocomposites*, American Chemical Society: 2006; Vol. 938, pp 114.
[189] J. DLOUHA, L. SURYANEGARA, H. YANO, *Soft Matter* **8**, 8704 (2012).
[190] K. SUZUKI, H. OKUMURA, K. KITAGAWA, S. SATO, A. NAKAGAITO, H. YANO, *Cellulose* **20**, 201 (2013).
[191] A. N. NAKAGAITO, H. YANO, *Appl. Phys. A* **80**, 155 (2005).
[192] A. N. NAKAGAITO, S. IWAMOTO, H. YANO, *Appl. Phys. A* **80**, 93 (2005).
[193] S. IWAMOTO, A. N. NAKAGAITO, H. YANO, *Appl. Phys. A* **89**, 461 (2007).
[194] T. ZIMMERMANN, E. PÖHLER, T. GEIGER, *Adv. Eng. Mater.* **6**, 754 (2004).
[195] T. ZIMMERMANN, E. PÖHLER, P. SCHWALLER, *Adv. Eng. Mater.* **7**, 1156 (2005).
[196] M. KETTUNEN, R. J. SILVENNOINEN, N. HOUBENOV, A. NYKÄNEN, J. RUOKOLAINEN, J. SAINIO, V. PORE, M. KEMELL, M. ANKERFORS, T. LINDSTRÖM, M. RITALA, R. H. A. RAS, O. IKKALA, *Adv. Funct. Mater* **21**, 510 (2011).
[197] C. AULIN, A. SHCHUKAREV, J. LINDQVIST, E. MALMSTRÖM, L. WÅBERG, T. LINDSTRÖM, *Colloid Interf. Sci.* **317**, 556 (2008).
[198] H. SEHAQUI, M. SALAJKOVA, Q. ZHOU, L. A. BERGLUND, *Soft Matter* **6**, 1824 (2010).
[199] H. JIN, M. KETTUNEN, A. LAIHO, H. PYNNÖNEN, J. PALTAKARI, A. MARMUR, O. IKKALA, R. H. A. RAS, *Langmuir* **27**, 1930 (2011).
[200] J. KORHONEN, M. KETTUNEN, R. H. A. RAS, O. IKKALA, *ACS Appl. Mater. Interfaces* **3**, 1813 (2011).
[201] W. ZHANG, Y. ZHANG, C. LU, Y. DENG, *J. Mater. Chem.* **22**, 11642 (2012).
[202] H. KOGA, A. AZETSU, E. TOKUNAGA, T. SAITO, A. ISOGAI, T. KITAOKA, *J. Mater. Chem.* **22**, 5538 (2012).
[203] R. T. OLSSON, M. A. S. AZIZI SAMIR, G. SALAZAR ALVAREZ, L. BELOVA, V. STRÖM, L. A. BERGLUND, O. IKKALA, J. NOGUES, U. W. GEDDE, *Nature Nanotech.* **5**, 584 (2010).
[204] H. SEHAQUI, Q. ZHOU, L. A. BERGLUND, *Compos. Sci. Technol.* **71**, 1593 (2011).
[205] Z. M. ALI, L. J. GIBSON, *Soft Matter* **9**, 1580 (2013).
[206] M. D. GAWRYLA, O. VAN DEN BERG, C. WEDER, D. A. SCHIRALDI, *J. Mater. Chem.* **19**, 2118 (2009).
[207] J. T. KORHONEN, P. HIEKKATAIPALE, J. MALM, M. KARPPINEN, O. IKKALA, R. H. A. RAS, *ACS Nano* **5**, 1967 (2011).
[208] H. SEHAQUI, Q. ZHOU, O. IKKALA, L. A. BERGLUND, *Biomacromolecules* **12**, 3638 (2011).
[209] L. HEATH, W. THIELEMANS, *Green Chemistry* **12**, 1448 (2010).
[210] C. AULIN, J. NETRVAL, L. WÅGBERG, T. LINDSTROM, *Sof Matter* **6**, 3298 (2010).
[211] L. J. GIBSON, F. R. S. ASHBY, *Proc. R. Soc. Lond. A* **382**, 43 (1982).
[212] L. J. GIBSON, *J. Biomech.* **38**, 377 (2005).
[213] W. SURAPOLCHAI, D. SCHIRALDI, *Polym. Bull.* **65**, 951 (2010).
[214] J. R. CAPADONA, K. SHANMUGANATHAN, D. J. TYLER, S. J. ROWAN, C. WEDER, *Science* **319**, 1370 (2008).
[215] T. ZHANG, T. OYAMA, A. AOSHIMA, H. HIDAKA, J. ZHAO, N. SERPONE, *J. Photochem. Photobiol. A* **140**, 163 (2001).
[216] V. PORE, A. RAHTU, M. LESKELÄ, M. RITALA, T. SAJAVAARA, J. KEINONEN, *Chem. Vap. Dep.* **10**, 143 (2004).

[217] H. JIN, A. MARMUR, O. IKKALA, R. H. A. RAS, *Chem. Sci.* **3**, 2526 (2012).
[218] T. NISHINO, M. MEGURO, M. NAKAMAE, Y. UEDA, *Langmuir* **15**, 4321 (1999).
[219] A. TUTEJA, W. CHOI, M. MA, J. M. MABRY, S. A. MAZZELLA, G. C. RUTLEDGE, G. H. MCKINLEY, R. E. COHEN, *Science* **318**, 1618 (2007).
[220] L. CAO, T. P. PRICE, M. WEISS, D. GAO, *Langmuir* **24**, 1640 (2008).
[221] H. M. CHOI, R. M. CLOUD, *Environ. Sci. Technol.* **26**, 772 (1992).
[222] Q. F. WEI, R. R. MATHER, A. F. FOTHERINGHAM, R. D. YANG, *Mar. Pollut. Bull.* **46**, 780 (2003).
[223] J. G. REYNOLDS, P. R. CORONADO, L. W. HRUBESH, *J. Non-Cryst. Solids* **292**, 127 (2001).
[224] A. VENKATESWARA RAO, N. D. HEGDE, H. HIRASHIMA, *J. Colloid Interface Sci.* **305**, 124 (2007).
[225] J. GURAV, A. V. RAO, D. Y. NADARGI, H.-H. PARK, *J. Mater. Sci.* **45**, 503 (2010).
[226] X. GUI, J. WEI, K. WANG, A. CAO, H. ZHU, Y. JIA, Q. SHU, D. WU, *Adv. Mater.* **22**, 617 (2010).
[227] J. YUAN, X. LIU, O. AKBULUT, J. HU, S. L. SUIB, J. KONG, F. STELLACCI, *Nature Nanotech.* **3**, 332 (2008).
[228] N. CERVIN, C. AULIN, P. LARSSON, L. WÅGBERG, *Cellulose* **19**, 401 (2012).
[229] H. MERTANIEMI, A. LAUKKANEN, J.-E. TEIRFOLK, O. IKKALA, R. H. A. RAS, *RSC Adv.* **2**, 2882 (2012).

Aalto-DD 114/2013

ISBN 978-952-60-5255-7
ISBN 978-952-60-5256-4 (pdf)
ISSN-L 1799-4934
ISSN 1799-4934
ISSN 1799-4942 (pdf)

Aalto University

Department of Applied Physics
www.aalto.fi

BUSINESS +
ECONOMY

ART +
DESIGN +
ARCHITECTURE

SCIENCE +
TECHNOLOGY

CROSSOVER

**DOCTORAL
DISSERTATIONS**